AUTOMATED CRACK CONTROL ANALYSIS FOR CONCRETE PAVEMENT CONSTRUCTION

A Thesis

by

SE HOON JANG

Submitted to the Office of Graduate Studies of
Texas A&M University
in partial fulfillment of the requirements for the degree of

MASTER OF SCIENCE

August 2005

Major Subject: Civil Engineering

AUTOMATED CRACK CONTROL ANALYSIS FOR CONCRETE PAVEMENT

CONSTRUCTION

A Thesis

by

SE HOON JANG

Submitted to the Office of Graduate Studies of
Texas A&M University
in partial fulfillment of the requirements for the degree of

MASTER OF SCIENCE

Approved by:

Chair of Committee,	Dan G. Zollinger
Committee Members,	Robert Lytton
	Mohammed Haque
Head of Department,	David Rosowsky

August 2005

Major Subject: Civil Engineering

ABSTRACT

Automated Crack Control Analysis for Concrete Pavement Construction. (August 2005)

Se Hoon Jang, B.S., Kungpook National University

Chair of Advisory Committee: Dr. Dan G. Zollinger

The focus of this research is on the control of random cracking in concrete paving by using sawcut notch locations in the early stages of construction. This is a major concern in concrete pavement construction. This research also addresses a probabilistic approach to determine the optimum time and depth of sawcutting for newly constructed portland cement concrete pavements.

Variability in climate conditions and material characteristics during the hardening process affects the potential of cracking at any sawcut depth. Several factors affecting the probability of crack initiation are material strength parameters, method and quality of curing, slab/subbase stiffness, the amount and depth of steel reinforcement, friction between the slab and the subbase, and concrete shrinkage. Other factors relevant to concrete mixture characteristics such as cement content and type of coarse aggregate affect development of early aged stresses caused by shrinkage and thermally induced contraction.

A probabilistic analysis of the factors that affect crack control using sawcut notches is presented in relation to different weather conditions (concrete placement temperature) at the time of construction, and concrete mixture characteristics such as fly ash replacement (FA) and cement factor (CF). Both of these significantly affect sawcut timing and depth

requirement. The determination of crack initiation is based on fracture mechanics. Estimation of the time of cracking is based on predicted tensile strength and stress in the concrete at the bottom of the sawcut notch to assess the feasibility of crack control in the early stages of construction.

DEDICATION

I would like to dedicate this thesis to my wife, Eunjeong Jung, and parents who have been supporting and encouraging me constantly. I would like to express my respect to my father who passed away on November 23, 2004, during my study.

ACKNOWLEDGMENTS

I would like to express my deep gratitude to my advisor, Dr. Dan G. Zollinger, for his advice and help in completing this thesis. I would also like to thank Dr. Robert L. Lytton and Dr. Mohommed Haque for serving as advisory committee members. I am grateful to Dr. Mukhopadhyay Anol for his encouragement and advice. I am sincerely indebted to all my professors in the faculty of Materials Engineering for contributing to my education in the subject.

TABLE OF CONTENTS

LIST OF FIGURES

FIGURE   Page

LIST OF TABLES

CHAPTER I

INTRODUCTION

OBJECTIVES

The purpose of this thesis is to present a rational analysis of the strength and stress occurring in newly constructed jointed concrete pavements due to variations with depth in moisture and temperature (so called warping and curling stresses), and restraint caused by reinforcing steel. Furthermore, it presents a probabilistic approach to appropriate sawcut timing and depth for newly constructed concrete pavements to control incidences of random cracking.

Joints in concrete slabs can be created by forming grooves, tooling, sawcutting, and placement of joint formers. Although a variety of methods are available for crack control, the discussion in this thesis is limited to those based on the use of a sawcut notch in the pavement surface. The placement of a notch at the appropriate time and depth is a key for the successful control of cracking. The control of cracking using sawcut notches in the surface of a concrete pavement is a complicated process involving several material properties, construction and weather related factors, and pavement design.

_____

This thesis follows the style and format of the *Transportation Research Record.*

CRACK CONTROL IN CONCRETE PAVING

Most random cracks in concrete pavements typically occur at an early age due to improper design and construction practices, such as omission of isolation and contraction joints and improper jointing practices. During the curing process at an early age, temperature and moisture gradients form vertically through the slab, which induce stresses through the depth of the slab. These gradients also cause the slab to deform and possibly to lift off in the corner areas. However this tendency to lift off is restrained by the self-weight of the slab. Thus, random cracks can occur when provisions to accommodate these movements are not made in design and construction. Therefore, the sawcutting on the surface of a concrete pavement forms into a joint and a line of separation within the slab if the tensile stresses exceed the tensile strength of concrete ensuring that cracking occurs at this point.

Theses types of joints are called contraction joints and are introduced as a means to relieve the stresses in the slab. Sawcut notches should be placed at appropriate locations from a few to several hours after the initial setting of concrete. If the sawcut notches are placed too late random cracks may occur at the point where high stresses are induced whether or not at the tip of the sawcut notches. Sawcutting too soon in some cases, results in some spalling and raveling along the joint face. Therefore, a well-timed placement of the surface notch works to the advantage of the pavement engineer to initiate a crack and form a contraction joint.

CHAPTER II

LITERATURE REVIEW

SAWCUT OPERATIONS

Sawcutting is the most common and reliable method of forming contraction joints. The initial sawcut provides a plane of weakness where cracking may begin. The timing of this sawcut in the pavement after placement is critical and requires judgment; sawcutting too late could lead to uncontrolled cracking in the slab. The depth of the sawcutting will vary with concrete strength. The sawcutting should begin as soon as the concrete has obtained adequate strength to resist raveling of the joint edges, typically between 4 and 24 hours. Weather conditions (temperature, wind, solar radiation, and humidity) have a large influence on concrete strength gain and thus on the optimal time to begin sawing. The concrete mix design also affects proper sawcut timing. Mixes with soft limestone aggregates require less strength development than do mixes with hard coarse aggregates such as river gravel. The modulus of subgrade reaction, k value, also affects proper timing. If the k value is high in case of stiff stabilized subbases, the timing of sawcut typically is earlier than for lower k values in case of natural subgrade or granular subbases.

Sawcutting should begin as soon as possible after adequate strength is obtained. Under normal weather conditions, sawcut operation can begin between 4 to 12 hours after placement, depending on curing conditions and support type. Severe climatic conditions

require even greater attention to detail. Hot weather conditions can cause concrete pavements to increase the rate of drying shrinkage requiring sawcut operations to start within four hours after placement. Cold weather conditions may retard concrete strength gain, prohibiting sawing operations for up to 24 hours or more after placement. Sawcutting operation in construction site is shown in Figure 2-1.

Figure 2-1 Timing of sawing contraction joint is critical.

The initial sawcutting for a weakened plane in adequately cured concrete paving is in the form of sawcut notches that have at least one-third the thickness of the slab (D/3) with a minimum width of l/8 inch. Under most circumstances, each joint should be sawed as soon as possible after placement. In some cases, such as hot and windy weather conditions, initial contraction joints generally are sawed with spacing of 60 to 80 feet intervals, while the intermediate joints are sawed at a later time. However, stiff stabilized subbases require that all transverse contraction joints be sawed continuously to prevent random cracking.

Timing of sawcut operations for longitudinal contraction joints is thought not to be as critical as for transverse contraction joints (1). On stiff stabilized subbases, longitudinal joint sawing should start as soon as possible, with the longitudinal sawing proceeding after transverse joints are initially sawn. During periods with large temperature fluctuations (spring, fall, or sudden thunderstorms), sawing should start as early as possible.

A widening cut is occasionally used as a secondary sawcut to establish the proper shape factor for a sealant material. Contractors use saws equipped with multiple blades and spacer combinations to get the necessary widths. Widening cuts are generally made within 7 days after paving and initial sawcutting.

The selection of saw blade type (abrasive/dry or diamond/wet) depends on the aggregates in the concrete. Aggregates hardness varies from soft to hard being more difficult to saw. General aggregate hardness classifications are shown in Table 2-1. Size and a mount of aggregate used in the mix design can also affect the ease of sawing regardless of overall aggregate hardness.

Table 2-1 General aggregate hardness table (1)

SOFT	MEDIUM	HARD
Limestone Dolomite Coral	River Gravel Trap Rock	Granite Flint Chert Quartz

Purpose of Joints

The purpose of sawing joints at an early age in concrete pavements is to create a point of weakness which will induce cracking at a desired location. Cracks in a concrete slab cannot be prevented entirely, but they can be controlled and minimized by properly designed joints. Concrete is typically weak in tension. If its natural tendency to shrink is restrained, tensile stresses that exceed its tensile strength can develop resulting in cracking. In addition, in some cases, cracking is caused by temperature changes or by the slight contraction that takes place as the concrete sets and hardens. Later, as the concrete hardens, it will shrink further and either additional cracks may form, or preexisting cracks may become wider. Joints, if properly formed, provide relief from the tensile stresses. Also, they are more easily maintained and are less objectionable than uncontrolled or irregular cracks.

A sawcut may be thought of as a "notch" in the pavement's surface. The notch toughness of an early age concrete is fairly low compared to other materials (such as steel, aggregate, and hardened concrete). Notch toughness for early age concrete slabs is controlled by the strength of the weakest component of the concrete, the cement paste, and

aggregate bond. This is supported by studies and field observation (2). Cores taken through successfully formed contraction joints typically show the concrete cracks through the paste and around the aggregate. Cores taken through fatigue cracks that occur well after the concrete hardens, however, typically show the cracks fracture both paste and the aggregate (3).

Joint design for concrete pavements is to control incidences of random cracking and maintain pavement capacity (e.g., load transfer efficiency) and ride quality. In concrete pavement, joints are supposed to control transverse and longitudinal cracking from restrained contraction and the combined effects of restrained curling and warping and accommodate slab movements, and also must provide desired load transfer. In case of longitudinal joints, a suitable means is provided to divide pavements into practical construction increments (e.g. traffic lanes), but suitable joint layout and construction is key to pavement performance. Poorly designed joints are prone to cause many distresses such as spalling, early cracking, and pavement serviceability loss. In addition, well-timed placement of the sawcut is an important factor in establishing an effective joint system.

Types of Joints

Widely used types of joints in concrete pavement construction are:

- Transverse Contraction Joints: Joints that are constructed transverse to the traffic direction and spaced to control cracking from stresses caused by temperature and moisture changes. Generally, transverse contraction joints are oriented at right angles to the centerline and edge of the pavement lanes.

- Transverse Construction Joints**:** Joints installed at the end of a day-long paving operation or other placement interruptions (e.g. bridge approach). These joints need to be installed at the location of a planned and expected joint location to the extent possible.

- Transverse Expansion/Isolation Joints**:** Joints placed at locations that allow movement of the pavement without damaging adjacent structures such as bridges, drainage structures, or the pavement itself.

- Longitudinal Contraction Joints**:** Joints that typically divide traffic lanes and control cracking where two or more lane widths are placed. However, it is not necessary that longitudinal contraction joints be installed on exact traffic lines.

- Longitudinal Construction Joints**:** Joints that are constructed adjacent pavement lanes which are paved at different periods of time.

Transverse Contraction Joints

The primary function of transverse contraction joints is to control transverse cracking formation. Figure 2-2 shows typical details for transverse contraction joints. Dowel bars are often placed at transverse contraction joints to provide load transfer. To determine transverse joint spacing that will optimally control cracking, it is necessary to consider the slab thickness and subgrade or subbase type. Material properties such as the amount and type of aggregates, concrete mixture design, or curing method also affect the optimum joint spacing.
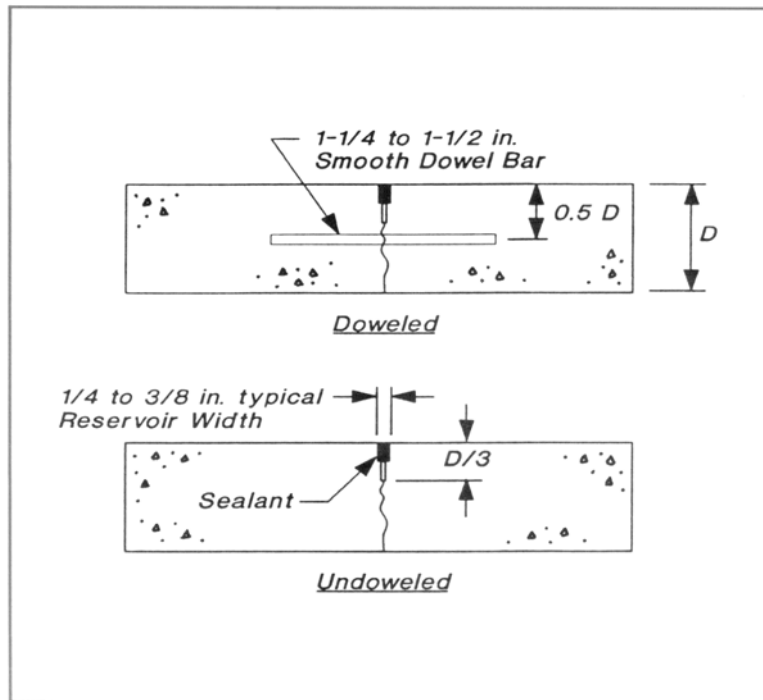
Figure 2-2 Transverse contraction joint (4).

Recommended joint spacings for different slab thickness and support conditions are shown in Figure 2-3. A design of transverse contraction joint should also consider the effect of longitudinal slab movement, and load transfer performance. For most concrete pavements, a range of spacing of transverse joints is from 12 to 20 feet, depending on slab thickness. No more than 20 feet is recommended according to Federal Highway Administration (FHWA) Report-RD-77-111 (5).

In this report, for reinforced concrete slabs the maximum advisable spacing is 30 feet. However, in this instance it is obviously not to minimize early aged cracking. The assumption is apparently based on that some random cracking will occur and that enough steel will be provided to keep the cracks tight.
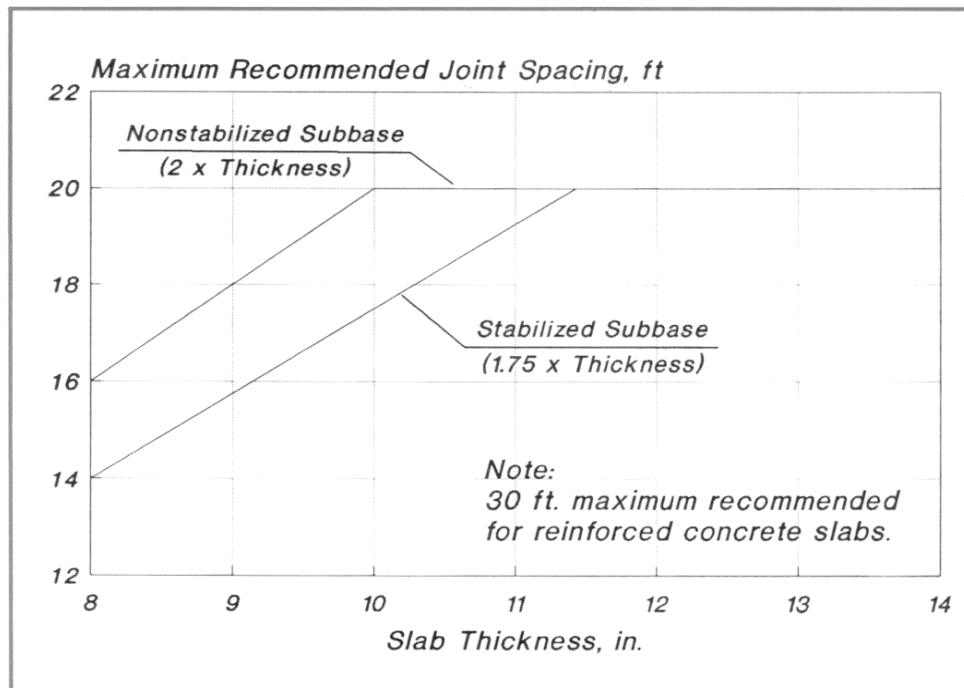
Figure 2-3 Recommended maximum joint spacing for concrete pavements (1).

Dowel Placement – Dowel bars can be placed at the contraction joint using a mechanical inserter or dowel baskets as shown in Figure 2-4. Mechanical insertion requires an attachment to the slipform paver that installs dowel bars by a vibrating process. Dowel baskets consist of dowel assemblies in a steel frame which holds and supports the dowel bars at a proper location and depth during placement.

Dowel bars at transverse contraction joints play an important role in the structural capabilities of a concrete pavement joint. Its shear capacity restrains movement at the edge of two adjacent slabs. Load transfer efficiency is highly dependent on the dowel bar shear capacity.

Figure 2-4 (Left) Dowel baskets in place prior to paving, (Right) Dowel bar inserter in operation.

It is best, in terms of freedom of movement, if dowels are properly aligned with the joint. Dowels should be placed perpendicular to the orientation of the joint and parallel to traffic lanes and the surface of the pavement. Dowel bar alignment may be a key for successful joint performance and long pavement life. Although unnecessary, dowel bars are some times lubricated to facilitate movement at the joint due to shrinkage and expansion caused by temperature and moisture changes. There are several lubricants commonly used in construction such as: parafin based lubricant, asphalt emulsion, form oil or standard grease. Some state agencies recommend that dowel bars have a maximum pull-out resistance of 200 pounds per dowel. However, there is a variance of values under actual field conditions.

Dowels should be smooth and free from any projected surface, however, to get a tight fit and good consolidation of concrete around the dowel, lubrication thickness is recommended less than 5 mils. If the lubrication layer is too thick, it may result in dowel

looseness and reduced joint load transfer. Therefore, application of lubricants on dowels should be carefully carried out.

A lubricated, smooth dowel will allow the joint to move easily and provide good performance. The dowel should meet American Society of Testing Materials (ASTM) Specification A615 (6). Dowel bars should also have resistance to corrosion. The guidelines of corrosion resistant coating is shown in AASHTO Specification M254 (7) and recommended as the coating thickness exceeds 5 to 15 mils to get suitable corrosion resistance. Epoxy-coating is used on dowels since it provides a consistent separation between the concrete and the steel layer and good resistance to corrosion. Consolidation of the concrete in the vicinity of the joint and around dowels is also a critical issue. Consolidation affects concrete strength, durability, and pavement life in the long term.

Transverse Construction Joints

Transverse construction joints are used at planned interruption such as at the end of a day's paving, at bridge leave-outs, intersections and where unplanned interruptions suspend operations for an extended time. Figure 2-5 shows typical details for construction joints. It is recommended that transverse construction joint locations coincide with the transverse contraction joint location. Transverse construction joints are always oriented perpendicular to the centerline.

Transverse construction joints are butt type joints that need dowel bars since joint opening may be so wide that there is no aggregate interlock to provide load transfer. The

same situation applies to joints placed adjacent to an existing concrete slab where dowels are required to get good load transfer at joints.
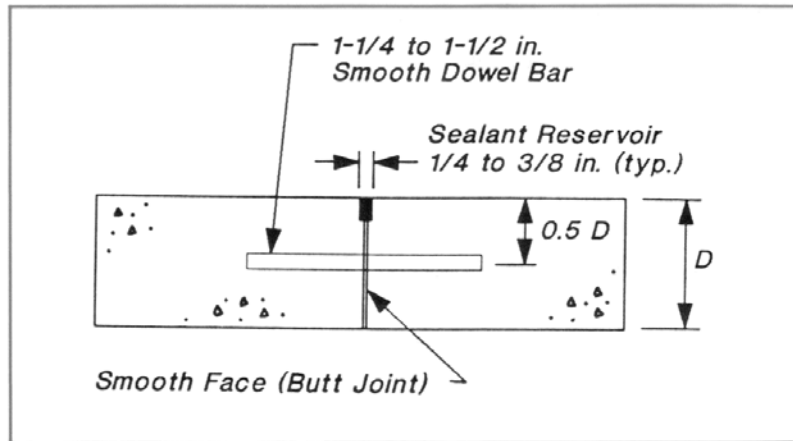
Figure 2-5 Transverse construction joint (4).

Transverse Expansion Joint

In the past, some engineers used various spacing combinations of expansion joints in an attempt to relieve pavement compressive stresses and prevent blow-ups. However, this practice led to other failures and distresses resulting in poor pavement performance since in many cases the expansion joints allowed too much opening of adjacent transverse contraction joints which led to loss of aggregate interlock and sealant damage. Thus, concrete pavements do not normally require transverse expansion joints. Experimental highway pavements show that expansion joints are only necessary at fixed structures such as bridges, drainage structures, or at locations where the difference in the thermal expansion point of reference (i.e. concrete set temperature) is more than 20°F. None the

less, eliminating unnecessary expansion joints, failures are minimized and the pavement provides better performance.
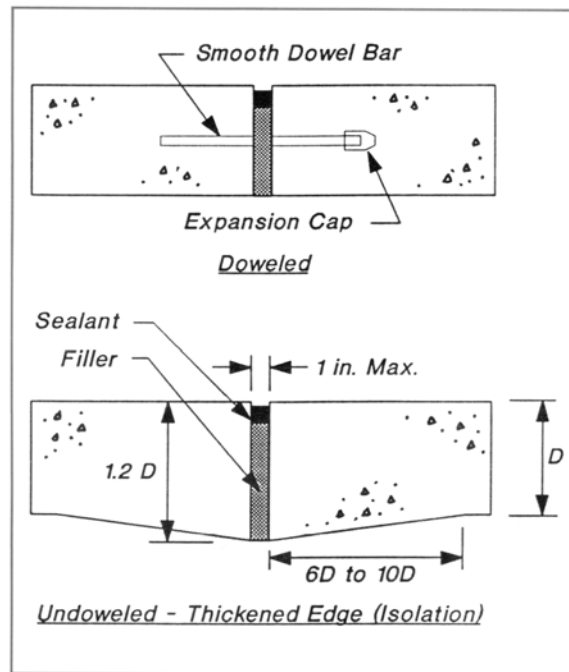
Figure 2-6 Transverse expansion joint (8).

Pavement expansion joints are only needed when the pavement is divided into long panels (60 feet or more) without contraction joints in-between and the contraction joints are allowed to be infiltrated by large incompressible materials or the adjacent pavement was constructed under low ambient temperature conditions causing a low set temperature. In most cases, theses criteria do not apply. Therefore, expansion joints are not normally used in pavement joints system. However, if they are used to isolate an on-line structure, such as a bridge, dowels to increase load transfer and joint effectiveness should be included.

It is recommended that expansion joints should be 3/4 to 1 inch wide. Otherwise, slab migration may occur if greater widths are involved. In expansion joints, the gap between the subbase or subgrade and the joint sealant is occupied by a preformed joint filler material as shown in Figure 2-6. Contraction joints within 60 to 100 feet of an expansion joint should be doweled. The expansion joint may allow adjacent contraction joints to open more than other contraction joints. If not doweled, adjacent contraction joints may lose load transfer efficiency.

Pressure relief joints have the same purpose as expansion joints. However, installation may not occur for years after the original pavement construction. Pressure relief joints relieve pressure against structures and alleviate potential blowups, and other similar problems. Although for most pavements they are not needed, pressure relief joints may provide appropriate relief against structure damage from excessive compressive stresses.

Doweled Expansion Joints

In doweled expansion joints, one end of the dowel must be equipped with a closed-end expansion cap into which the dowel bars can move smoothly as the joint expands and contracts. The cap must be long enough to cover at least 2 inches of the dowel and have a suitable stop to hold the end of the cap at least the width of the isolation joint plus ¼ inch away from the end of dowel bar by preventing the cap from slipping off of the dowel during placement. The cap must fit the dowel bar tightly and be watertight. The half of the dowel with the capped end must be coated to prevent bond and permit horizontal movement. A doweled expansion joints is shown at the top of Figure 2-6.

The same dowel placement and alignment requirements used for doweled contraction joints apply to doweled expansion joints. The dowels are typically installed at mid-depth, spaced 12 inches apart (center to center), and have a diameter of l-l/4 inches for 8 to 9-l/2 inches slabs, and l-1/2 inches diameter dowels for thicknesses of 10 inches or greater. Epoxy coating for corrosion resistance may be used for severe climates.

An expansion basket is placed in an attempt to support and align the dowel bars while also supporting the preformed filler material. The filler material must extend completely through the entire width of the slab and fit snugly into the basket frame as well as it occupies the gap between the slabs and must be continuous from one pavement edge to the other.

Undoweled Expansion Joints (Isolation Joints)

Undoweled expansion joints are normally made with thickened edges to reduce the stresses developed at the slab bottom. The abutting edges of both slabs should be thickened by 20 percent along the expansion joint. The thickness transition is tapered at a slope of 6 to 10 times the pavement thickness. For example, a thickness transition from 10 inches to a 12 inches thickened edge, would occur over 60 to 100 inches. A thickened-edge expansion joint is shown at the bottom of Figure 2-6.

Longitudinal Contraction Joints

Longitudinal contraction joints prevent irregular longitudinal cracks that would otherwise occur. Typical longitudinal contraction joint is shown in Figure 2-7. Longitudinal

contraction joints are typically placed in an attempt to divide lanes of traffic as well as control random cracking where two or more lane widths are placed at one time. Longitudinal joints are necessary when slab widths exceed 15 feet and when integral concrete curbs and gutters are involved. Longitudinal contraction joints typically are cut one-third the depth of the slab with initial saw cut l/8 to 3/8 inch width.
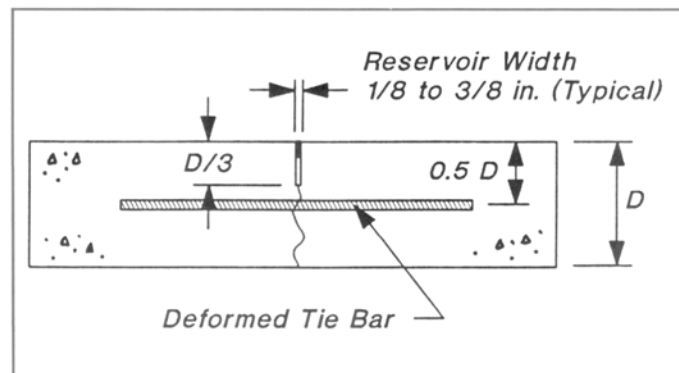
Figure 2-7 Longitudinal contraction joint (4).

Aggregate interlock is a common way to achieve load transfer effectiveness at longitudinal contraction joints. To maintain the interlock effectively, tiebars are often used to hold the longitudinal joints tight. Tiebar spacing varies with the thickness of the pavement and the distance of the joint to the nearest free edge. However, concrete pavement movements rarely develop stresses which approach the strength of the steel tiebars.

It is advised that tiebars should not be placed within 15 inches of transverse joints or they may interfere with joint movement. Tiebars also should be resistant to corrosion. Guidelines for protection from corrosion from AASHTO Specification M284 (9) and

ASTM Specification D3963 (10) recommend that the coating thickness should not exceed 5-12 mils. Thicker coating may cause tiebars to loose gripping ability of the deformations.

Longitudinal Construction Joints

Longitudinal construction joints are used between construction lanes which are paved in separate passes. This includes concrete shoulders and traffic lanes and may be keyed. A keyed joint is formed in the slab edge either by extrusion with a slipform paver of by attaching to the side form a metal or wooden key of the correct shape and dimensions at the proper depth. Tiebars are commonly used to provide load transfer as shown in at the bottom of Figure 2-8.
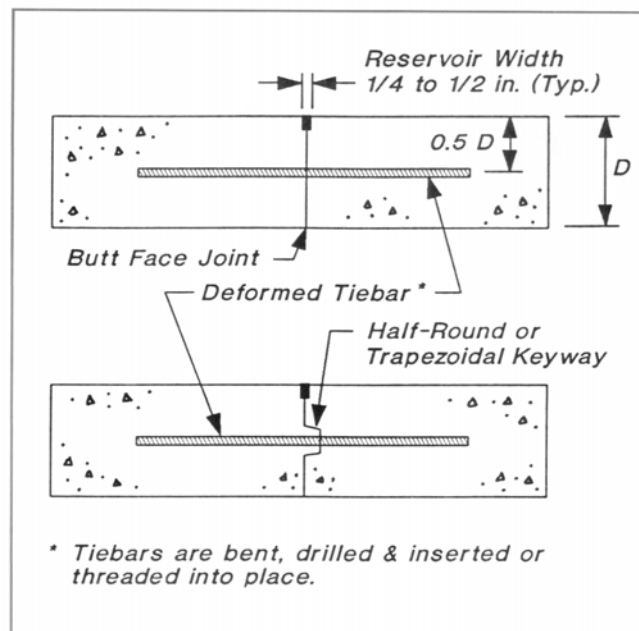
Figure 2-8 Longitudinal construction joint (4).

Typically, the keyway is a half round or trapezoidal shape meeting the dimensions as shown in Figure 2-9. The keyway should be located at mid-depth of the slab to provide maximum strength. It is important that these keyway dimensions are used. Larger keys tend to reduce the strength of the joint and may result in keyway failures. If wooden keyway forms are used, they must be maintained in good condition and well lubricated before each use. When slipform pavers are used, the keyway is formed by the traveling slipform as it advances.

When the keyways are built too large or are above mid-depth of the slab, keys are prone to fail easily in shear and resulted in spalling along the joint, especially when the slab thickness is less than 10 inches. For these reasons, keyways are often eliminated in longitudinal construction joint design.
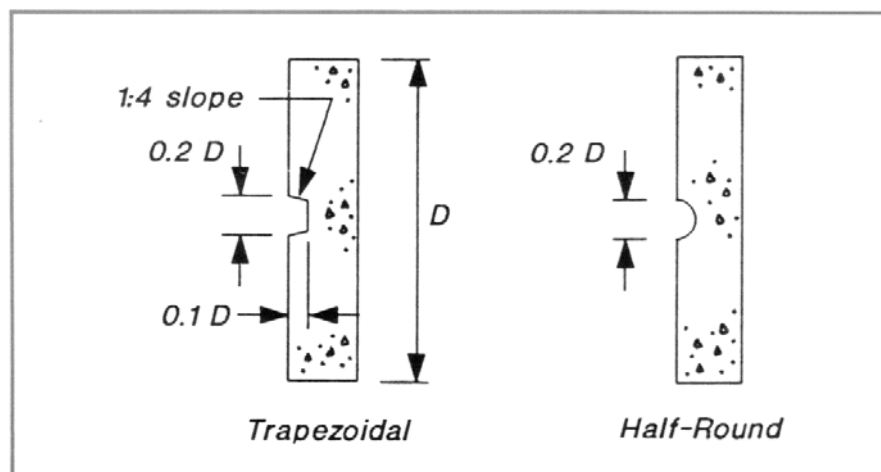
Figure 2-9 Standard dimensions for basic keyway designs (4).

To maintain load transfer effectively, tiebars are usually required regardless of using keyways. Tiebars hold both the side of previous and extended longitudinal joint surface

together. Tiebar requirements for keyed longitudinal construction joints are similar to those for longitudinal contraction joints.

Tiebars are typically all that is required to provide the necessary load transfer. Because traffic load is not constantly crossing these smooth longitudinal joints, dowel bars are not necessary to provide slab edge support. Tiebars that have small diameter such as #4 or #5 are suitable for this situation, but the tiebar spacing should be reduced to 12 to 24 inches to transfer traffic load effectively and reduce slab stresses and deflections.
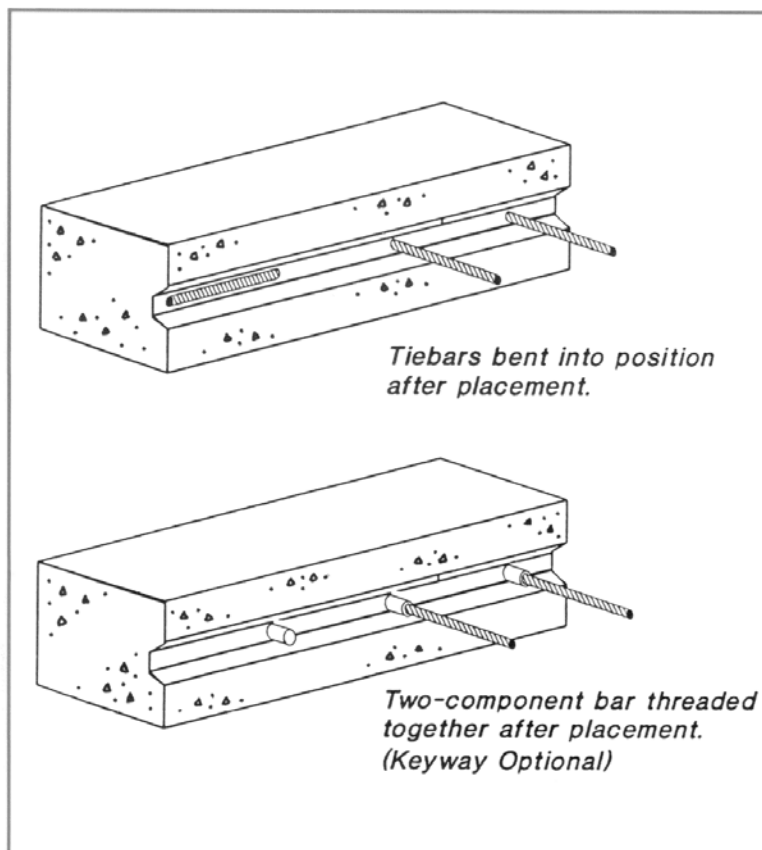
Figure 2-10 Typical placement of tiebars in fresh concrete (1).

There are two basic methods for tiebar installment for longitudinal construction joints as shown in Figure 2-10. One of the common methods is to drill holes along the side of the longitudinal joints. Then, later tiebars are inserted into the holes and fixed with a grout as shown at the bottom of Figure 2-10. Another method is to use right angle bent tiebars. The bent tiebars are inserted into the side of the concrete slab during paving operation as shown at the top of Figure 2-10. The bars are needed to be straightened before constructing adjacent lanes. In this process, however, the straightened point at the tiebar is prone to be corroded after paving, which is often a source of joint widening and should be avoided when possible.

CONCRETE SLAB BEHAVIOR RELATIVE TO CRACK CONTROL

The deflection behavior of a concrete slab due to a temperature differential through its depth is called curling while deflection behavior caused by a moisture differential between the top and bottom surfaces of the slab is called warping. Understanding slab behavior in concrete pavements is essential to understanding stress development and the role of materials in crack development. In addition, slab behavior at early stages, from placement of concrete mix to final setting time, plays an important role in the development of slab cracking. Past research efforts in curling and warping behavior are described to aid in understanding the cracking behavior of concrete.

Curling and Warping Stresses

Stresses due to temperature and moisture gradients within concrete slab can contribute to cracking. These stresses generally occur while concrete is hardening. The exposed top surface undergoes fairly large daily variations in temperature and moisture content. The daily changes in temperature and moisture content are much smaller at and near the bottom of the pavement.

As previously stated, curling is a result of temperature gradients through the depth of the pavement structure. Temperature gradients vary with weather conditions and time of day. Daytime curling arises when the top portion of the slab is at a higher temperature than the bottom. The top of the slab expands more than the bottom portion causing a tendency to curl. The weight of the slab resists the curling action and induces tensile stresses toward the bottom, and compressive stresses toward the top of the slab as shown in Figure 2-11. At night the stress pattern reverses. Tensile stresses are developed toward the top and compressive stresses toward the bottom of the slab.
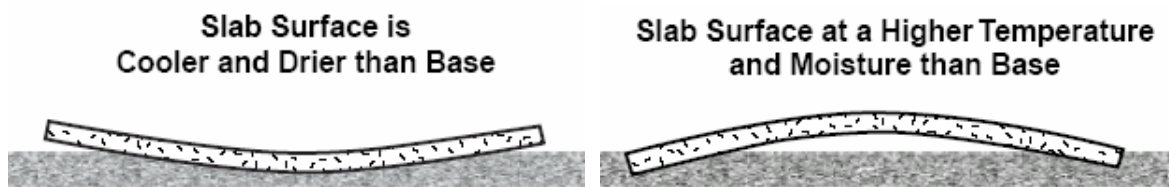
Figure 2-11   Curling and warping action in a concrete slab: (left) upward concave
slab (night time); (right) downward concave slab (daytime).

Moisture warping is a factor which works to counteract daytime curling. Moisture warping results from a moisture differential from the top to the bottom of a slab. The top of a slab is typically drier than the bottom. A decrease in the moisture content causes contraction and an increase in moisture causes expansion. The differential tends to develop compressive stresses at the base of the slab which counteract load and daytime curl developed tensile stresses.

Curling and warping result in a loss of support along the slab edges where the loss of support is greater as the subbase becomes stiffer. Curling and warping also result in restraint stresses within the concrete slab. If the slab was weightless, curling and warping would take place unhindered and no internal stresses would be induced. However, the weight of the slab prevents full curling and warping to take place and as a result restraint stresses are induced within the slab (11).

Evaluating the combined effect of restrained temperature curling and moisture warping is complicated due to their opposing nature. Because of these and other factors, curling stresses computed from formulas which only consider temperature gradients are too high when compared to measured values and pavement performance. Combined curling and warping stresses measured on one research project were only half the values computed on the basis of temperature alone. Figure 2-12 shows the resulting natural crack pattern due to curling and warping behavior. Proper jointing provides a series of joints spaced to control the formation (location & geometry) of these cracks (Figure 2-12(B)) (12).
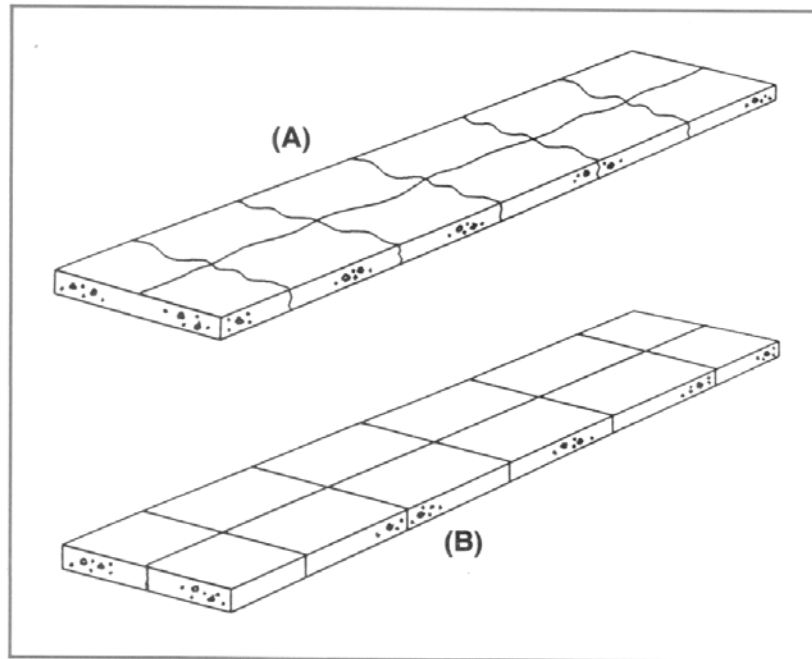
Figure 2-12 (A) Crack pattern in concrete pavements without crack control

(B) Proper joints control location and geometry of cracks (1).

Shrinkage Effects on Crack Control

Shrinkage is a very important characteristic of concrete because it is one of the primary causes of cracking in concrete slabs. Much of the anticipated concrete shrinkage occurs very early in the pavement life. A major source of early shrinkage is from temperature change. The heat of hydration and temperature of pavement normally peak a short time after final set. After peaking, the temperature of concrete declines due to both reduced hydration activity and lower air temperature during the first night of pavement life.

Another factor contributing to initial shrinkage results from the reduction of volume through loss of mix water. Concrete mixes for roadway applications require more mix water than is required to hydrate the cement The extra water helps attain adequate

workability for placing and finishing operations. During consolidation and hardening, most of the excess water bleeds to the surface and evaporates. With the loss of the water the concrete occupies less volume. Subgrade or subbase friction resists the contraction of the pavement from reduced volume and temperature. This resistance produces tensile stresses within the concrete. If not considered, the tensile stresses cause a transverse crack pattern like that shown in Figure 2-13. Spacing of initial cracks varies from about 40 to 150 ft. and is dependent on concrete properties, thickness, subbase friction, and climatic conditions during and after placement.
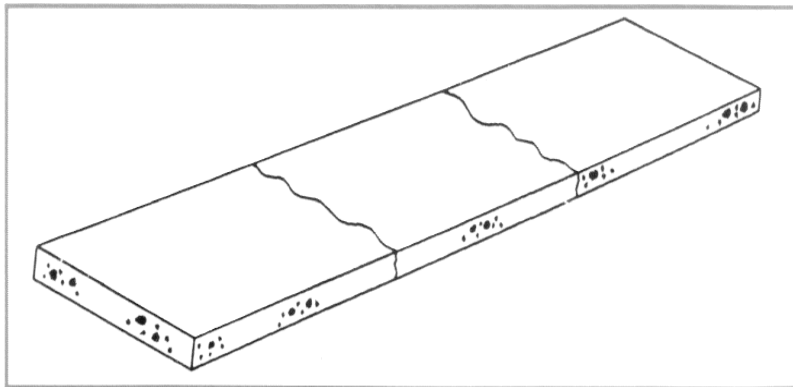
Figure 2-13 Initial cracking in concrete pavement without contraction joints (1).

The occurrence and interval of early cracks are important. Cracking intervals are shorter with stiff stabilized subbases so there is less opening at each individual crack. Crack spacing may be much longer for concrete placed on granular subbases or natural subgrades. With longer initial crack spacing, much greater opening and movement can be anticipated at each crack (13).

Autogenous Shrinkage

If no additional water beyond that added during mixing is provided during hardening, concrete will begin to dry internally, even if no moisture is lost to the surroundings as water is consumed by hydration. However, bulk shrinkage is only observed in concretes with a low w/c ratio and is increased by the addition of reactive pozzolans.

The phenomenon is known as self-desiccation and is manifested as autogenous shrinkage because, as the name implies, it is self produced by the hydration of cement. However when concrete is cured under water, the water taken up by cement during hydration is replaced from outside, and, furthermore the gel particles absorb more water thus producing a net increase in the volume of cement paste and an expansion of the concrete.

Drying Shrinkage

Loss of water from hardening concrete is referred to as drying shrinkage. Concrete exposed to ambient conditions undergoes drying shrinkage where some of it is not reversible. Drying shrinkage is influenced by the ambient humidity, aggregate content, volume to exposed surface ratio, and the water cement ratio of the concrete mix. When concrete that has been allowed to dry out is subjected to a moist environment, it swells. However, the magnitude if this expansion is not sufficient to recover all the initial shrinkage, even after prolonged immersion in water. Concrete subjected to cyclic drying and wetting approaches the same shrinkage level as that caused by completed drying (14).

Plastic Shrinkage

Shrinkage that takes place before concrete has set is known as plastic shrinkage. This occurs as a result of the loss of free water with, or without, significant settlements of solids in the mix. Because evaporation usually accounts for a large proportion of the water losses, plastic shrinkage is most common in slab or pavement construction and is characterized by the appearance of surface cracks, which can extend deeply into the concrete. Crack patterns associated with significant settlement generally coincide with the line of reinforcement. Preventive methods are usually based on methods of reducing water loss.

Plastic shrinkage cracks appear in the surface of fresh concrete soon after it is placed and while it is still plastic. These cracks appear mostly on horizontal surfaces. 1 to 3 feet apart, relatively shallow, and generally do not intersect the perimeter of the slab. Plastic shrinkage cracking is highly likely to occur when high evaporation rates causes the concrete surface to dry out before it has set. Plastic shrinkage cracks are unsightly but rarely impair the strength or durability of concrete floors and pavements.

Plastic shrinkage cracks are caused by a rapid loss of water from the surface of concrete before it has set. The critical condition exists when the rate of evaporation of surface moisture exceeds the rate at which rising bleed water can replace it. Water receding below the concrete surface has formed menisci between the fine particles of cement and aggregate causing a tensile force to develop in the surface layers. If the concrete surface has started to set and has developed sufficient tensile strength to resist the tensile forces, cracks do not form (15).

If the surface dries very rapidly, the concrete may still be plastic, and cracks do not develop at that time; but plastic cracks will surely form as soon as the concrete stiffens a little more. Synthetic fiber reinforcement incorporated in the concrete mixture can help resist the tension when concrete is very weak. Conditions that cause high evaporation rates from the concrete surface, and thereby increase the possibility of plastic shrinkage cracking, include:

• Wind velocity in excess of 5 mph

• Low relative humidity

• High ambient and/or concrete temperatures

Small changes in any one of these factors can significantly change the rate of evaporation. ACI 305 (16) provides a chart to estimate the rate of evaporation and indicates when special precautions might be required. However, the chart isn't infallible because many factors other than rate of evaporation are involved. Concrete mixtures with an inherent reduced rate of bleeding or quantity of bleed water are susceptible to plastic shrinkage cracking even when evaporation rates are low. Factors that reduce the rate or quantity of bleeding include high cementitious materials content, high fines content, reduced water content, entrained air, high concrete temperature, and thinner sections. Concrete containing silica fume requires particular attention to avoid surface drying during placement.

Any factor that delay setting increases the possibility of plastic shrinkage cracking. Delayed setting can result from a combination of one or more of the following: cool

weather, cool subgrades, high water contents, lower cement contents, retarders, some water reducers, and supplementary cementing materials.

Creep Effects on Crack Control

Creep of concrete resulting from the action of a sustained stress is a gradual increase in strain with time. Creep can thus be defined as the increase in strain under a sustained stress and, because this increase can be several times as large as the strain on loading, creep is of considerable importance in crack control. It may be regarded as very slow yielding of a material at stresses, which, in the short term, would result only in elastic deformation. Moisture susceptible materials may exhibit creep. Materials, which, for example, swell when damp, are likely to exhibit creep, and this may be related to the moisture flow of material.

Therefore, more porous materials, such as concrete, are subject to creep. It is commonly stated that creep and drying shrinkage are interrelated phenomena because there are a number of similarities between the two. The strain-time curves are very similar, experimental parameters affect creep in much the same way as shrinkage, the magnitudes of the strains are the same, and they include a considerable amount of irreversibility. Like shrinkage, creep is a paste property, and the aggregate in concrete serves to act as a restraint.

Mechanism of Creep in Tension

The origin of creep may be due to water contained in the cement gel. The exact mechanism has been the subject of much debate; theories include the effect of "viscous shear" in the

cement gel, the movement of adsorbed water in the gel, and micro cracking. However, the effect, in all cases, is a release of stress in the most heavily stressed areas typically associated with larger aggregate particles in the cement paste (17).

Creep in tension, a time-dependent deformation of concrete that is most prevalent at early concrete ages, develops with curling and warping behavior and tends to reduce the level of tensile related restraint stresses. The creep mechanism centers within the material and pore structure of the hydrated product.
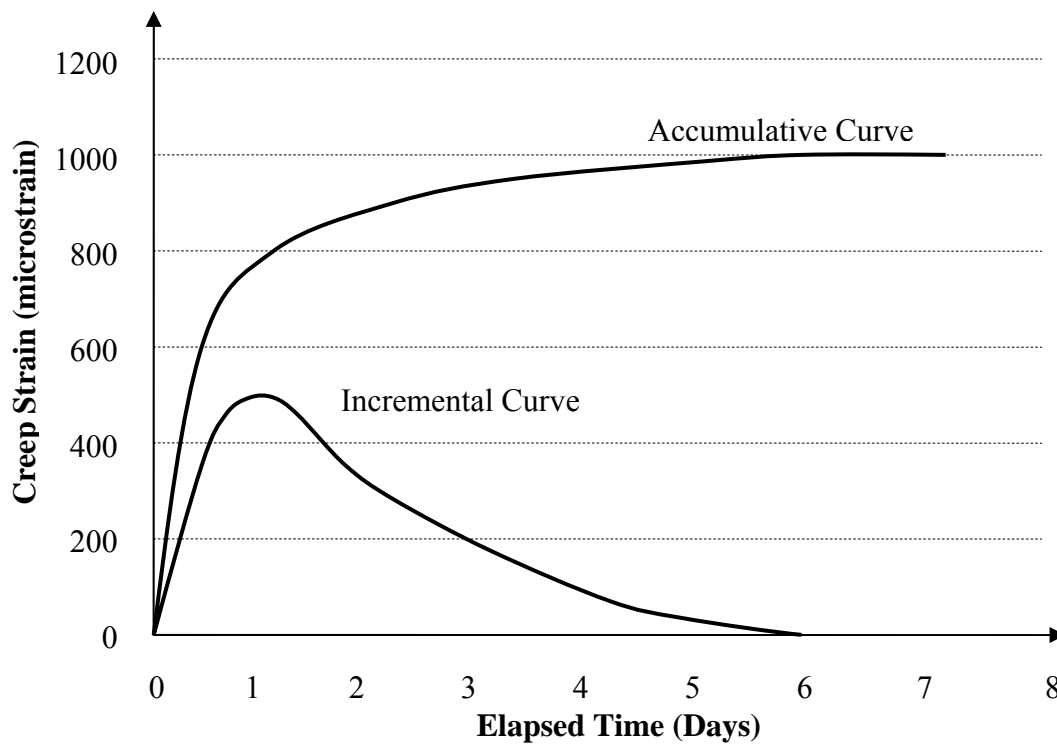
Figure 2-14 Typical creep curve for plain concrete in tension.

Specifically, creep reduces the tensile stress due to the viscous movement within the hydrated cement paste and is closely associated with the loss of moisture and the development of shrinkage. Creep in tension is of considerable interest in estimating cracking potential due to stresses imposed by moisture or thermal changes. Reduction of tensile stresses by tensile creep can minimize cracking in water-retaining structures, where impermeability is important. Although it is difficult to measure accurately because of the low tensile strength of concrete, it does appear in general trends as shown in Figure 2-4 that the initial rate of creep is higher in tension and tensile creep is therefore greater for relatively short durations after concrete placement (18).

Factors Influencing Creep in Tension

Strength of concrete has a considerable influence on creep in tension and within a wide range creep is inversely proportional to the strength of concrete at the time of application of load. From this it follows that creep is closely related to the water-cementitious ratio. Also the modulus of elasticity of aggregate controls the amount of creep that can be realized and concretes made with different aggregates exhibit creep of varying magnitudes.

The influence of concrete's constituent materials, on creep is somewhat complex. The different types of cement influence creep because of the different associated rates of gain in concrete strength. For example, concrete made with rapid hardening portland cement such as a Type III shows less creep than concrete made with ordinary portland cement (19).

Normal concrete aggregates have a restraining effect on concrete creep, and the use of large, high modulus aggregates can be beneficial in this respect. They act as a restraint to

reduce the potential deformations of the paste. Thus, the aggregate content and modulus of elasticity are the most important parameters affecting creep of concrete. Aggregate size, grading and surface textures have little influence. Therefore, creep strain in tension is affected by:

- The ingredients of concrete

- Curing history

- Strength of concrete

- Age of concrete

- A relative magnitude of the applied stress with respect to concrete strength (stress to strength ratio)

In summary, for a given concrete, and stress to strength ratio:

- Creep strain increases as cementitious content increases.

- Creep strain increases as water to cementitious ratio increases.

- Creep strain decreases as relative humidity at loading increases.

- Creep strain decreases as the age of concrete at loading increases.

CRACKING IN CONCRETE SLABS AT SAWCUT NOTCH

Variability in climate conditions and material characteristics during the curing of concrete pavements affects the potential of cracking at any sawcut. Several factors such as material strength parameters, method and quality of curing, slab and subbase stiffness, and concrete shrinkage affect the early-aged crack initiation. Others are relevant to concrete mixture

characteristics and reinforced steel bars properties that affect development of early aged stresses caused by shrinkage and thermally induced contraction.

Mechanism of Cracking in Concrete Pavements

If the concrete slab has a different temperature moisture gradients with depth, curling and warping stresses is occurred along with depth of the slab which makes concrete slab curls upward or downward 3-20 hours after paving is conducted. Once a concrete slab deformed, the slab weight itself should restrain its curling behavior. Therefore, cracks occur at the place where maximum tensile stress is induced regardless of being temperature and moisture related. In case of continuously reinforced concrete pavements, the stresses induced at an early age are a bit more higher than the joint plain concrete pavements because the reinforced steel bars is believed to restrain to concrete slab movement.

Crack Control Factors in Concrete Pavements

The need for a jointing system in concrete pavements is a result of the desire to control transverse and longitudinal cracking. Cracking results from the combined effects of concrete drying shrinkage, temperature and moisture changes, subbase restraint, and certain material characteristics. In order to design a suitable pavement jointing system, the following considerations must be evaluated (20).

Environmental Conditions

Temperature and moisture changes induce movement of the slab, resulting in stress

concentrations, warping, and curling. Thus, daily temperature difference (maximum daily temperature, minimum daily temperature), daily moisture difference, solar radiation, and wind speed should be considered in the potential of a jointing system of succeeding.

Concrete Material Characteristics

Constituent materials affect concrete strength. The materials selected for the concrete determine slab shrinkage. As previously stated the amount and type of cement used in concrete have their great effect upon the cracking potential. In addition, inferior materials have a detrimental affect on controlling early age cracking.

Subbase Type

The support values and interface friction characteristics of different subbase types affect movement and support of the slabs.

Slab Thickness

Pavement thickness affects curling stresses. If slab thickness increases, it results in decreasing curling stresses.

Water/Cement Ratio

Its increase tends to increase shrinkage and, at the same time, to reduce the strength of concrete by determining the amount of evaporable water in the cement paste and rate at which water can move towards the surface of a concrete slab.

Amount and Type of Aggregate

If large amount of aggregate are used in concrete mix it permits the use of a leaner mix, and thus results in low shrinkage and reduced tensile stresses at an early age. Aggregate type is also one of crack control factors by influencing a concrete thermal coefficient and bond strength.

CHAPTER III

SYNTHESIS AND DEVELOPMENT

DEVELOPMENT OF C^{4}M PROGRAM

The focus of this study is on the control of random cracking of concrete paving to sawcut notch locations in the early stages of construction. For this purpose, the crack control and management in the curing concrete (C^{4}M) program was developed to present a rational analysis of the tensile strength and stress occurring in newly constructed jointed concrete pavements due to variations in depth of moisture and temperature (so called warping and curling stresses) and restraint caused by reinforcing steel. Furthermore, it presents a probabilistic approach to sawcut timing and depth for newly constructed concrete pavements to account for the inherent variabilities associated with sawcutting and similar crack control operations.

Concept of C^{4}M Program

The crack control and management in the curing concrete (C^{4}M) program development is based on a rational analysis of tensile strength and stress at the tip of sawcut notch as shown in Figure 3-1. Figure 3-1 shows that probability of cracking has 50% when the tensile stress is equal to tensile strength and higher than 50% when the tensile stress is greater than tensile strength. Therefore, it is shown that the proper sawcut location and

depth design suitable to avoiding random cracking on concrete surface can be accomplished using the C^4M program on this basis.
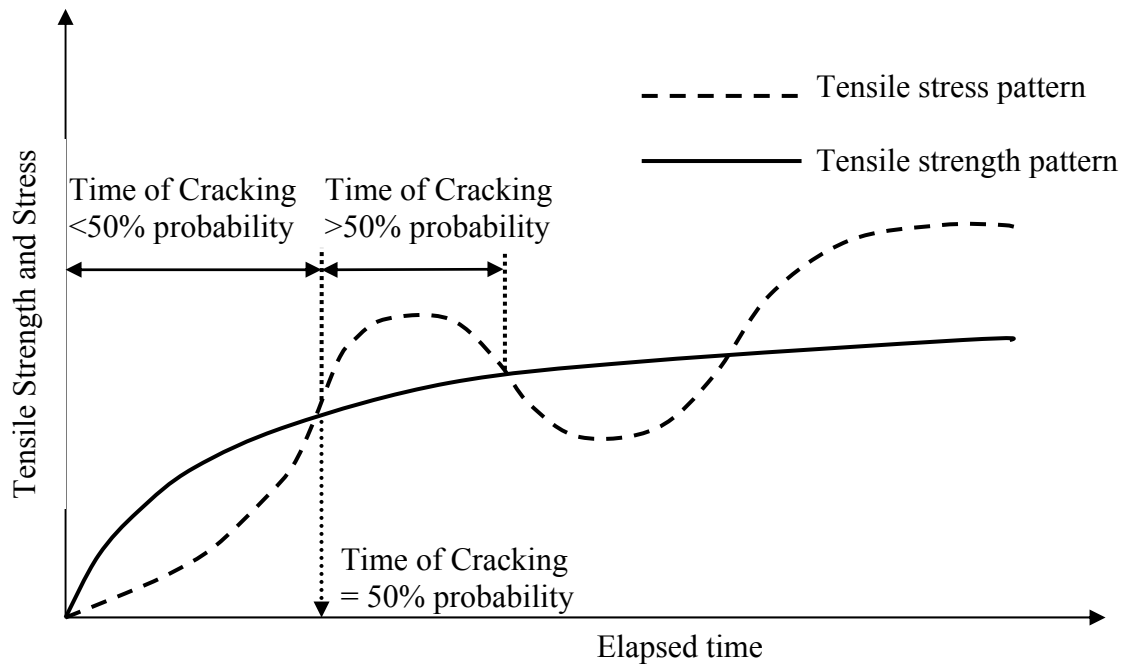
Figure 3-1 Concept of C^4M program.

C^4M Program Components

The C^4M program has been developed to predict tensile stress and strength at the tip of the sawcut notch under specified environmental conditions. A system for analyzing tensile stress and strength at a concrete slab at an early age is introduced along with some important parameters that are used as inputs for the C^4M program and included in the C^4M program outputs.

C⁴M Program Inputs

There are several significant factors to be considered for controlling early aged cracking. Factors affecting the probability of crack initiation are material strength parameters, method and quality of curing, slab/subbase stiffness, the amount and depth of steel reinforcement, friction between the slab and the subbase, slab thickness, amount and type of aggregate, and variability in climatic conditions during the hardening process. Table 3-1 listed significant input data for C⁴M program.

Table 3-1 Input data for C⁴M program

	Input Data	Unit
Climatic Data	Ambient temperature	°F
	Ambient relative humidity	%
	Solar radiation	kW/m^2
	Wind speed	mile/hour
Mix Design	Water cementitious material ratio, w/cm	
	Cement type (ASTM type I,II,III,IV, or V)	
	Fly ash type (class F, C, or N)	
	Fly ash replacement ratio	
	Cement factor	
Material Properties	Coefficient of thermal expansion, CoTE	$\times 10^{-6}$/°F
	Total heat developed, Hu	J/g
	Activation energy, E (cementitious)	J/mol
	Fracture toughness at 28 days, K_{If}	psi(inch)$^{1/2}$
	Process zone length at 28 days, c_f	inch
	Set temperature gradient	°F/inch
	Compressive strength at 28 days, f'_c	psi
	Modulus of subgrade reaction, k-value	pci

Table 3-1 Continued

	Input data	Unit
Construction & Design	Time of placement (0~24)	
	Slab thickness, *h*	inch
	Sawcut notch depth	inch
	Sawcut location	feet
	Curing type (mat, plastic sheet, curing compound, or no curing)	

Strength and Stress Patterns at Bottom of Sawcut

Initial 36 hours tensile strengths at the tip of the sawcut notch can be predicted using the tensile strength development model by Bazant and Kazemi (19):

$$f'_t = c_n \frac{K_{If}}{\sqrt{g'(\alpha)c_f + g(\alpha)d}} \tag{3.1}$$

where:

f_t' = Tensile strength of the concrete

K_{If} = Fracture toughness ($FL^{-2}L^{1/2}$),

c_n = A constant based on specimen geometry (=1.5(s/d)),

s = Length of span, (L)

d = Slab thickness, (L)

a = Sawcut depth, (L)

α = Initial crack ratio (=a/d),

c_f = length of the fracture process zone, (L)

$g(\alpha)$ = $\pi\alpha c_n^2 F^2(\alpha)$,

$g'(\alpha)$ = $\pi F^2(\alpha) + 2\pi\alpha c^2 nF(\alpha)F'(\alpha)$,

$F(\alpha)$ = $1.122 - 1.4\alpha + 7.33\alpha^2 - 13.08\alpha^3 + 14\alpha^4$, and

$F'(\alpha)$ = $-1.4 + 14.66\alpha - 39.24\alpha^2 + 56\ \alpha^3$.

Tensile strength is compared to the tensile stress occurring at the tip of sawcut notch. When the tensile stress of concrete at the tip of the sawcut notch is larger than the tensile strength, it is assumed that a crack propagates from the tip of a sawcut notch to bottom of the slab. The tensile stress at the tip of sawcut notch with time can calculated following equation:

$$f_t = (\sigma_{curling\ +\ warping})\left(1 - \frac{2a}{h}\right) + L\left(\frac{f}{2}\right) + L\left(\frac{U_m \cdot P_b}{C_{1ki} \cdot d_b}\right) \tag{3.2}$$

where:

h = Concrete slab thickness, (L)

a = Depth of sawcut notch, (L)

f = Subgrade friction coefficient

L = Mean crack spacing in longitudinal direction, (L). ($\approx 4.44l$)

U_{mi} = Peak bond stress for age increment i, (FL^{-2}) $= 0.0020k_{1i}$

k_{1i} = $(0.1172 f'_{ci})*1000$

P_b =   Percent of steel, in fraction

d_b =   Reinforcing steel bar diameter, (L)

C_1 =   First bond stress coefficient

$$\left[C_1 = 0.577 - 9.499e^{-9}\frac{\ln \varepsilon_{tot-\varsigma i}}{(\varepsilon_{tot-\varsigma i})^2} + 0.00502L(\ln L) \right]$$

L_k =   Joint spacing, (L)

$\varepsilon_{tot\varsigma i}$ =   Total strain at the depth of the steel for the time increment i
             (typical range = 150 to 600 micro-strains)

In accordance with Equation (3.2), the term $f_i = (\sigma_{curling+warping})\left(1-\frac{2a}{h}\right)$ represents the

tensile stress due to curling and warping behavior, the term $\overline{L}\left(\frac{f}{2}\right)$ represents the tensile

stress due to friction between subgrade and concrete slab, and the term $\overline{L}\left(\frac{U_m \cdot P_b}{C_{1ki} \cdot d_b}\right)$, if

reinforcing steel is used, represents the tensile stress induced from reinforcing steel.

Equations equation (3.1) & (3.2) will be subsequently discussed in detail.

Figure 3-2 illustrates the pattern of strength and stress due to all the types of restraints

involved including warping and curling, subgrade friction, and reinforcing steel using

equation (3.1) and equation (3.2) respectively on an hourly basis for the first 36 hours after

placement concrete.
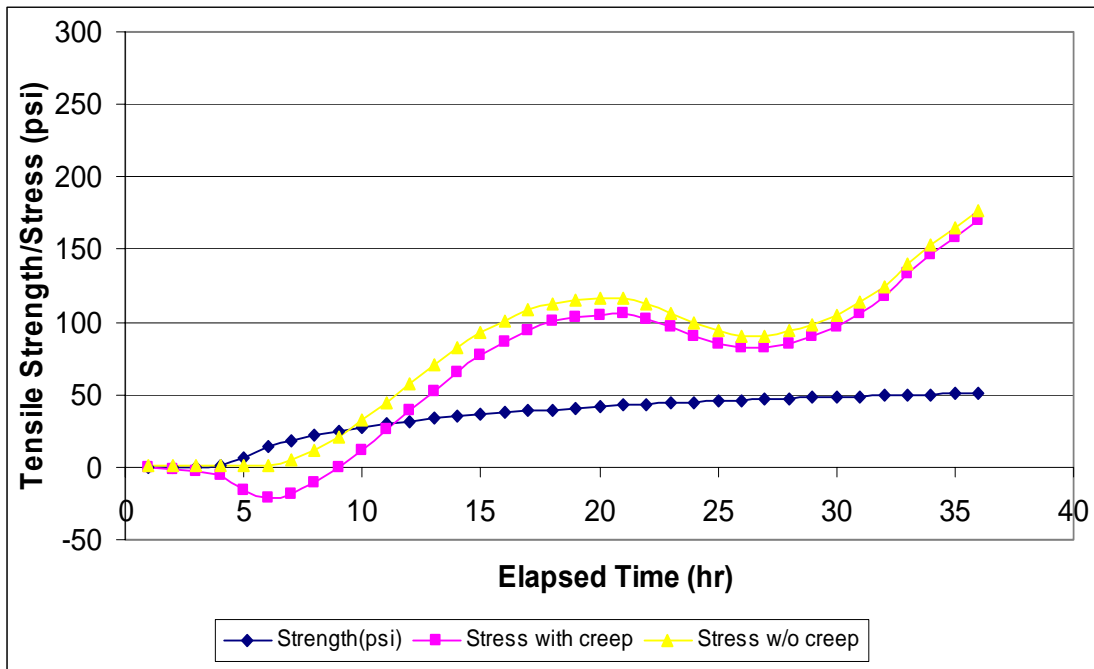
Figure 3-2 Strength and stress pattern at the tip of sawcut notch with time.

Stress Pattern at Surface

The stress of random cracking is only based on the amount of shrinkage in the concrete at the pavement surface due to the loss of moisture. The random cracking is determined from applying a shrinkage strain to the surface of the slab and calculating the tensile stress. The prediction of cracking at the sawcut notch was based on a combination of shrinkage and thermally induced strains.

$$\sigma_{surface} = \left[\left(0.98 - RH^3\right)\varepsilon_\infty - \varepsilon_{crp}(t)\right]E(t) \tag{3.3}$$

where:

$\varepsilon_{crp}(t) =$ Creep strain as a function of time, (creep is varied from 25 to 100 micro

strains over the 30 hour period)

In the same manner as the analysis of cracking at the tip of sawcut notch, the analysis of random cracking can be calculated by comparing tensile strength, equation (3.1) with tensile stress at surface, equation (3.3). When the tensile stress at maximum stress occurring location is larger than the tensile strength at the same point, it is assumed that random crack propagates from a surface to bottom of the slab with greater than 50% probability. The maximum random cracking location is calculated at approximate intervals of $4.44l$. The position of maximum random cracking may vary for early aged concrete since l changes during the period of time. It will be subsequently explained on page 66.

Probabilistic Approach for Cracking

Several factors, which contribute to the variability of strength and stress, should be considered. The effects of factors on the variation above and below the mean of each of these parameters were assumed to be normally distributed. Based upon this distribution, the probability that the difference between the stress and the strength of the concrete at the tip of the sawcut notch is greater than zero is determined as a function of time from zero to 36 hours after placement of the concrete as the probability that a crack will form the tip of the notch as shown in Figure 3-3.
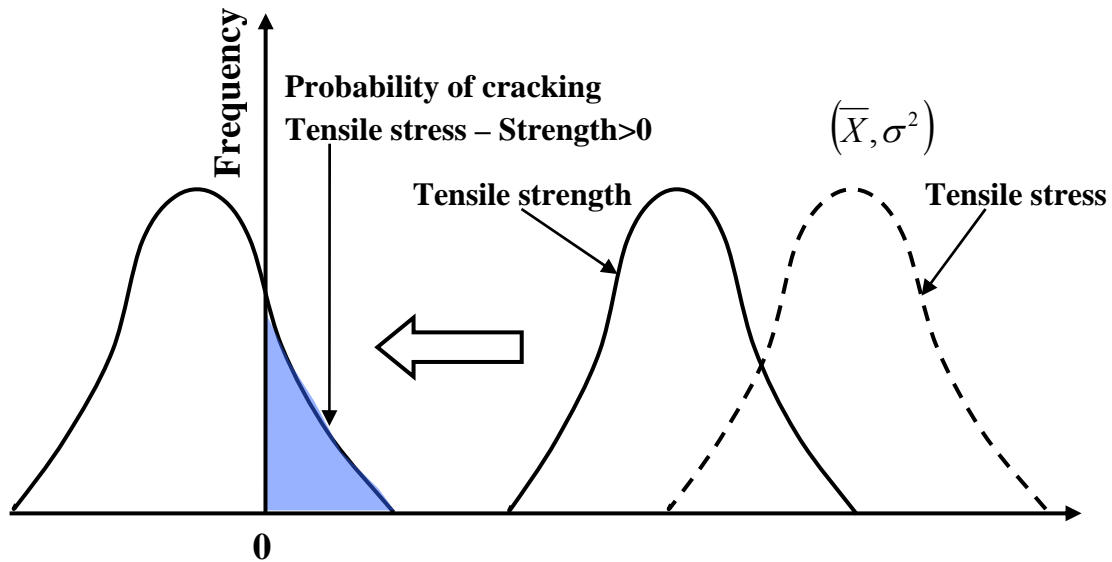
Figure 3-3 Probabilistic approach for controlling cracks.

In order to calculate this difference, both the variance of the distribution of stress and the strength of the concrete at the tip of the sawcut should be defined. The variances were developed from the expressions of stress and strength previously noted and the first order, second moment method (21):

$$\sigma^2(Y) = \sum \left[\frac{\partial Y}{\partial X}\right]^2 Var(X_i) + \sum \sum \frac{\partial Y}{\partial X} Var(Y) \frac{\partial Y}{\partial X} Var(X) \rho$$

where:

Y = stress or strength

X = variance factor (listed in Table 3-1.)

ρ = correlation factor

Examples of the probability of random cracking at surface and controlled cracking at the tip of sawcut notch as a function of time are shown in Figure 3-4 using probabilistic method as mentioned previously. When the tensile stress of concrete is equivalent of the tensile strength at the tip of sawcut notch, a 50% probability of a crack occurring at the sawcut notch exists.

Table 3-2 Stress variance factors

Type	Factors	COV(%)
Stress	Young's Modulus	15
	Slab thickness	20
	k-value	20
	CoTE	5
	Temperature difference	5
	RH difference	5
	Ultimate shrinkage	15
Strength	K_{If}	10
	c_f	10
	Sawcut depth to thickness Ratio(α)	10
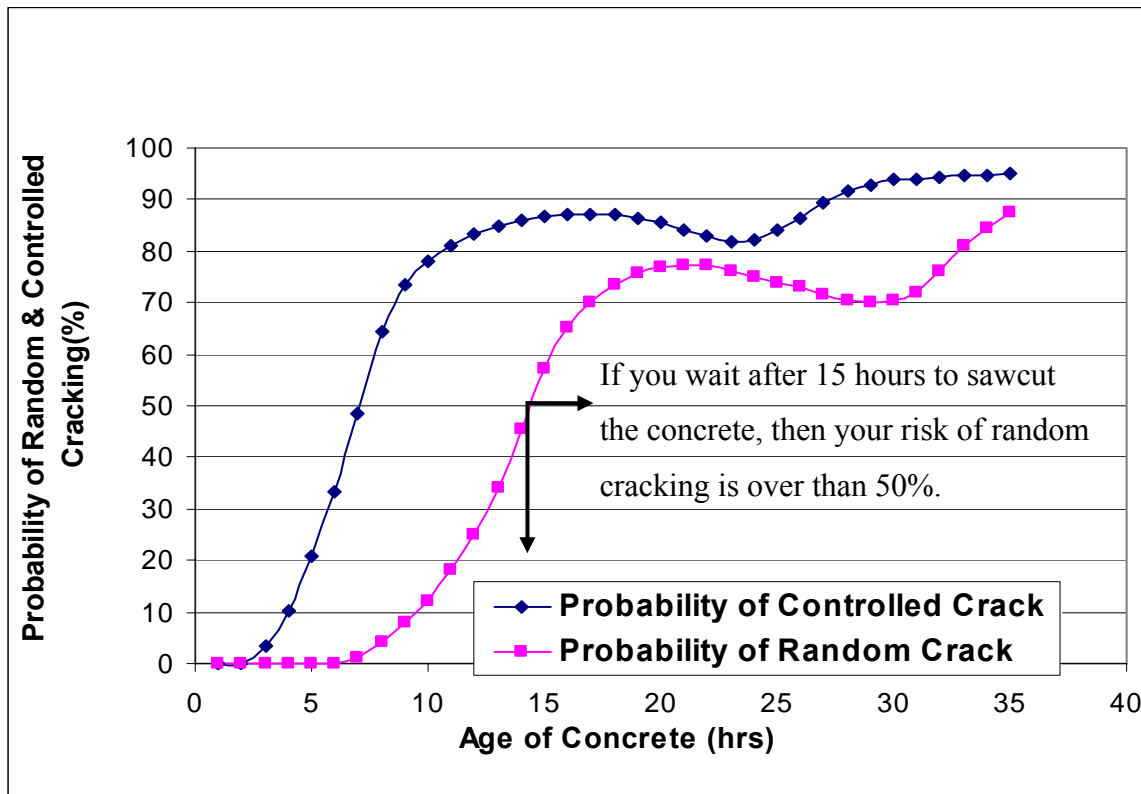
Figure 3-4 Probability of random and controlled cracking at the tip of sawcut notch.

By subtracting the probability of random crack from the probability of controlled crack at the tip of the sawcut notch, probability of crack control can be obtained as shown in Figure 3-5. An indicator of the best time to exercise crack control that can be defined as window of sawcutting is shown in Figure 3-5 by having at least greater than 10% of probability of crack control. If the difference or probability of crack control is high, it's possible to control cracking with good reliability. A low value indicates cracking can be controlled by sawcutting but with a lower degree of reliability. And a negative value means there's no possibility to control cracking by sawcutting and that it is too late to sawcut or not deep enough.
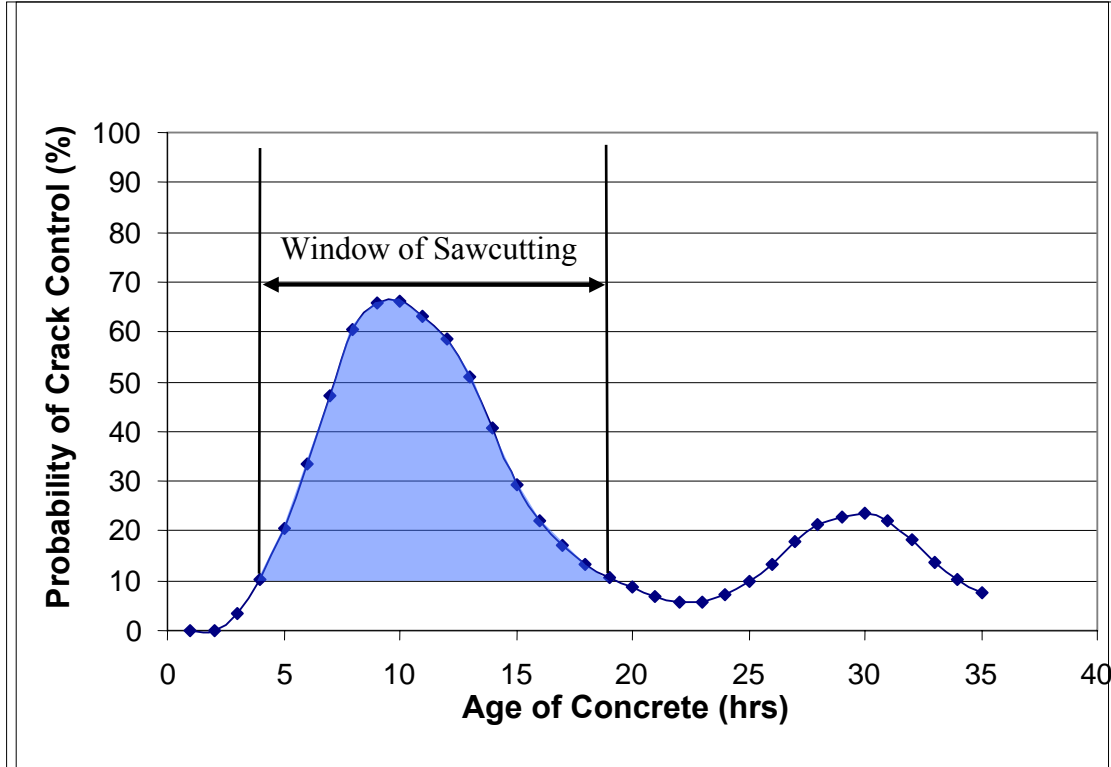
Figure 3-5 Probability of crack control with time.

Using the above procedure, the crack control and management in the curing concrete (C^4M) program can be used to calculate the optimum sawcut timing in concrete pavement construction and reduce risk of random cracking. The optimum sawcut timing and depth that creates maximum probability of crack control can be calculated with confidence using this approach. Furthermore, using the C^4M program the proper sawcut joint layout and design to avoid random cracking can be determined. The flow chart for C^4M program is shown in Figure 3-6.
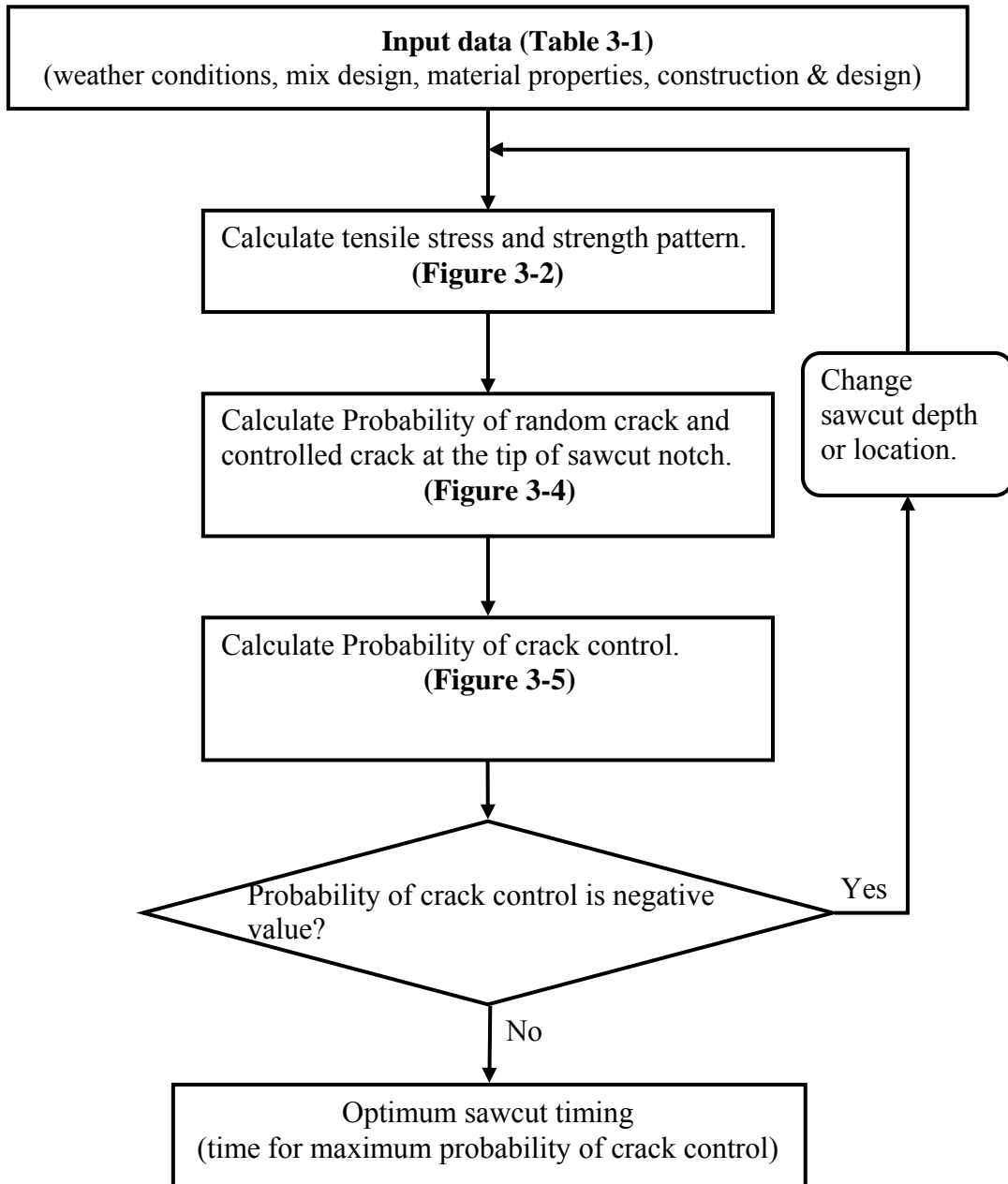
Figure 3-6 Flow chart for C^{4}M program algorithms.

Determination of C^{4}M Program Inputs

As mentioned previously, there are several significant inputs to run the C^{4}M program. Mix design factors such as cement type, amount and type of coarse aggregate, w/cm, cement factor, and fly ash replacement can be input directly. Some of them such as material properties (fracture parameters, activation energy, and coefficient of thermal expansion) are determined by laboratory tests. It is subsequently explained. Construction design factors are selected by the user.

Determination of Fracture Parameters

Fracture toughness (K_{If}) and the length of the fracture process zone (c_f - a factor related to the brittleness of the concrete) play an important role for predicting tensile strength with time. Concrete brittleness is descriptive of a material's resistance to crack growth or the rate at which a crack may grow and, at an early age, is very sensitive to these fracture parameters in a concrete mixture. To determine the fracture parameters (K_{If} and c_f ; it will be elaborated later on page 67), tensile strength test can be conducted at several different days typically 1, 3, 7, and 28 days according to modified ASTM C 496 procedure. These parameters of concrete can be used to determine the tensile cracking strength over time based on the use of fracture mechanics.

Cylindrical specimens are commonly used since they have the advantage of being easily cast or cored from concrete pavements. The split tension of concrete cylinders, also known as the Brazilian disk test, is a standardized ASTM 496 test method (ASTM 1995) typically used to obtain concrete tensile strength. In order to evaluate the fracture parameter,

modified split tensile specimens were developed as shown in Figure 3-7 (b), (c).

The hole drilled at the center of the specimen in Figure 3-7 (c) alters the specimen geometry and dramatically changes the ratio $g(\alpha)/g'(\alpha)$ (Tang et al. 1996). Cylinders without a hole (only with a notch) and cylinders with a hole are called notched and holed cylinders, respectively. Sawcutting of cored specimens or coated inserts in cast specimens were used to form the notch of both notched and holed cylinders. In the split tensile specimens shown in Figure 3-7 (b), (c), the notch length is denoted as $2a$ because of the symmetry of the specimen. Therefore, $\alpha = 2a/d = a/R$. where d is the diameter and R is the radius of the cylinder.
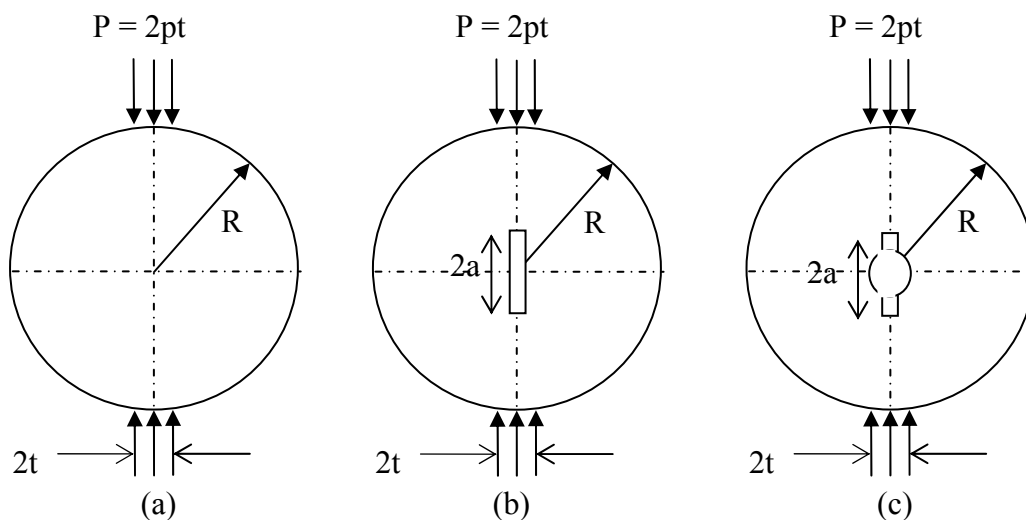
Figure 3-7 Split tensile test specimens for modified ASTM C 496.

In Figure 3-8, t/R is 0.16, and r/R for the holed cylinder is 0.125 (t is the width of the distributed load and r is the radius of the hole). The geometry factors, $F(\alpha)$ for the notched and holed cylinders are as follows (Tang et al. 1996)

Notched : $\quad F(\alpha) = 0.964 - 0.026\alpha + 1.472\alpha^2 - 0.250\alpha^3$

Holed : $\quad F(\alpha) = 2.849 - 10.451\alpha + 22.938\alpha^2 - 14.940\alpha^3$

Along with the notched and the holed cylinders, the proposed method includes a notchless specimen ($\alpha_0 = 0$). A combination of notched and notchless specimens increases even more the range of $X = g(\alpha_0)d/g'(\alpha_0)$ resulting in a very effective one-size version of the size effect method. Although results incorporating notchless specimens have been previously reported for bending beam and eccentric compression tests, this study presents original results utilizing split tensile cylinders (22).

Correlation of Fracture Parameters with Time and Compressive Strength

From the modified ASTM C 496 tests (split tensile test) and compressive strength tests on concrete using river gravel as the coarse aggregate, Tang and Zollinger developed the correlation curve between stress intensity factors and compressive strengths in 1996 (23). According to the previous research, the K_{If} increases with the age ranging from 12 hours to 28 days following an equation as:

$$\left[\frac{K_{If}}{K_{If}{}^{28}} \right] = \sqrt[4]{\frac{Age}{28}} \tag{3.4}$$

where, $K_{If}{}^{28}$ is the K_{If} value at the 28-day age. This curve does not fit the data for the first 12 hours after placement, but shows the trend of increase in K_{If} with the age of concrete. By assuming a linear relationship, the following equation is obtained for change in K_{If} during the first day:

$$\frac{K_{If}}{K_{If}{}^1} = 1.333\left[\frac{Age}{1}\right] - 0.333 \qquad (3.5)$$

where, $K_{If}{}^1$ is the K_{If} value at the one-day age. According to this equation, K_{If} remains zero for a couple of hours after specimen casting. This may be reasonable since the concrete needs some time to take on a set. Therefore, K_{If} at any point of time can be calculated using equation (3.4) and (3.5). Also, compressive strength cannot be measured before concrete has taken on a set. By comparing the compressive strength to stress intensity factor with time, more accurate correlation within the first day can be obtained:

$$\frac{K_{If}}{K_{If}{}^1} = 0.818 \times 10^{-4}\, fc' + 0.244 \qquad (3.6)$$

where, f_c' is compressive strength in unit of psi.

Analysis of Tensile Stresses in Concrete Slab

The analysis of curling and warping behavior previously elaborated that is included in the C⁴M program is subsequently explained. The analysis of stress in the slab includes not only

curling and warping behavior but also the friction between subgrade and concrete slab and restraint caused by reinforced steel if it was used.

Curling Stress

Tensile stresses and thermal cracking in a concrete pavement result from temperature and shrinkage effects during the early stages of hydration while the concrete is developing an increasing stiffness. Due to exposure to ambient conditions, a concrete pavement may cool to a minimum temperature after cycling through a maximum temperature such that tensile stresses can be induced in the concrete slab. The tensile stress distribution through the pavement thickness can be assumed to be linear for the sake of simplicity (24). Stress development may become significant very soon after placement, perhaps even before the concrete has attained a certain degree of stiffness. Crack development in concrete pavement has been noted to be sensitive to diurnal temperature effects. The tendency to curl is restrained by concrete slab weight in which the resulting level of stress development is a function of the stiffness of the subbase layer as reflected in the radius of relative stiffness (*l*). When the slab curls in an upward configuration, tensile stresses are induced in the lower part. Analysis of stress induced by a linear temperature gradient in rigid pavements was developed by Westergaard and others (25).

The Westergaard solution for concrete slab stresses under temperature gradients will only be briefly elaborated here to include an approach for concrete slab stresses caused by moisture gradients. Westergaard presented solutions which considered curling stresses in a slab of infinite and semi-infinite dimensions based on the following governing equations:

$$l^4 \frac{d^4 w}{dy^4} + kw = 0 \tag{3.7}$$

where:

$l \quad = \quad \sqrt[4]{\dfrac{E \times h^3}{12(1 - v^2)k}}$ is called the radius of relative stiffness,

$E \quad = \quad$ Elastic modulus of concrete, (FL^{-2})

$v \quad = \quad$ Poisson's ratio of concrete (=0.15),

$k \quad = \quad$ Modulus of subgrade reaction (k-value), (FL^{-3})

$h \quad = \quad$ Slab thickness, (L)

$w \quad = \quad$ Slab deflection, (L)

Equation (3.7) encompasses a spring model that was proposed for to represent the reaction of the supporting layer in terms of a spring modulus known as the *k*-value. Although the slab weight restrains the curling, the weight is not included in the equation. However, the displacement (*w*) caused by curling can be considered only part of the slab displacement.

There are two boundary conditions that Westergaard announced to solve equation (3.7), which are described as Westergaard's stress solution for an infinitely long slab of a finite width and for a semi-infinite slab. When the pavement slab is considered to be of infinite extent with respect to the length of the slab, the tendency to curl in longitudinal direction is fully restrained or $w \equiv 0$. With a positive Δt, the maximum tensile stress is at the top surface of the slab in longitudinal direction, whose value is:

$$\sigma_0 = \frac{E\alpha\Delta t}{2(1-\nu)}$$

(3.8)

Tensile stress pattern at an early age in concrete slab is shown in Figure 3-8. For a slab of finite dimensions, Bradbury (1938) suggested an approximate formula to estimate the maximum stress, where two coefficients were given based on the Westergaard analysis. Bradbury developed a chart to determine the correction factors that were applied to the Westergaard equation to determine the total stress in the slab. The Bradbury coefficient depends on radius relative stiffness of the slab, length of the slab, modulus of elasticity of concrete, thickness of the slab, Poisson ratio of concrete, and modulus of subgrade reaction as shown in Figure 3-9.

Base
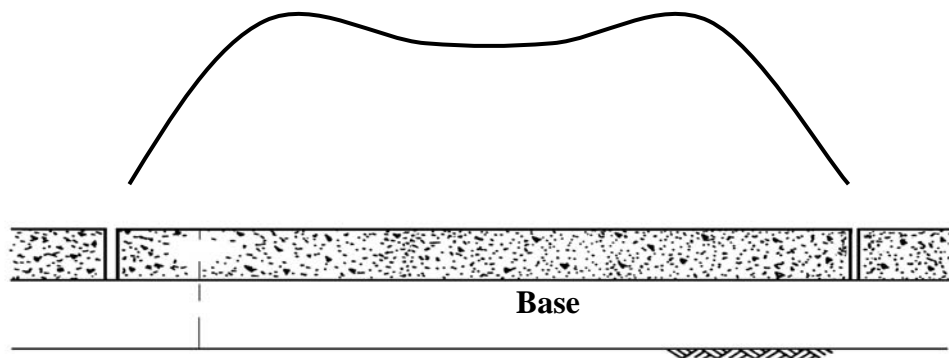
Figure 3-8 Tensile stress pattern at an early age in slabs.

When a slab with a finite length L_x and a finite width L_y on a spring model is curled in a concave configuration as subjected to a negative temperature gradient, stress distributions can be found analytically. For estimating the maximum σ_y in a finite slab, Bradbury proposed an approximate fomula as follows:

$$\sigma = \frac{E\alpha\Delta t}{2}\left(\frac{C_1 + \nu C_2}{1-\nu^2}\right) = \frac{E\varepsilon^t}{2}\left(\frac{C_1 + \nu C_2}{1-\nu^2}\right) \tag{3.9}$$

where:

α = Thermal coefficient of expansion (/°F)

Δt = Temperature change or drop

ε^t = Temperature strain only, $(\alpha \cdot \Delta t)$

C = Bradbury Coefficient

$$= 1 - \left(\frac{2\cos\lambda\cosh\lambda}{\sin 2\lambda + \sinh 2\lambda}\right)\left[\begin{array}{l}(\tan\lambda + \tanh\lambda)\cos\dfrac{y}{l\sqrt{2}}\cosh\dfrac{y}{l\sqrt{2}} \\ + (\tan\lambda - \tanh\lambda)\sin\dfrac{y}{l\sqrt{2}}\sinh\dfrac{y}{l\sqrt{2}}\end{array}\right]$$

The coefficients C_1 and C_2 for the appropriate slab dimensions were given based on Westergaard's stress solution for an infinitely long slab of a finite width in terms of the ratio of the maximum σ_y/σ_0. The coefficients are shown in Figure 3-9 and are used in equation (3.9). If $C_1 = C_2 = C$, then

$$\sigma = \frac{CE\alpha\Delta t}{2(1-\nu)} \tag{3.10}$$
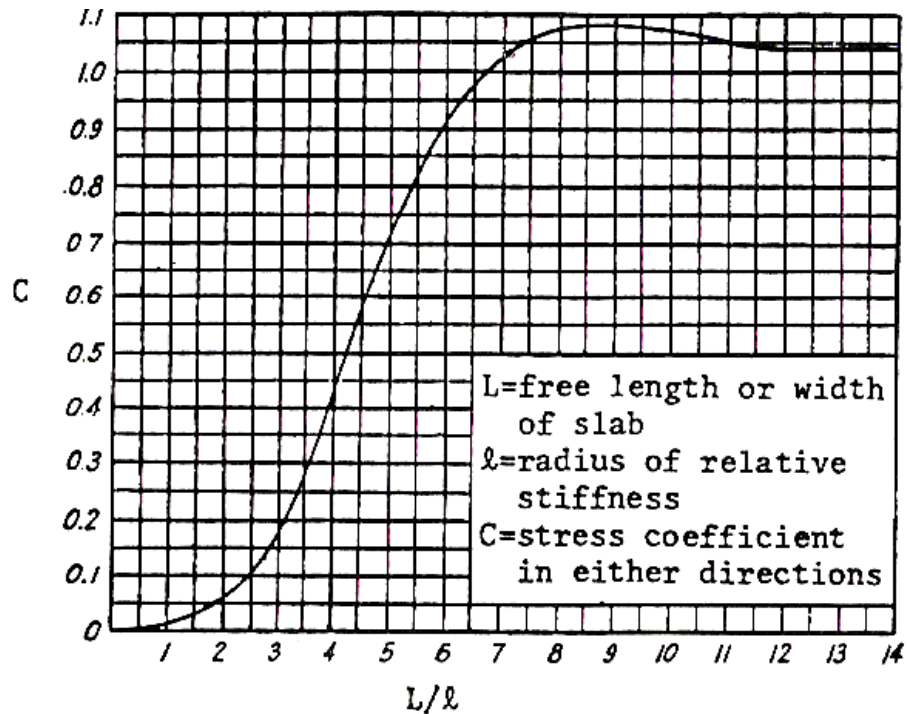
Figure 3-9 Coefficients for Maximum stress in finite pavement slab curled up due to temperature gradient (after Bradbury) (26).

The coefficient C_1 is the desired direction, whereas C_2 is for the direction perpendicular to this direction. Coefficient C increases as the ratio L/l increases, having a value of C = 1.0 for L = 6.7l, reaching a maximum value of 1.084 for L=8.88l.

In summary, the magnitude of the restraint stress is affected by slab dimensions and support stiffness. When the coefficient C has a maximum value of 1.084, and poisson's ratio is 0.15, the maximum tensile stress due to curling is 0.638 $E\varepsilon^{total}$ according to equation (3.10). It implies that the maximum curling stress cannot exceed 63.8% of total possible restrained tensile stress. Any additional contributors to the tensile stress in the slab such as those induced by reinforced steel bar and friction between subgrade and slab may add to the balance of stresses, but the total tensile stress should not exceed $E\varepsilon^{total}$.

Warping Stress

Similarly, the interaction of drying shrinkage (ε^{sh}) of concrete and pavement restraint can induce warping stress in a concrete slab. According to Bazant and Wu, the shrinkage of concrete can be described by the following function of humidity:

$$\varepsilon^{sh} = \varepsilon^{sh\,\infty}(1\text{-}RH^3) \tag{3.11}$$

where, RH is relative humidity and $\varepsilon^{sh\,\infty}$ is a material parameter, which is the ultimate concrete shrinkage at the reference relative humidity of 50%. Ultimate drying shrinkage ($\varepsilon^{sh\,\infty}$) is defined as the shrinkage strain long after the end of initial curing. To calculate the equivalent total strain difference, equation (3.11), can be used and the following equation:

$$\varepsilon^{sh\,\infty} = \text{ultimate drying shrinkage} = 1330 - 970y$$

$$y = (390z^{-4}+1)^{-1}$$

$$z = 0.381\sqrt{f'_{c28}}\left[1.25\sqrt{\frac{a}{cm}} + 0.5\left(\frac{g}{s}\right)^2\right]\left(\frac{1+s/c}{w/cm}\right)^{1/3} - 12$$

where:

a/cm = aggregate-cementitious material ratio,

g/s = gravel-sand ratio,

s/c = sand-cement ratio,

w/cm = water-cementitious material ratio,

f'_{c28} = compressive strength at 28days in ksi

It is assumed that the drying shrinkage stress distributes linearly through the thickness of the slab. The solutions provided by Bradbury can be implemented by only replacing ε^t in all the equation (e.g. Eq (3.9)) with ε^{sh}.

Frictional Stress

The concrete slab tends to move from both ends toward the center, but the subgrade prevents it from moving; thus, frictional stresses are developed between the slab and the subgrade. Maximum frictional stresses (σ_f) at the mid-slab area of a concrete pavement may be calculated from the traditional expressions elaborated by Yoder and Witzak (27). If the unit weight of concrete is taken as lbs/CF then:

$$\sigma_f = \frac{L}{2} f \tag{3.12}$$

where, f is the coefficient of subgrade friction and L is the length of the slab. Equation (3.12) suggests that σ_f will increase directly with L (for a given value of f); however, a practical limit does exist for frictional stress in the same manners as curling and warping stresses when it equals the maximum frictional stress (σ_m) that results from complete restraint at the bottom of the slab of the climatic induced strains:

$$\sigma_m = E(\varepsilon^t + \varepsilon^{sh}) = E \, \varepsilon^{total}$$

According to equation (3.12), as the friction coefficient increases, σ_f approaches the value of σ_m. Friction coefficients depend upon the type of subgrade.

Stress Due to Reinforcing Steel

In case of reinforced concrete pavement, the reinforcing steel is also a factor inducing tensile stress in the concrete slab. The following equation can be used to calculate the tensile stress caused by reinforced steel bars:

$$\bar{L}\left(\frac{U_m \cdot P_b}{C_{1ki} \cdot d_b}\right) \tag{3.13}$$

where:

L = Mean crack spacing in longitudinal direction, (L). ($\approx 4.44l$)

U_{mi} = Peak bond stress for age increment i, (FL^{-2}) $= 0.0020k_{1i}$

k_{1i} = $(0.1172f'_{ci})*1000$

P_b = Percent of steel, in fraction

d_b = Reinforcing steel bar diameter, (L)

C_1 = First bond stress coefficient

$$\left[C_1 = 0.577 - 9.499e^{-9}\frac{\ln \varepsilon_{tot-\varsigma i}}{(\varepsilon_{tot-\varsigma i})^2} + 0.00502L(\ln L)\right]$$

L_k = Joint spacing, (L)

$\varepsilon_{tot\varsigma i}$ = Total strain at the depth of the steel for the time increment i, (typical range = 150 to 600 micro-strains)

Total Tensile Stress

The maximum curling and warping stresses reaches 63.8% of total possible tensile stress as mentioned previously. When all the above equations superposed, the actual tensile stress in

concrete slab can be obtained following equation (3.2)

The term, $\sigma_{curling+warping}$ presents curing and warping stresses at the top of surface on concrete slab and need to be multiplied by $\left(1-\dfrac{2a}{h}\right)$ to get the tensile stress at the tip of sawcut notch as shown in Figure 3-10.
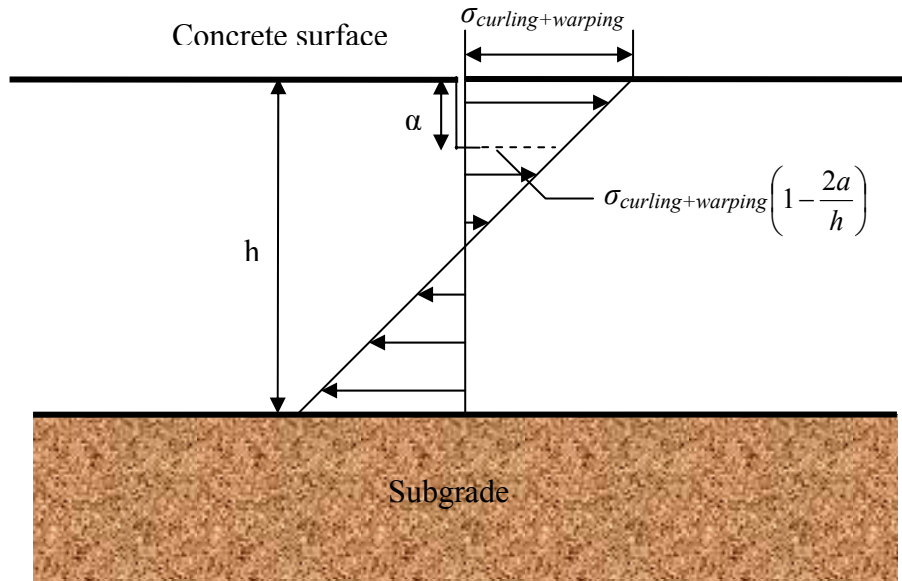
Figure 3-10 Curling and warping stress at the tip of sawcut notch.

Thus, curling and warping stress at the tip of sawcut notch can be obtained as following equation:

$$ft_{at\ sawcut} = (\sigma_{curling\ +\ warping})\left(1-\frac{2a}{h}\right) = C\times\sigma_o\left(1-\frac{2a}{h}\right) \tag{3.14}$$

where:

h = Concrete slab thickness, (L)

a = Depth of sawcut notch, (L)

C = Bradbury stress coefficient (Typical range for C is 0 to 1.084)

λ = $\dfrac{L}{l\sqrt{8}}$

y = Distance of sawcut notch location from the center

l = Radius of relative stiffness

σ_0 = Westergaard nominal stress factor

  = $\dfrac{E\varepsilon_{tot}}{2(1-v)}$ (typical range for 0 is 0 to 300psi)

v = Poisson's ratio (0.15)

E = Concrete modulus of elasticity

ε_{tot} = Equivalent total strain difference between pavement surface and bottom.

  = $[\alpha_t\Delta T_{eq}+\varepsilon_\infty\Delta(1\text{-}RH^3)_{eq}]$

Equivalent Nonlinear Temperature Difference

The temperature and moisture distribution typically is not linear throughout the depth of slab as shown in Figure 3-11. The ΔT_{eq} and $\Delta(1\text{-}RH^3)_{eq}$ terms are equivalent temperature and relative humidity difference between the pavement surface and bottom based on formulations given by Mohamed and Hansen. These equivalent differences are suggested to account for non linear effects in either the temperature or humidity gradients on the curing and warping stress. In the case of the temperature gradient, ΔT is defined at four locations

below the pavement surface. The coordinate z is zero at mid depth of the slab where upward is negative and downward is positive, and used in order to define coefficients B and D based on following regression equation:

$$\Delta T(z) = A + Bz + Cz^2 + Dz^3 \tag{3.15}$$

where, A, B, C, and D is regression coefficients. From these coefficients, ΔT_{eq} can be determined as:

$$\Delta T_{eq} = -12\left(\frac{Bh}{12} + \frac{Dh^3}{80}\right) \tag{3.16}$$

A similar approach can be applied to $\Delta(1-RH^3)_{eq.}$
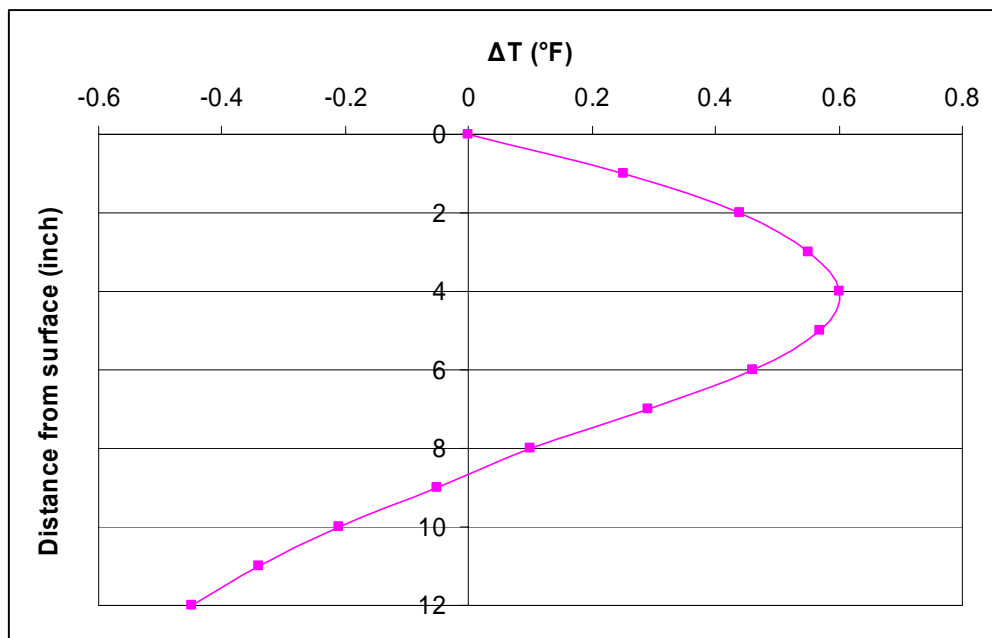
Figure 3-11 Actual temperature differentials in a hardening 12 inch concrete slab after 11 hours of placement.

Location of Maximum Tensile Stress

To determine the spacing of the transeverse joint or sawcut for a newly placed concrete pavement, it is assumed that that a newly constructed concrete pavement is infinitely long. Therefore, the maximum total tensile stress can calculated from coefficient graph by Bradbury as shown in Figure 3-9. According to the graph, maximum tensile stress occurs at approximate intervals of 4.44*l*. The position of maximum stress may vary for early-aged concrete since radius of relative stiffness (*l*) changes during this period of time. As the concrete ages, maximum stress locations typically stabilize at 13-16 foot intervals, depending on the subbase type and slab thickness, which provides some guidance as to the recommended joint spacing for design and construction purposes.

The same analysis may apply to the spacing of the longitudinal sawcut locations; however, the focus in this instance is normally to examine the suitability of standard joint locations which often serve as lane dividers. In a two-lane pavement, the longitudinal tensile stress at the pavement top is calculated at the longitudinal joint location (such as along the center line where the pavement is divided to two 12 feet wide strips).

Analysis of Tensile Strength in Concrete Slab

Concrete tensile strength in a concrete slab at sawcut notch can be derived from fracture mechanics. Failure of concrete is a process of crack formation and growth. With these fracture parameters that is defined in size effect law (SEL), resistance of concrete material against fracturing can be appropriately and correctly evaluated.

Size Effect Law

According to brittle fracture concepts, material fracture occurs when stress intensity factor (K_I) reaches a critical value. However, it has been long observed that a steady crack growth takes place in concrete before the peak load. In addition, many microscopic-scale investigations have indicated that a process zone (*c*) exists around the concrete crack tip as shown in Figure 3-12.
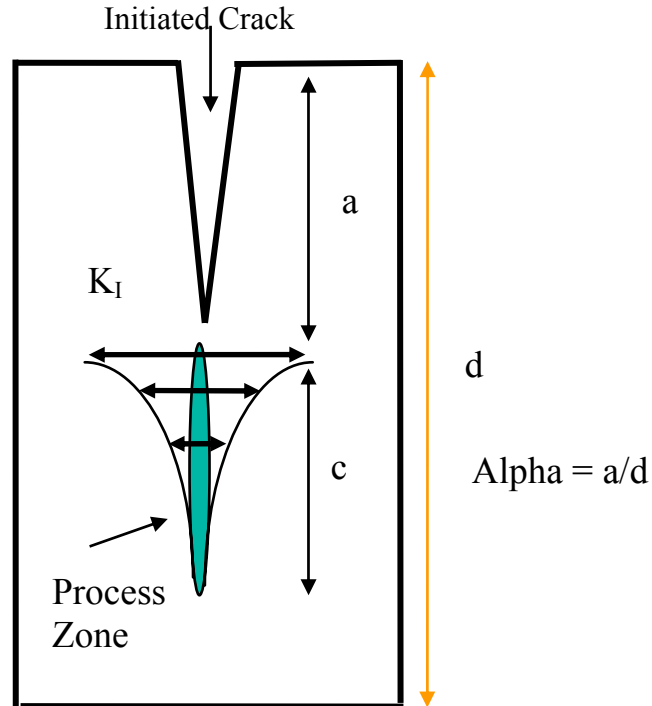
Figure 3-12 Illustration of cracking mechanism.

Microcracking in the process zone consumes energy, and therefore, toughens the material and causes nonlinear fracture behavior, which, in turn, results in the size effect on the nominal strength of the concrete structure as shown in Figure 3-13. The size effect low

(SEL) proposed in 1984 by Bazant gives a fomula to describe the size effect for the geometrically similar structures as follows:

$$\sigma_N = \frac{Bf'_t}{\sqrt{1 + \dfrac{d}{d_0}}}$$

(3. 17)

where, f'_t is the tensile strength of the concrete, d is a specimen dimension, B and d_0 depend on material, structure geometry and load type. A modification of the SEL proposed in 1990 by Bazant and Kazemi attributes the nonlinearity of concrete fracture in an infinite specimen to two material constants: the critical stress intensity factor in an infinite specimen K_{If}, and the critical effective crack length or the process zone length in an infinite specimen c_f. Although the fracture parameters K_{If} and c_f refer to an infinitely large structure, they can be conservatively applied to pavement slab dimensions. Equation (3.17) characterizes the size effect for the given geometry as shown in the log (σ_N) – log(d) plane. By taking the log on both sides of the strength expression above gives log(σ_N) as a linear function of the logarithm of the slab thickness d as shown by the slanting line with slope (-1/2) as shown in Figure 3-13.
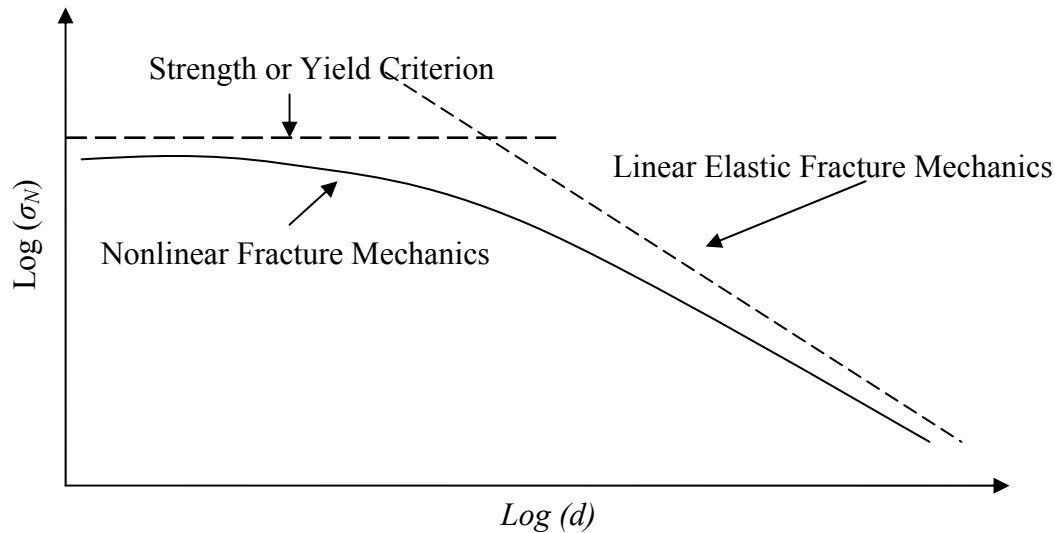
Figure 3-13 Size effect for geometrically similar structures of different sizes. (28)

However, the size effect of quasi-brittle materials such as concrete does not follow the straight line shown in Figure 3-13. Rather, it follows a transitional curve that approaches the limit stress criterion for very small specimens and approaches the limit defined by linear elastic fracture mechanics (LEFM) for large specimens. This transitional curve encompasses the structure sizes of interest for most practical applications (Bazant and Kazemi 1990). Deviating from LEFM, the size effect of concrete is due to the presence of a fracture process zone of numerous micro-cracks in front of a microscopic crack. Formation and growth of these micro-cracks consume a large amount of energy in the cracking process serving as a mechanism of concrete toughening. Unstable crack growth does not occur until the fracture process zone develops a certain length.

Consider a non-dimensional geometry function $g(\alpha) = \pi \alpha c_n^2 F^2(\alpha)$, in which $F(\alpha)$ is a geometry factor. Based on K_{If} and c_f, for any structure of finite size d, the nominal strength

can be determined from the final form of the size effect law proposed by Bazant and Kazemi (1990):

$$f'_t = c_n \frac{K_{If}}{\sqrt{g'(\alpha)c_f + g(\alpha)d}}$$

(3.18)

Equation (3.18) can be used to calculate a concrete tensile strength in a concrete slab at sawcut notch.

where:

f_t' = Tensile strength of the concrete

K_{If} = Fracture toughness ($FL^{-2}L^{1/2}$),

c_n = A constant based on specimen geometry ($=1.5(s/d)$),

s = Length of span, (L)

d = Slab thickness, (L)

a = Sawcut depth, (L)

α = Initial crack ratio ($=a/d$),

c_f = length of the fracture process zone, (L)

$g(\alpha)$ = $\pi \alpha c_n^2 F^2(\alpha)$,

$g'(\alpha)$ = $\pi F^2(\alpha) + 2\pi \alpha c^2 n F(\alpha)F'(\alpha)$,

$F(\alpha)$ = $1.122 - 1.4\alpha + 7.33\alpha^2 - 13.08\alpha^3 + 14\alpha^4$, and

$F'(\alpha)$ = $-1.4 + 14.66\alpha - 39.24\alpha^2 + 56\,\alpha^3$.

TMAC^2 SOFTWARE PROGRAM

The crack control and management in the curing concrete (C^{4}M) program uses a two-dimensional element program, temperature and moisture analysis for curing concrete (TMAC^2), to calculate ΔT_{eq} and $\Delta(1\text{-}RH^3)_{eq}$ as well as the temperature and relative humidity of concrete slab at a selected locations, such as the depth of steel. TMAC^2 was developed to predict the temperature and relative humidity distributions in hardening concrete pavement under specified environmental conditions. As an application of TMAC^2, maturity can be estimated by predicted temperature and moisture change through the concrete slab depth over the time since placement.

Basic Models for Temperature and Moisture Prediction

The models that are used by TMAC^2 Program will be subsequently explained.

Temperature Prediction

The two dimensional governing equation of heat transfer for temperature prediction in an early age concrete pavement taking heat of hydration and ambient temperature conditions into account is:

$$\frac{\partial}{\partial x}\left(K_x \frac{\partial T}{\partial x}\right) + \frac{\partial}{\partial y}\left(K_y \frac{\partial T}{\partial y}\right) + Q_h(t, T) = \rho c_p \frac{\partial T}{\partial t} \tag{3.19}$$

where:

T =   temperature in concrete pavement, °C

t =   time, hr,

x, y =   depth and longitudinal coordinates in concrete pavement, m

K_x, K_y =   thermal conductivities of concrete in x and y directions, W/m°C

ρ =   concrete density, kg/m^3

c_p =   specific heat, J/kg°C

Q_H =   generated heat from heat of hydration of cement and external source

The thermal parameters in equation (3.19) are determined by standard test procedures. The boundary conditions associated with a concrete pavement are associated with both the pavement top and bottom surface since these are the areas where the majority of heat exchanges take place. Also the heat transfer within a concrete pavement involves the generation of heat by hydration of cement during early age (29).

Moisture Prediction

Similar to heat transfer, mass diffusion is a transport process that originates from molecular activity. A higher concentration implies more molecules per unit volume. Mass diffusion is in the direction of decreasing concentration.

The drying process of concrete through diffusion due to humidity gradients is such a process which involves the transfer of water vapor into dry air due to the presence of moisture concentration gradients. There are modes of mass transfer that are similar to modes of heat transfer. Mass transfer by convection is analogous to convection heat transfer, while mass transfer by diffusion is analogous to conduction heat transfer (30).

Drying of concrete is a complicated moisture transport process. It includes primarily the effects of capillary pressure, disjoining pressure, and liquid and vapor diffusion. It is generally accepted that the drying process in porous concrete can be purely described by diffusion theory based on Fick's law. It is assumed phenomenologically that the rate of transfer of moisture content gradient as the solely driving force measured normal to the section. The diffusion equation for the drying concrete under variable temperature conditions is can be obtained as following equation:

$$\frac{\partial H}{\partial t} = kc\frac{\partial^2 H}{\partial x^2} + k\frac{\partial c}{\partial x}\frac{\partial H}{\partial x} + \frac{\partial H_s}{\partial t} + K\frac{\partial T}{\partial t} \tag{3.20}$$

where:

t = Curing time,

y = Distance from the surface of concrete,

k = Slope of the moisture isotherm where the mass of water is described as a function of humidity (H),

c = Permeability as a function of temperature and humidity of concrete,

∂H_s = Change in humidity due to hydration at a constant water content and time,

K = Hygrothemic coefficient.

Permeability (c) is also a function of the porosity and indirectly a function of position x. Because permeability change with position x is assumed to be very small, the second

term in the equation (3.20) is considered to be negligible and is consequently dropped from

the diffusion equation as:

$$\frac{\partial H}{\partial t} = D\frac{\partial^2 H}{\partial y^2} + \frac{\partial H_s}{\partial t} + K\frac{\partial T}{\partial t}$$

(3.21)

where:

$D\ (k \cdot c) =$ Moisture diffusivity (L^2/t)

CHAPTER IV

VALIDATION USING CRACKING FRAME

NEED FOR VALIDATION

A test program in the laboratory was undertaken to analyze and verify to the extent possible the concepts introduced in Chapter III relative to their application to cracking control. The cracking frame test is essentially used to monitor cracking stress and strain over time relative to shrinkage, temperature change, and creep strain. It is necessary to compare and validate the results from mathematical equations that consists of basic concepts of C^4M program with the analysis data from experimental test.

LABORATORY TESTING PROGRAM

An important factor for laboratory tests is the concrete placement temperature which is affected in part by the concrete mixture constituents such as the amount of fly ash (FA) and the amount of cement. Both of these significantly affect sawcut timing and depth requirement. Thus, the cracking analysis at a sawcut notch for a newly concrete pavement provided in C^4M program can be systematically validated by considering three different factors of concrete temperature, fly ash content, and cement content.

A factorial design with these factors was prepared for the laboratory and listed in Table 4-1 with their corresponding levels. Three levels of placement temperature, i.e., 75, 95 and 105°F were considered whereas each two levels were assigned to the other two factors, i.e., FA content and cement factor. The factorial design is shown in Table 4-1 consists of 12 combinations. Seven test combinations out of the 12 were selected for the laboratory testing and are listed in Table 4-2.

Table 4-1 Three factors with their corresponding levels for the laboratory program

Placement Temperature	FA replacement	Cement factor
75°F	25	5
95°F	40	6
105°F		

Table 4-2 Physical layout of the seven test combinations

Experiments	Placement Temperature	FA replacement	Cement factor
1	75°F	25	5
2	95°F	25	5
3	95°F	25	6
4	105°F	25	5
5	105°F	25	6
6	105°F	40	5
7	105°F	40	6

Note: CAF = 0.72, w/cm = 0.45, 0.5% air and 4% medium range water reducer

A total of four mixtures were used to make up the above 7 test combinations shown in Table 4-3. Mixture I was investigated at 75, 95 and 105°F whereas mixture II was investigated at 95 and 105°F. The mixtures III and IV were investigated at only 105°F. The required materials, i.e., coarse aggregate, fine aggregate, class F ash, cement (ASTM type-I), water reducing admixture etc., to conduct the previously described combinations were supplied by Lone Star Infrastructure.

Table 4-3 Four mixtures associated with 7 runs in Table 4-2

Mixture No.	*Mixture Proportion*
Mixture I	CF 5, FA 25%
Mixture II	CF 6, FA 25%
Mixture III	CF 5, FA 40%
Mixture IV	CF 6, FA 40%

The mixture proportions for each material in *mixture I, II, III, and IV* are shown in Table 4-3. Type I cement and a class F fly ash were used for all the tests. Air-entraining admixture and medium range water-reducing admixture were also used in all the mixtures.

CRACKING FRAME TEST

The cracking frame was developed in order to measure restraint stresses in young concrete during the hardening process. Researchers have used the cracking frame to study the

cracking tendency of a concrete mix as well as the cracking sensitivity of different cement types. The stiffness of the cracking frame restrains the deformation of the concrete due to shrinkage and thermal effects. Therefore, this testing devise is able to create a certain degree of restraint at early concrete ages. Tests conducted under constant temperature conditions allow the measurement of restraint stresses caused by early shrinkage and swelling. The cracking frame is shown in Figure 4-1, restraints the ends of the beam or slab segment by dovetails in two steel crossheads. To restrain movement between the two cross heads, they were connected with two steel longitudinal bars (steel and concrete approximately at equal cross sections). The steel used is special steel with an extremely low thermal expansion coefficient. In this research, a cracking frame test was conducted and monitored for test 4, i.e., mixtures with cement factor 5 and fly ash content 25% under constant temperature (105°F) and relative humidity conditions (40%) in an environmental chamber.

Figure 4-1 Cracking frame test for test 4.

The purpose of this test is to monitor the time of crack formation at the pre-fabricated notch in the concrete specimen as a function of strain gain and creep development and to validate analysis of stress, strength and creep strain for the given mixture as would be determined by the C^4M program.

The concrete specimen cross section at the center portion is 3.05 x 5.75 inches and at the ends of the dovetails is 3.05 x 12.95 inches. The length of the concrete specimen is 3.3 feet (1 meter). The concrete in the cracking frame was notched at mid span to induce cracking at that location. The crack formed at the notch of the concrete specimen at 62 hours after placement. The crack runs through the full depth of the test specimen as shown in Figure 4-2.
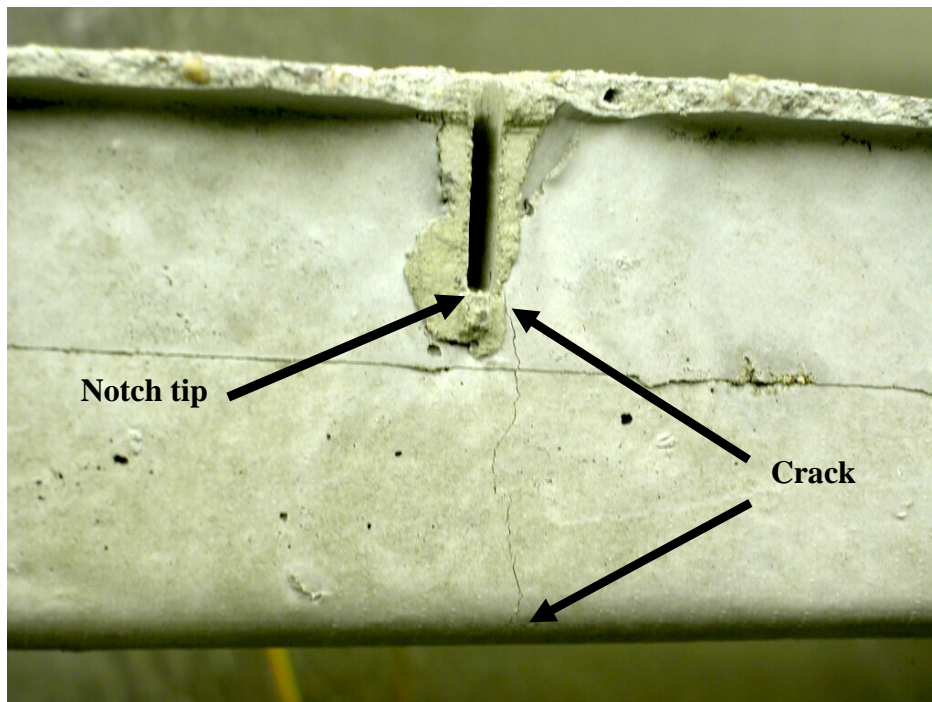
Figure 4-2 Crack formation at the notch.

Data Observed from Cracking Frame Test

Ambient temperature and relative humidity at laboratory with time is shown in Figure 4-3.
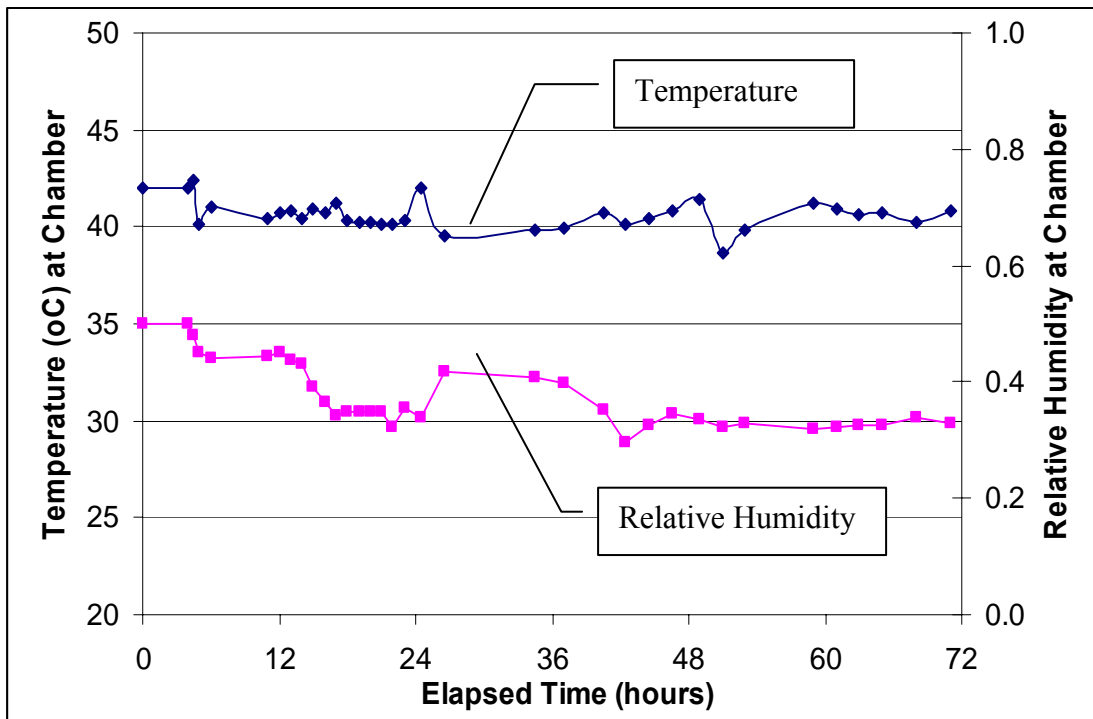
Figure 4-3 Ambient temperature and relative humidity at laboratory.

During the cracking frame test the concrete drying shrinkage was monitored with time, as shown in Figure 4-4, by use of vibrating wire gauge (VWG). This drying shrinkage strain data was used to calculate warping stress in the specimen due to change of moisture content inside concrete. Cracking frame strain data also was monitored every an hour during cracking frame test as shown in Figure 4-5.
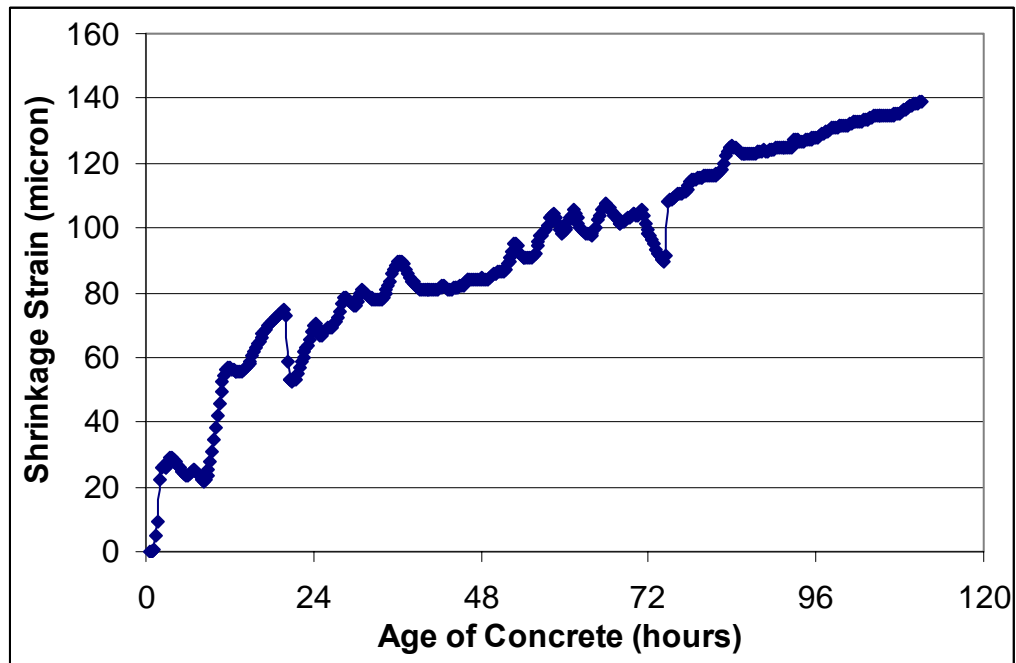
Figure 4-4 Drying shrinkage strain vs. age of concrete (hours).
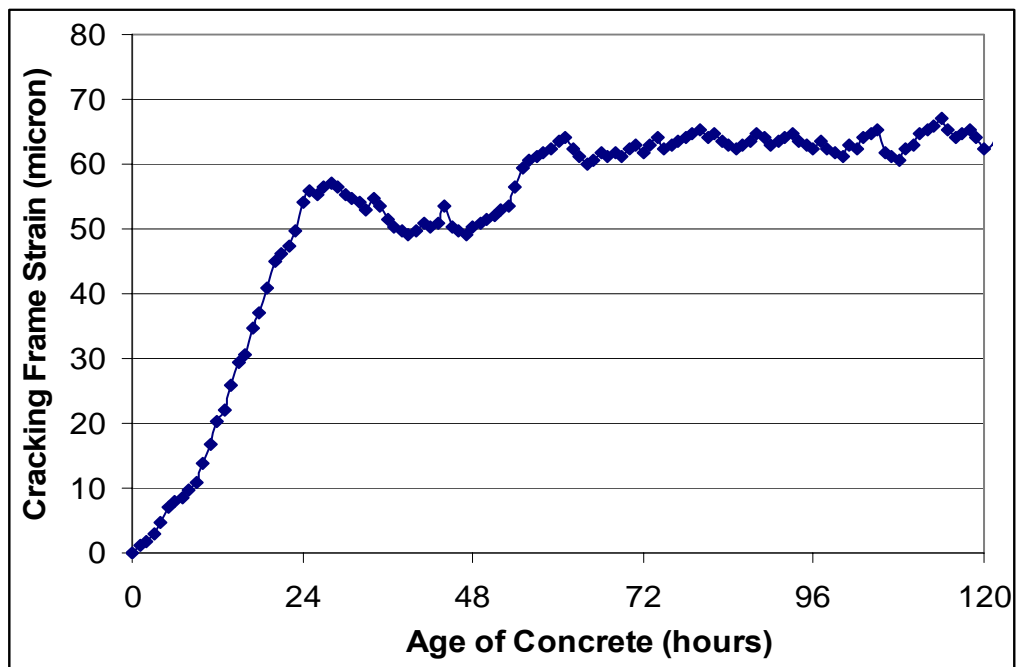
Figure 4-5 Cracking frame strain (micron) vs. age of concrete (hours).

Analysis of Cracking Frame Test Results

The concrete tensile stress in the cracking frame at laboratory was calculated by considering thermal strain (ε^t), shrinkage strain (ε^{sh}), and creep strain (ε_{crp}). In case of thermal strain, the equivalent temperature gradient was found using the temperature data at the top and bottom of specimen that was collected using the thermocouples. As shown in Figure 4-6, the trend in the temperature difference in the specimen over the initial hydration stages was not constant. This effect is due to the thermal diffusivity of the concrete that controls how rapidly the temperature will change at a given point. These equivalent temperature gradients at each time were subtracted by a set temperature gradient that was defined as the equivalent temperature gradient at final setting time of 6.5 hours.
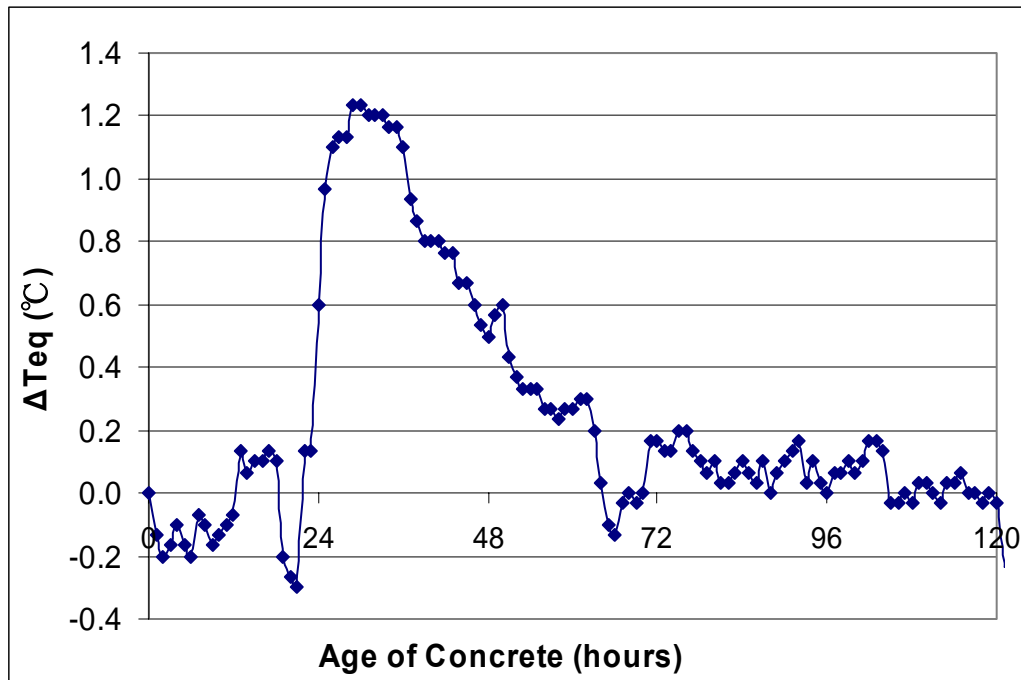
Figure 4-6 Equivalent temperature difference vs. age of concrete (hours).

Creep strain during the test was found using the following relation:

$$\varepsilon_{crp} = \varepsilon_v - \varepsilon_e - \left(\frac{F_s}{E_c A_c} \right)$$

(4.1)

where:

ε_{crp} = Creep strain

ε_v = Total shrinkage strain

ε_e = Cracking frame strain

F_s = Force in concrete (F)

E_c = Modulus of elasticity of concrete (F/L^{-2})

A_c = Specimen cross sectional area (L^2)

The cracking frame strain (Figure 4-5) was measured during the testing sequence. The creep strain was then obtained by subtracting cracking frame strain and the strain due to the load on the concrete (F_s) from total shrinkage strain that consisted of thermal and drying shrinkage strain.

The total creep strain (Figure 4-7) appeared to be on the order of 40% to 50% of the shrinkage strain at fracture. Reducing the total creep strain by the plastic strain which is the strain before the concrete began to stiffen may yield the creep strain that effectively reduces the cracking stress, which in this case is approximately 20% of the shrinkage strain at the time of cracking. From 13 to 34 hours after concrete placement, incremental creep strain has negative value which is due to the specimen's internal expansion. Therefore, it is clear

from the trend of stress and strength with time shown in Figure 4-8 that crack does not occur in concrete until the creep has diminished to a small value of approximately less than 50 micro-strain.
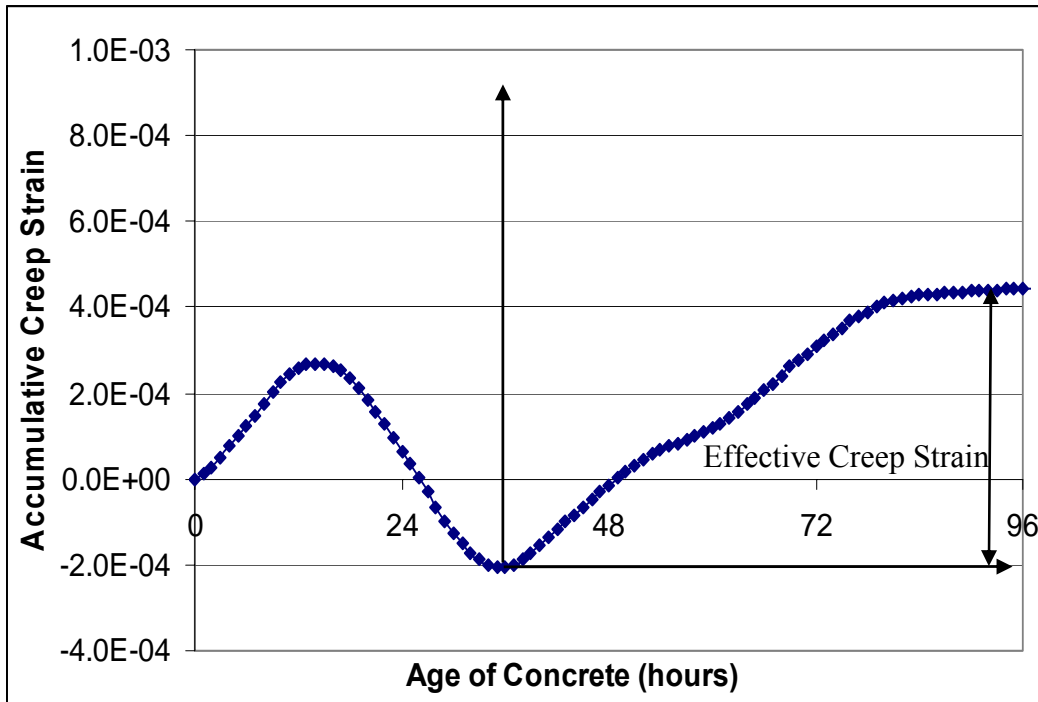
Figure 4-7 Laboratory total creep strain vs. time after placement.

The Figure 4-8 shows the stress and strength patterns with time obtained by calculating thermal, drying shrinkage, and creep strain. The tensile stress was calculated by using the first term of equation (3.2):

$$f_t = \frac{E\varepsilon^{tot}}{2(1-v)}\left(1 - \frac{2a}{h}\right)$$

(4.2)

where:

E = Elastic modulus ($57000\sqrt{f'_c}$)

ε^{tot} = Total strain ($\varepsilon^t + \varepsilon^{sh} - \varepsilon_{crp}$)

The total strain (ε^{tot}) was calculated by adding the shrinkage strain (ε^{sh}) and subtracting the creep strain (ε_{crp}) from thermal strain (ε^t). Shrinkage strain was obtained directly from observed data as shown in Figure 4.4, thermal strain was calculated by multiplying coefficient of thermal expansion (CoTE: $\alpha = 6\times10^{-6}$) from ΔT_{eq} (Figure 4.6), and creep strain was obtained by using equation (4.1) as previously explained. Notch depth (a) of 1.7 inches, specimen thickness (h) of 5 inches, and Poisson's ratio (v) of 0.15 was used in equation (4.2).

The laboratory tensile strength with time was obtained by conducting split tensile tests on cylindrical concrete specimens 6"x12" over a period of 1, 3, 7, and 28 days. From the split tensile tests the fracture parameters (K_{If} and C_f) were found and used to determine the tensile strength at each point of time from the equation (3.1). The parameters obtained are: $K_{If} = 987$ psi $\sqrt{in}$, and $c_f = 2.23$ inches.

From the tensile strength and stress curves in Figure 4-8, theoretical cracking formation time can be obtained approximately 60 hours after concrete placement, which is based on the same theoretical method as C⁴M program uses. This calculated cracking formation time of 60 hours is almost same as the observed time of cracking at the notch of 62 hours after concrete placement.
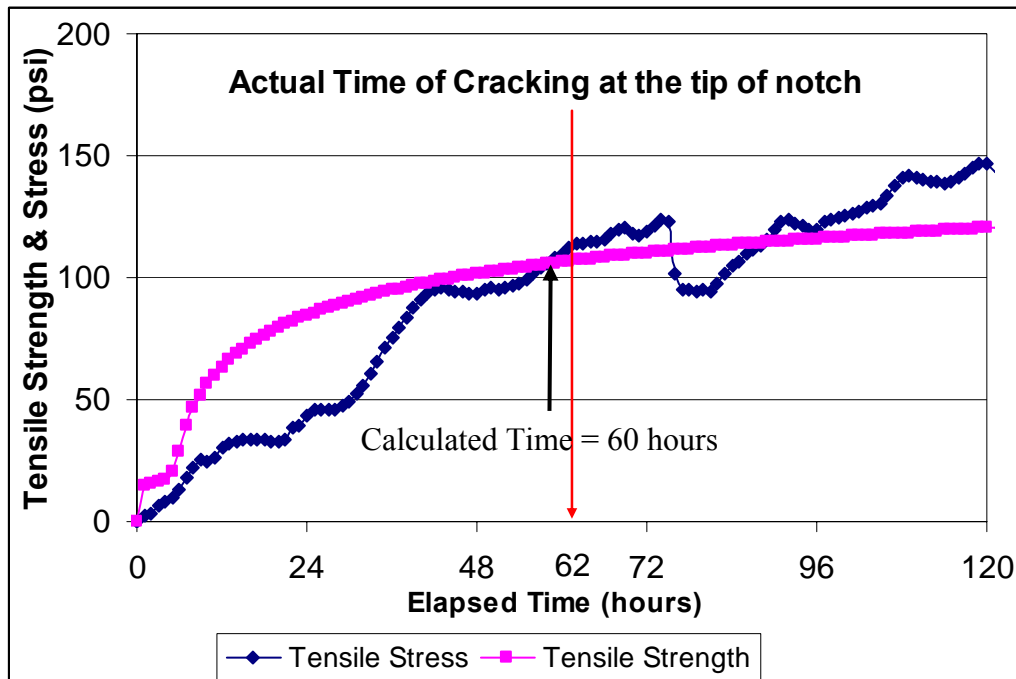
Figure 4-8 Tensile strength and stress pattern using cracking frame test.

Therefore, it can be concluded that the cracking formation time in the concrete slab can be estimated by appropriated theories such as fracture mechanics and mechanical method of concrete material.

PREDICTION OF CRACKING TIME FOR SEVEN RUNS

Test Methods

The following discussion addresses the tests that are carried out to obtain input data for C^4M program. Although a cracking frame test and predicted time of cracking was performed only in test run 4, by conducting below tests that will be subsequently explained

predicted time of cracking can be calculated for other 6 cases. The room temperature for each test run was pre-set 2 days prior to the commencement of the testing to allow sufficient time for the material temperature to come to equilibrium with the surrounding temperature. To this end, all the concrete components, i.e., coarse aggregate, fine aggregate, cement, water etc. were kept inside an environment chamber prior to mixing. Concrete mixing and specimen casting for each test run was carried out inside the chamber for a given placement temperature. Therefore, it can be assumed that the placement temperature of a particular test run was similar to the corresponding room temperature.

Compressive Strength

Relative to the effects of placement temperature on concrete, strength gain over time is a major factor for cracking control using sawcut notch. Accordingly, compressive strength testing was carried out. Cylindrical specimens (8x4 inch) were cast and tested for compressive strength at 1, 3, 7, and 28 days according to ASTM C39. The specimens were cast and cured inside an environmental chamber at a given temperature for 24 hours; thereafter all specimens were moist cured at 100% relative humidity and a constant temperature of 70°F.

Maturity

Maturity testing was performed according to ASTM C 1074. Temperature data for each test run were collected using a thermocouple placed inside selected cylindrical specimens (8x4 inches) and measured at hourly basis from the concrete placement time. From the measured

temperature history of the concrete, maturity data was calculated using following equation:

$$M(t) = \sum (T_a - T_0)\Delta t \qquad (4.3)$$

where:

$M(t)$ = Maturity at age t,

Δt = Time interval, hour

T_a = Average concrete temperature during time interval, and

T_0 = Datum temperature

Concrete Setting

Setting is a key property that needs to be considered when examining the crack occurrence on concrete slab. Setting in many respects is related to the rate of strength gain as well as the rate of hydration in concrete. Penetration testing (ASTM C 403) was conducted to determine (a) the time of initial and final set of the concrete – which is obtained by measuring the penetration resistance at different needle diameters and time, and (b) the concrete temperature over the setting-period.

Heat of Hydration

Possible placement temperature affects on concrete hydration were characterized in terms of adiabatic heat signature (AHS) and adiabatic temperature rise (ATR). AHS is defined as the heat of hydration and the rate of heat released as a function of curing age of a

cementitious mixture during hardening. ATR is defined as the adiabatic temperature rise and its rate as a function of curing age of a cementitious mixture during hardening. ATR is the maximum possible temperature increase of a concrete mixture when it is perfectly insulated. AHS and ATR were determined for all the seven test runs by using Quadrel Q-Drum device.

Collected Data for Each Test

The different early age concrete properties previously described were determined for each run listed in the factorial design. The results of test analysis and validation are subsequently described.

Compressive Strength

Compressive strength data was used to estimate fracture parameters K_{If} (stress intensity factor) and C_f (process zone length) at any point of time using equation (3.6). Therefore, compressive strength at 28 days is one of the inputs of C^4M program. Figure 4-9 shows that up to 28 days, the higher the temperature (up to 105^0F) the more rapid the cement hydration and the strength development. Therefore, the increase of placement temperature is of benefit for early age (up to 28 days) strength development in case of concrete with reasonable amount of fly ash. The amount of fly ash replacement of concrete mixture also affects the compressive strength of concrete at early age. The strength of concrete on 25% fly ash replacement tends to have a higher rate of strength gain compared to that containing

40% fly ash replacement at the same placement temperature. The high value of cement factor also tends to increase the compressive strength for any placement temperature.
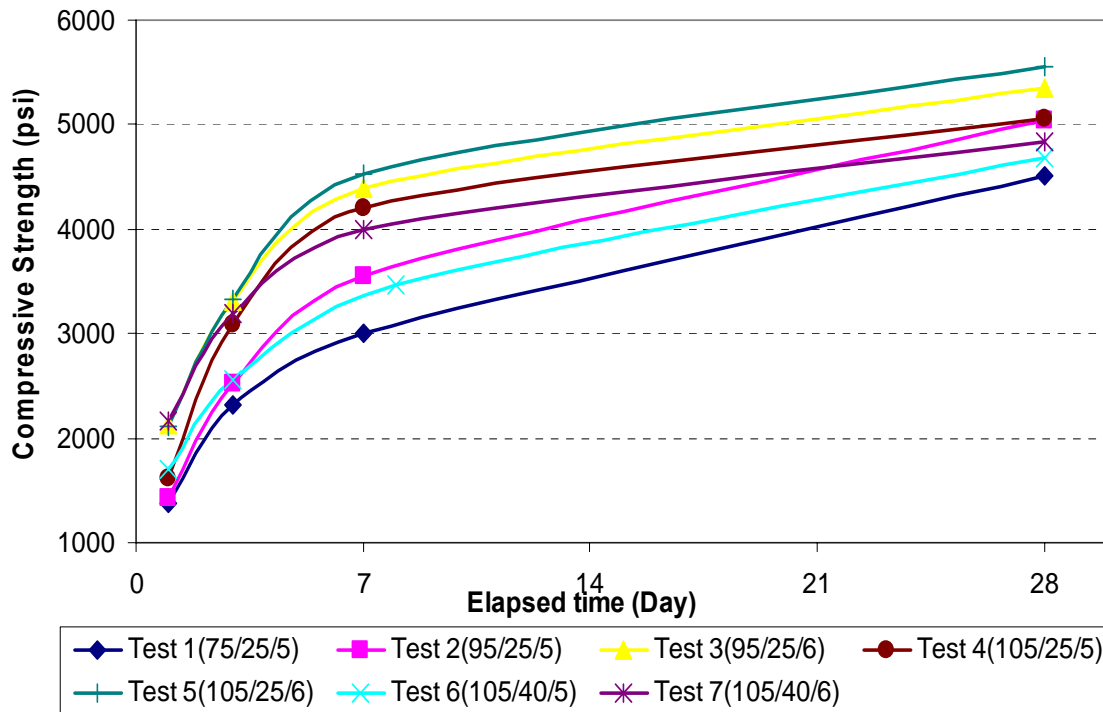
Figure 4-9 Compressive strength as a function of time for the seven runs.

The data in Figure 4-10 show strength – maturity (temperature – time) relations for the seven test runs at three different placement temperatures of 24, 35 and 41℃. The data shows that strength-maturity of a given concrete mixture is affected by the placement temperature.
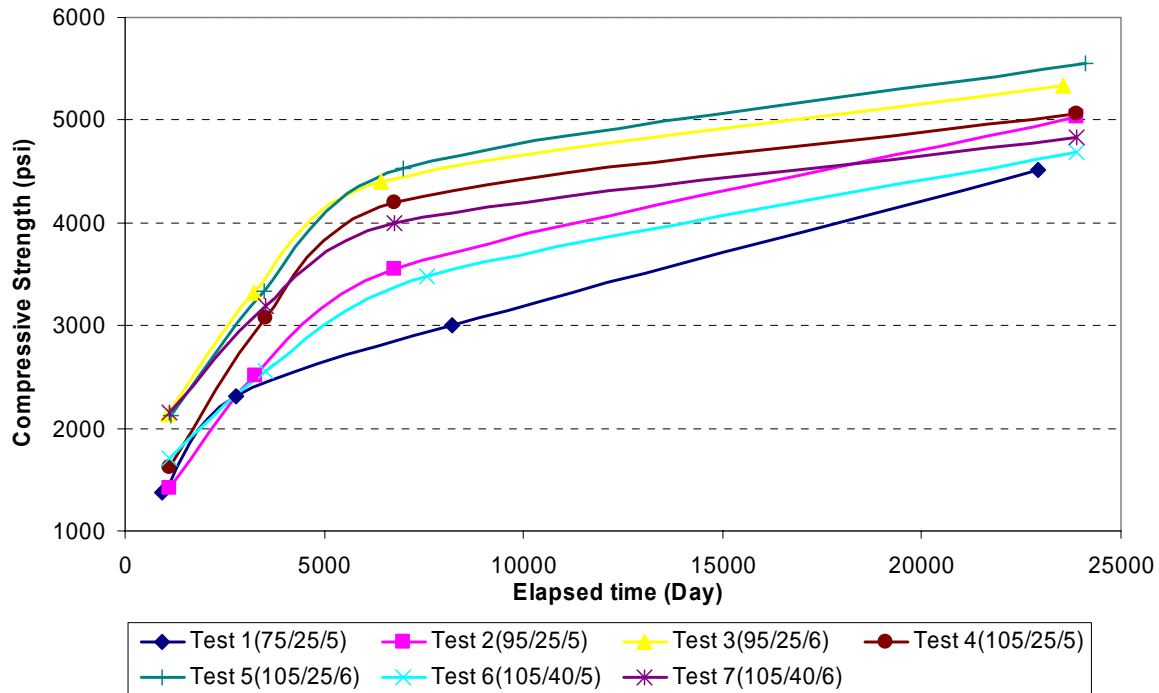
Figure 4-10 Compressive strength as a function of maturity for the seven runs.

Maturity

The maturity tests were conducted to estimate mathematical strength gain with time. The prediction equation was used to project the strength of a test specimen based upon its measured early-age strength. The general form of the prediction equation used in this test method is:

$$S_M = S_m + b(\log M - \log m) \qquad (4.4)$$

where:

S_M = Projected strength at maturity index M,

S_m = Measured compressive strength at maturity index m,

b = Slope of the line,

M = Maturity index under standard curing conditions, and

m = Maturity index of the specimen tested at early age.

The prediction equation was developed by performing compressive strength tests at various ages, computing the corresponding maturity indices at the test ages, and plotting the compressive strength as a function of the logarithm of the maturity index. In this test method, it is assumed that there is a linear relationship between strength and the logarithm of the maturity index. The relationship between the maturity and elapsed time for all seven test runs is shown in Figure 4-11. In hot weather condition, the maturity increments also steeper than those at lower ambient temperature condition. However, it can be realized that the maturity increments are reducing if we used higher fly ash replacement such as 40% compared with that of 25% at the same ambient temperature.
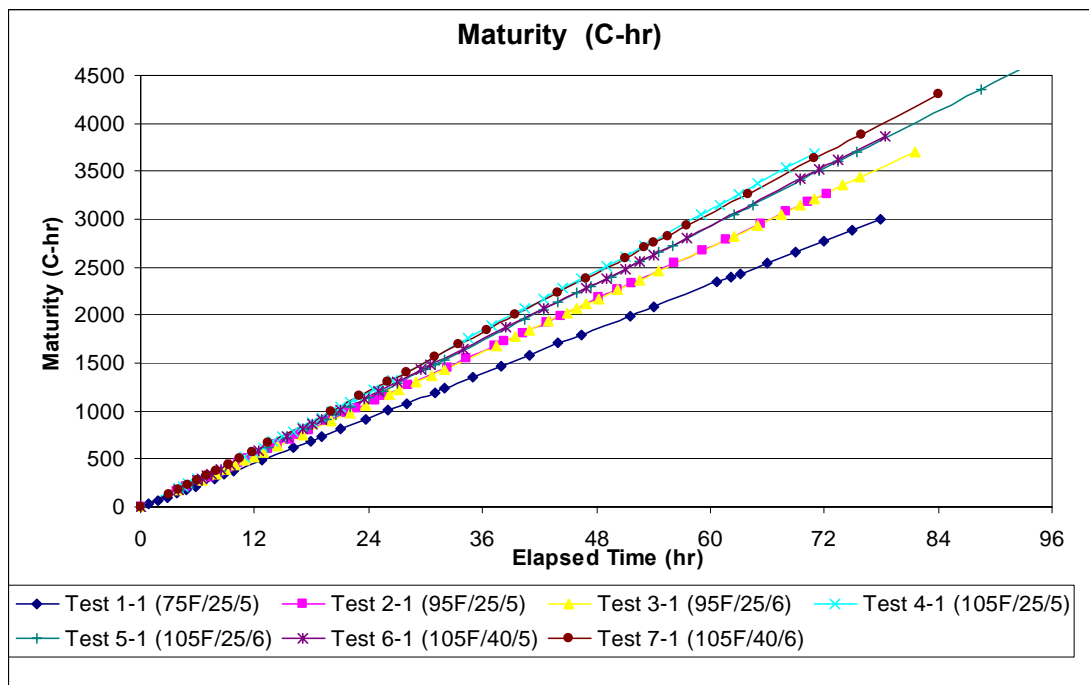
Figure 4-11 Maturity as a function of time for the seven runs.

Initial and Final Setting

Initial and final set time in concrete slab is an important characteristics related to sawcut operating timing. Typically, the notches placed with an early-entry saw can be placed as soon as one can walk on the concrete which coincides with approximately one-half to two-third of the elapsed time between initial and final setting of the concrete. The final set time also can be used to determine set temperature as defined by the temperature of concrete slab at final setting time.

The times of initial and final setting were determined for all the 7 runs by using the penetrometer test method (ASTM C 403). The results are presented in Figure 4-12. A perusal of Figure 4-12 shows that increasing placement temperature causes reduction in both initial and final set time. It is also observed that both initial and final set time slightly increases as the Class F fly ash content changes from 25% to 40%. Figure 4-12 indicates that the final setting time for mixture with 40% fly ash tends to be delayed by about 30 minutes. Temperature at 1 inch below the surface of the specimen for all the 7 test runs was monitored periodically during setting time measurement. Set temperature, temperature at final set time, was determined from these temperature measurements and presented in Table 4-4 along with time-temperature maturities. The set temperature was well above the ambient temperature at low temperature placement whereas it was either similar or slightly above the ambient temperature at high temperature placement.
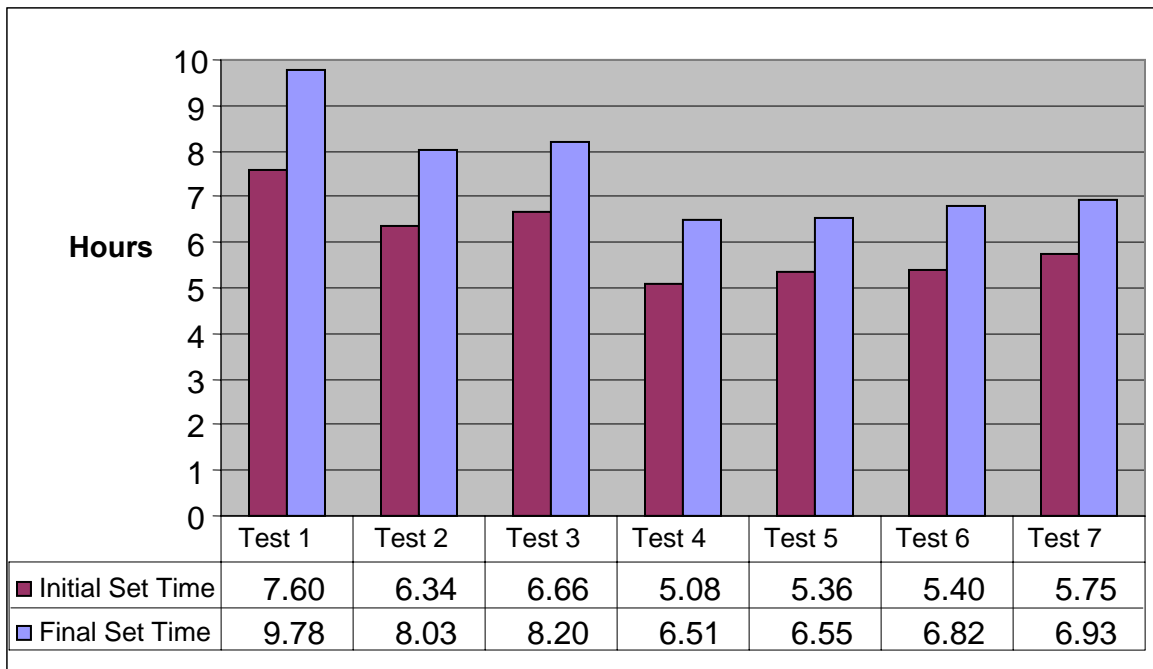
Figure 4-12 Initial and final set time for the seven runs.

Table 4-4 Maturity and set temperature at final set time for seven runs

Test runs	Initial set time (hours)	Final set time (hours)	Final set maturity (^{0}C-hr)	Final set temperature (^{0}F)
1	7.60	9.78	372.62	84.02
2	6.34	8.03	334.80	94.64
3	6.66	8.20	349.29	95.72
4	5.08	6.51	324.88	103.10
5 (*)	5.36	6.55	327.00	108.68
6	5.4	6.82	336.00	109.22
7	5.75	6.93	335.57	108.14

Note: (*) Conditions cracking frame test was conducted

Heat of Hydration

Heat of hydration data is required to estimate temperature profile throughout depth of slab with time as input data for the TMAC[2]. The results of adiabatic heat signature (AHS, J/gm) and adiabatic temperature rise (^{0}F) testing are presented in Figures 4-13 and 4-14. As indicated, the higher the placement temperature the greater the adiabatic heat signature (AHS, J/gm) and adiabatic temperature rise (^{0}F). The heat of hydration determined by Q-drum test at 75^0F, 95^0F and 105^0F placement temperatures are 287, 317 and 346 J/gm respectively for mixture I (Table 4-5). The high heat development within 3-4 days for concrete placed at 105^0F or high cement factor such as 6 might make earlier the cracking occurred time while the use of fly ash seems to delay the crack occurred time as it reduce the heat development at early an age.
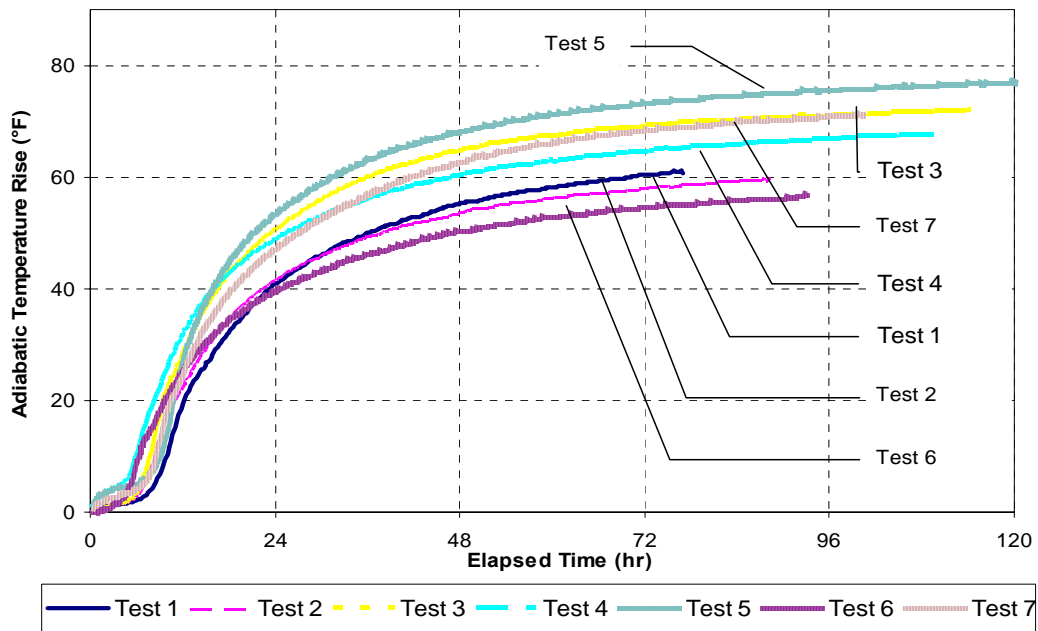
Figure 4-13 Adiabatic Temperature Rise (ATR) as a function of time for seven runs.
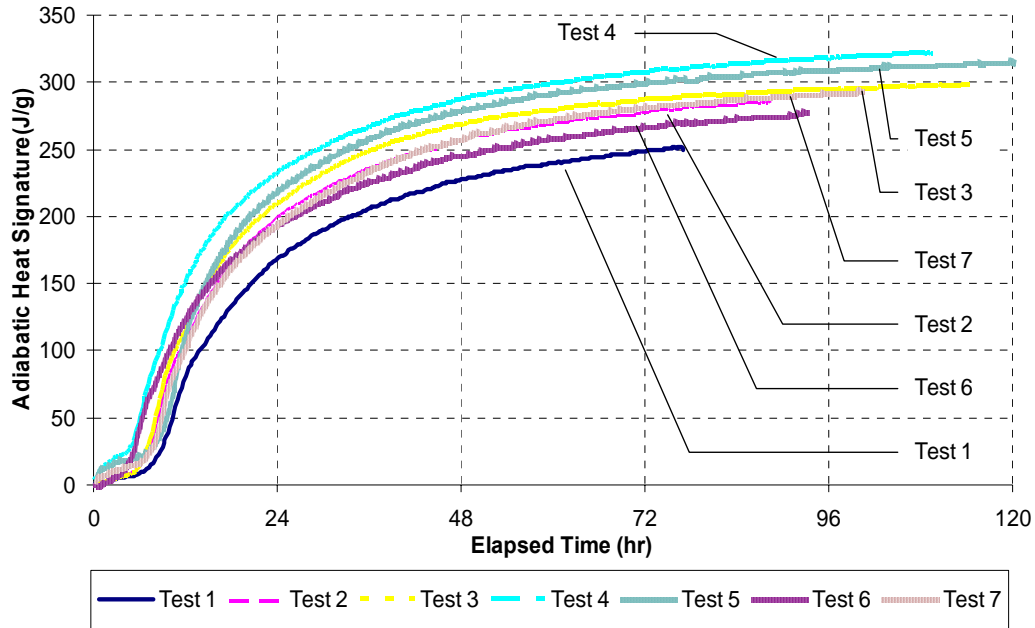
Figure 4-14 Adiabatic Heat Signature (AHS) as a function of time for the seven runs.

Table 4-5 Adiabatic Heat Signature (AHS) in J/gm for all seven mixtures

Test run	AHS (J/gm)					
	1 Day	2 Days	3 Days	4 Days	28 Days	90 Days
1	176.5	239.50	259.00	-	285.74	287.44
2	198.41	256.56	277.49	291.12	312.15	317.50
3	209.11	267.96	286.80	293.77	315.22	324.01
4	213.0	269.0	288.0	298.5	330.5	346.0
5	218.64	278.65	299.59	309.36	340.00	370.00
6	193.06	245.16	266.33	279.12	296.00	305.00
7	193.29	257.49	281.45	291.68	310.98	317.03

Analysis of Data

Set temperature and moisture gradients are the key factors affecting the tensile stress due to curling and warping behaviors in a concrete pavement. To predict time of cracking at the tip of the notch in cracking frame specimen size for the seven test runs, set temperature and moisture gradients in 3.75 inches thickness slab were predicted using the Temperature and Moisture Analysis for Curing Concrete (TMAC^2) program (Jeong et al. 2001) where, inputs [e.g., set maturity (Table 4-4), heat of hydration (Table 4-5)] were developed from the laboratory test results as previously described. The following are the required inputs for the TMAC^2 program.

a) Ambient temperature, ambient relative humidity, wind speed, and solar radiation

b) Set maturity and heat of hydration (J/gm) for each test run

c) Concrete mixture component for each test run

Set Temperature Profiles

Set temperature profiles for all 7 runs are computed by TMAC^2 and depicted in Figures 4-15, 4-16, 4-17, and 4-18. It was observed that from the figures below that the set temperature profiles become more positive slope as the placement temperature increases. Therefore, the temperature difference between top and bottom of slab at final setting time is more severe in hot weather conditions than cool weather conditions, which could make high positive set temperature gradient and cause a greater potential thermal stress. (discussed subsequently)

Temperture,(°F)
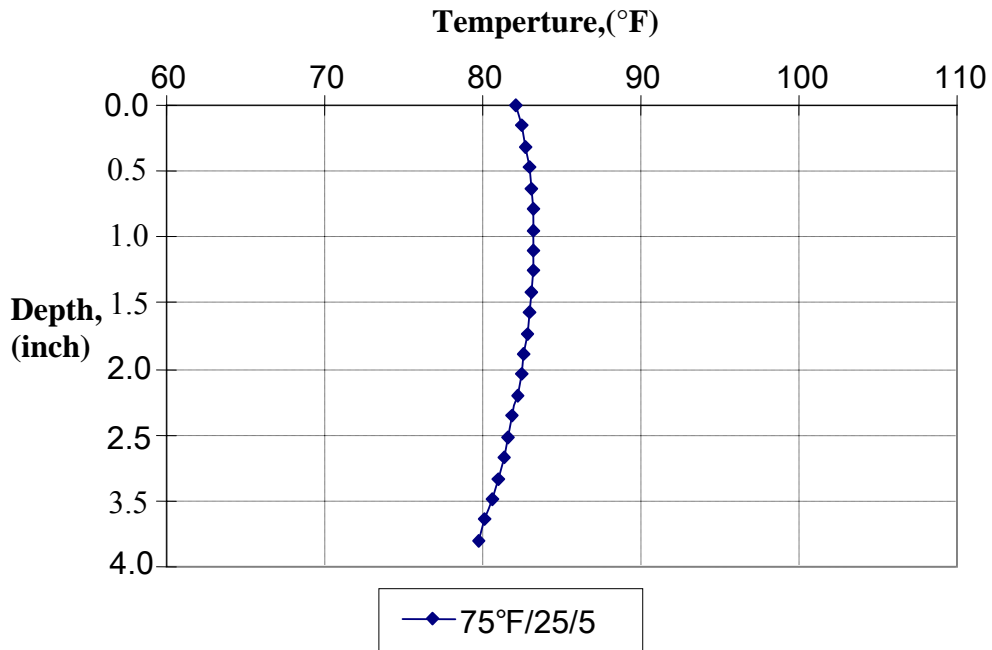
Figure 4-15 Set temperature profiles at 75℉ concrete placement.

Temperture,(°F)
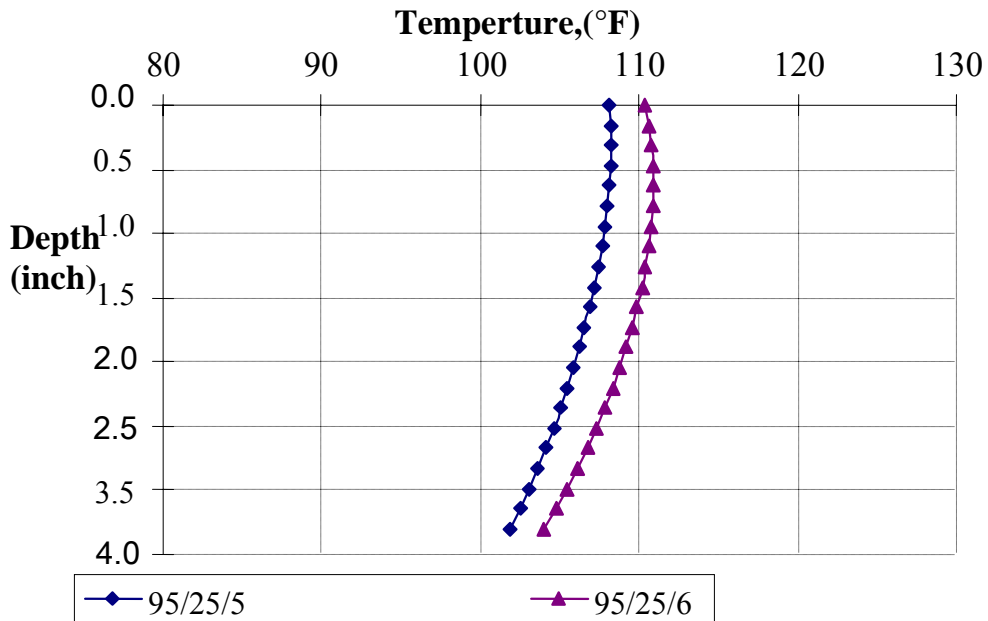
Figure 4-16 Set temperature profiles at 95℉ concrete placement, and 25% fly ash content.
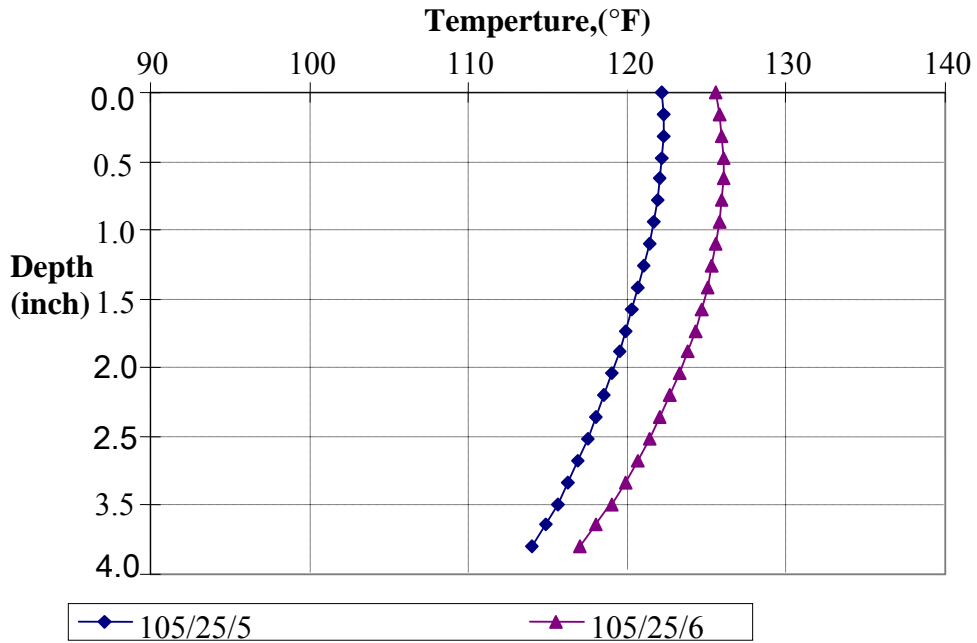
Figure 4-17 Set temperature profiles at 105℉ concrete placement, and 25% fly ash content.
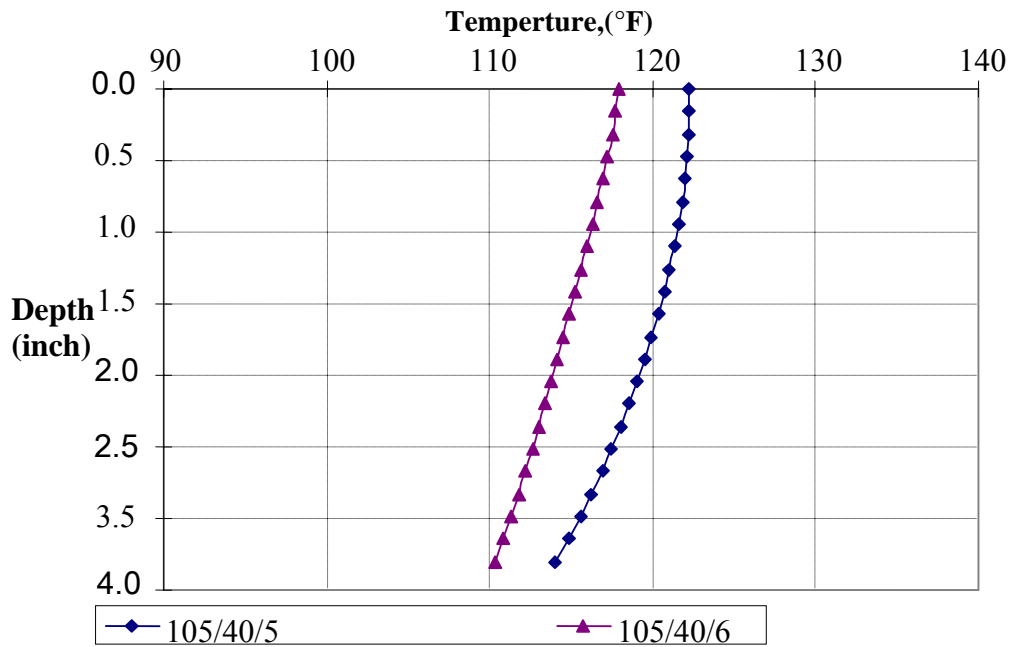
Figure 4-18 Set temperature profiles at 105℉ concrete placement, and 40% fly ash content.

Set Temperature Gradients

The set temperature gradient, i.e., the temperature difference between top and bottom of slab at final setting determines the thermal stress development in concrete pavement. It is observed from the previous discussion that the set temperature profiles are invariably non-linear in nature. Therefore, a non-linear pattern of set temperature profile was converted to linear type by linearization in order to calculate the set temperature gradient using equation (3.15) and (3.16).

The influence of set temperature gradient on the mechanism of crack formation is described below. The temperature drop at the top of the slab occurs during the night because the concrete surface temperature is lower than it is at the bottom due to ambient temperature effects. The upwards slab curvature occurs when the surface temperature is lower than the set temperature. Therefore, it is anticipated that the high positive set temperature gradient will lead a greater amount of liftoff at the corners due to the temperature difference and high probability of cracking.

On the other hand, it might be difficult to induce controlled cracking at the tip of sawcut notch if the concrete slab has a negative set temperature gradient which may occur under a afternoon placement in cool weather conditions because most time of tensile stress may occur at the bottom of the slab which makes difficult to induce controlled cracking at the tip of sawcut notch.

	Test 1	Test 2	Test 3	Test 4	Test 5	Test 6	Test 7
▣ Set temp. gradient	0.476	1.011	1.011	1.292	1.332	1.214	1.243
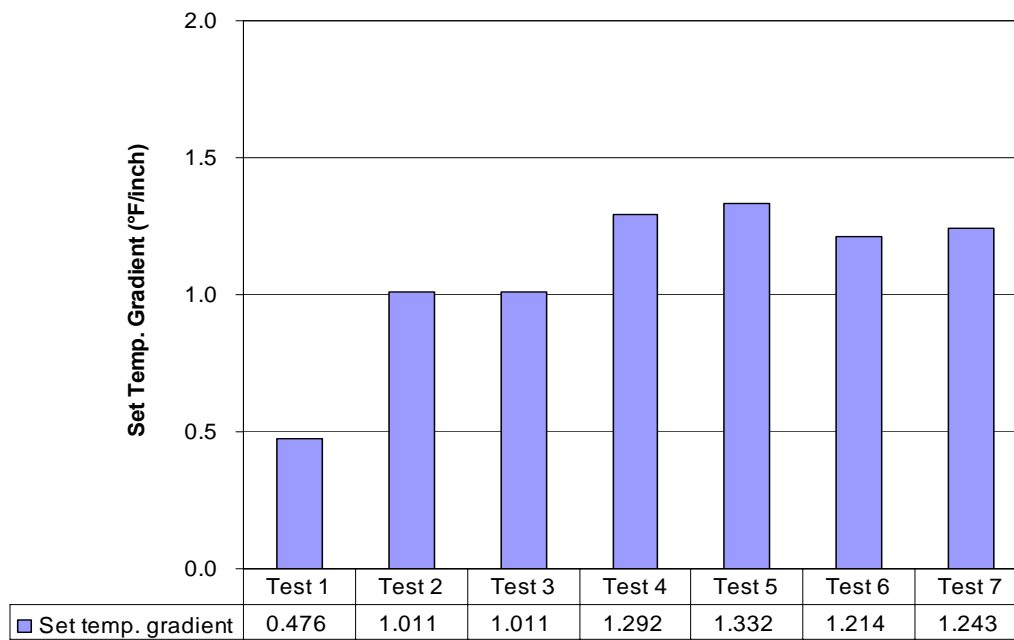
Figure 4-19 Set temperature gradient for seven runs.

In the same manner, set moisture gradient also was calculated using TMAC^2 program.

	Test 1	Test 2	Test 3	Test 4	Test 5	Test 6	Test 7
▣ Set moisture gradient	0.249	0.220	0.235	0.227	0.218	0.235	0.229
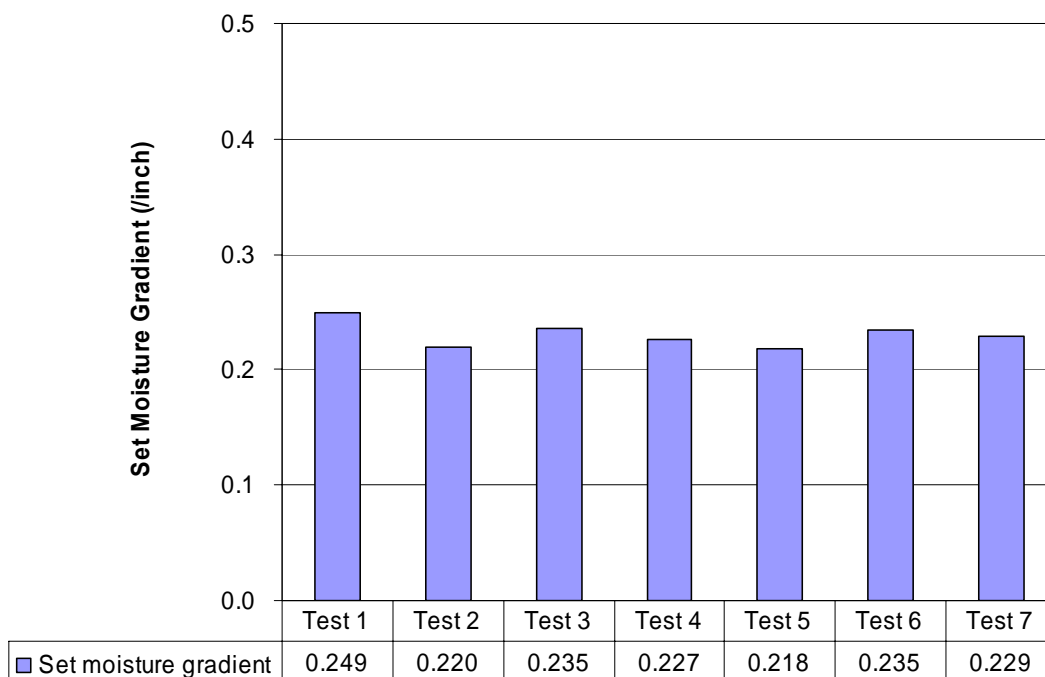
Figure 4-20 Set moisture gradient for seven runs.

From the conducted test results as described above, the C^{4}M program input data for seven runs was created to calculate predicted time of cracking at the same notch depth and slab thickness as a cracking frame specimen size. Table 4-6 listed the C^{4}M program input data for seven runs.

Table 4-6 C^{4}M program input data for seven runs

	Test 1	Test 2	Test 3	Test 4	Test 5	Test 6	Test 7
Ambient temp.	75°F	95°F	95°F	105°F	105°F	105°F	105°F
Ambient RH	50%	50%	50%	50%	50%	50%	50%
Fly ash content	25%	25%	40%	25%	25%	40%	40%
Cement factor	5	5	6	5	6	5	6
f'_c at 28days (psi)	4514.8	5039.9	5344.2	5057.3	5553.4	4686.8	5237.2
Total heat (J/gm)	260	317.5	314	336.0	349.4	355.65	317.1
Set temperature Gradient	0.476	1.011	1.011	1.292	1.332	1.214	1.243
Set moisture Gradient	0.249	0.220	0.235	0.227	0.218	0.235	0.229

Using the C^{4}M program with input data for seven runs (table 4-6), the predicted time of cracking at the tip of notch was obtained for each test run as listed in table 4-7.

Table 4-7 C^{4}M program output data for seven runs

	Test 1	Test 2	Test 3	Test 4	Test 5	Test 6	Test 7
Predicted time of cracking (hours)	67.2	63.5	59.2	60.7	53.4	65.6	62.2

CHAPTER V

ANALYSIS ON CRACK CONTROL

TWO EXAMPLES OF C⁴M PROGRAM APPLICATION

In this chapter, two examples for applications of the C^4M program that are commonly designed and constructed in pavement construction will be introduced below. The first example is transverse crack control under different weather conditions and methods of sawcutting. From this example, it will be shown that how different weather conditions and methods of sawcutting affect crack control. The second example is longitudinal crack control under different ambient temperature and depth of sawcut. This example of the C^4M procedure will be shown that how the depth of sawcut affects the probability of cracking in a concrete slab.

Example I of C⁴M Procedure (Transverse Crack Control)

The jointing layout for a concrete pavement is shown in Figure 5-1. This case considers a 10 inch thickness slab with a width of 18 feet and no reinforcing. It is assumed that sawcutting is carried out to create transverse contraction joints at 16 feet interval with h/4 notch depth of 2.5 inches. In this example, the effect of weather conditions on cracking control (in four combinations of weather conditions) will be demonstrated relative to two key factors of ambient temperature and relative humidity as illustrated in Table 5-1.

Table 5-1 Four combinations of different climatic factors

Case	Climatic Condition	Ambient Temperature	Relative Humidity
1	High Temperature High Relative Humidity	90~105˚F	50~95%
2	High Temperature Low Relative Humidity	90~105˚F	10~50%
3	Low Temperature High Relative Humidity	60~80˚F	50~95%
4	Low Temperature Low Relative Humidity	60~80˚F	10~50%

Transverse Sawcut with h/4 notch depth

16ft

Paving Direction

18ft

10in
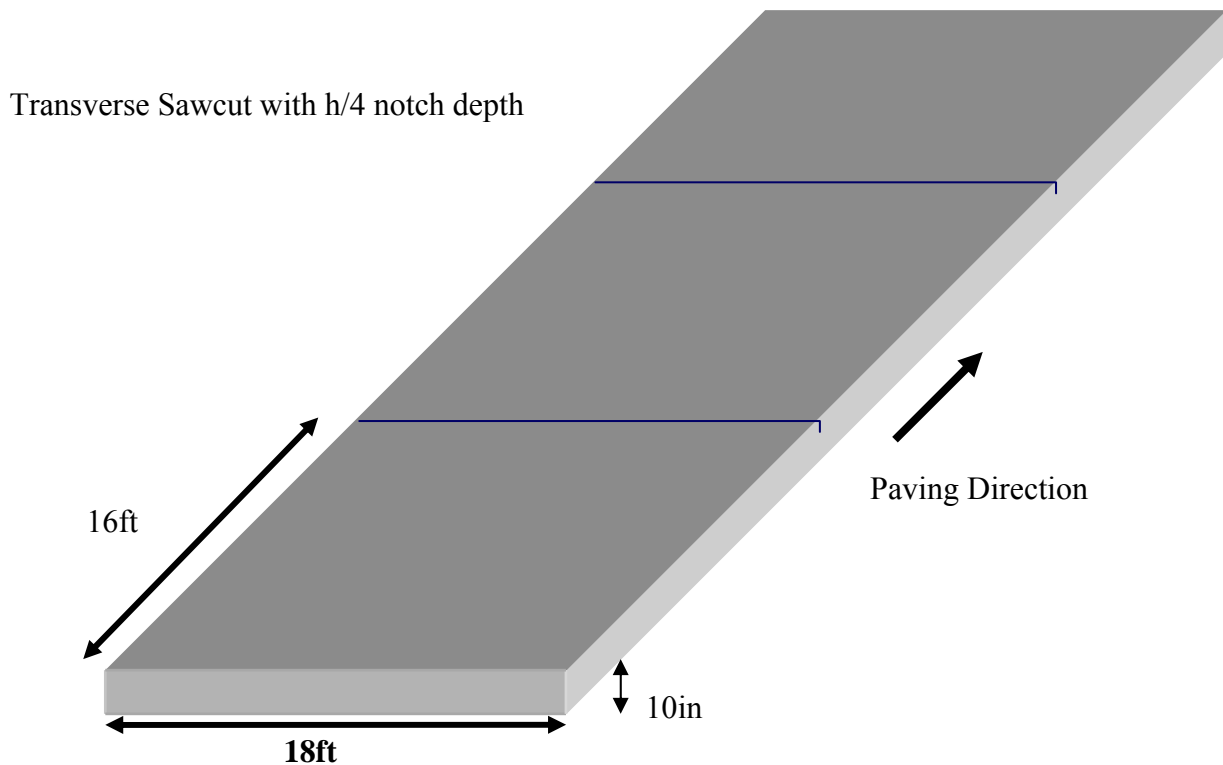
Figure 5-1 Designed slab for proper timing of sawcut.

This analysis presented below focuses on the control and incidence of transverse cracking as defined in terms of the difference between the probability of initiating a crack at the tip of sawcut notch and the greatest probability of a random crack developing at or prior to the time of initiation. Figure 5-2 shows that probability of controlled crack and random crack patterns as a function of time under high ambient temperature and relative humidity conditions.
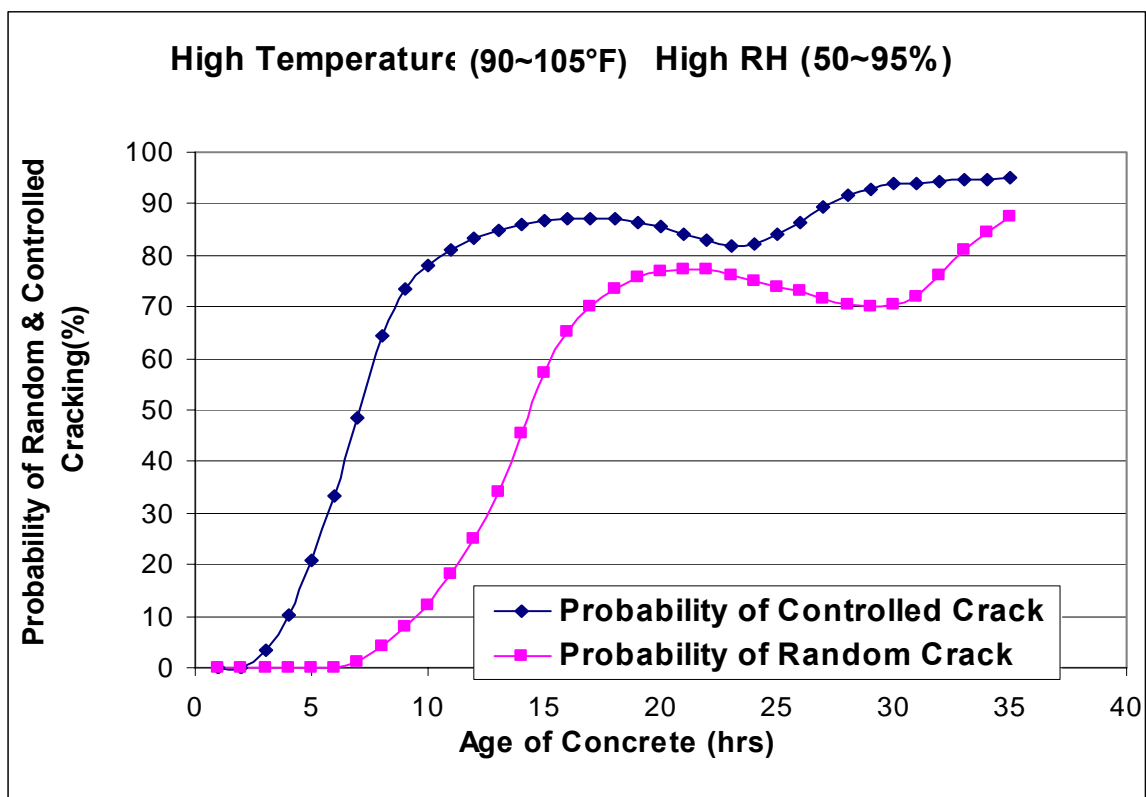
Figure 5-2 Probability of random and controlled cracking at high temperature and high RH weather condition.

By subtracting the probability of a random crack from the probability of initiating a crack at the tip of sawcut notch, an indicator of the best time for crack control can be obtained as shown in Figure 5-3.
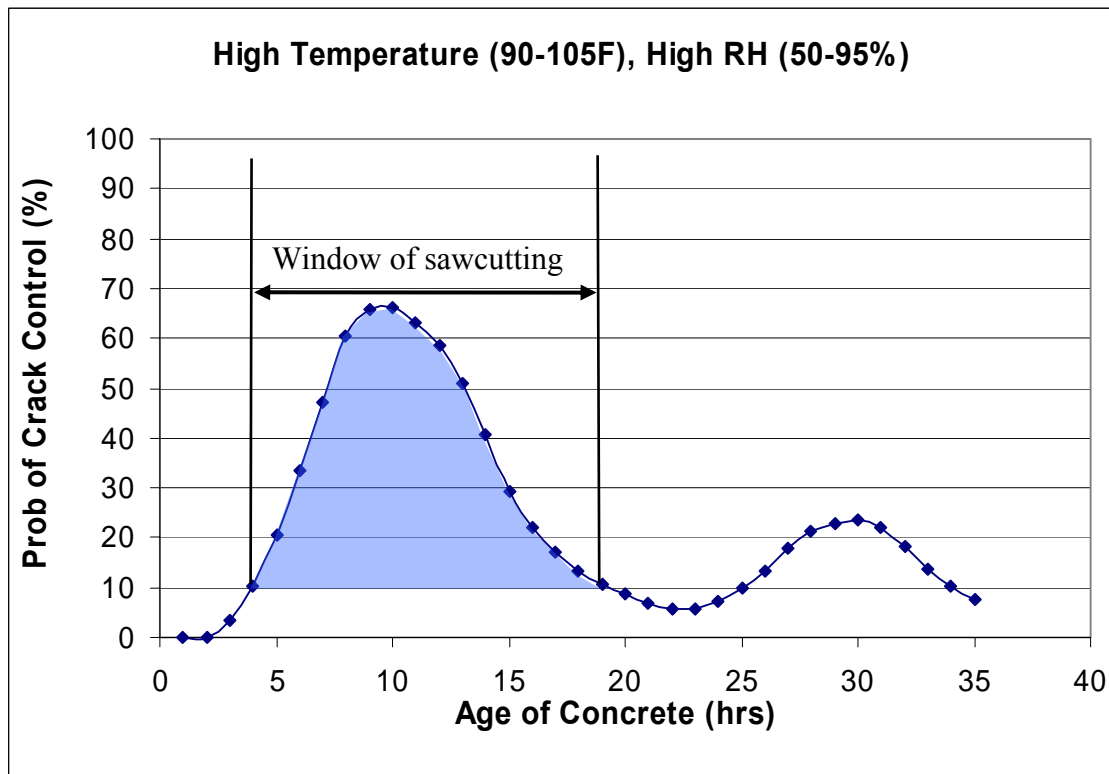
Figure 5-3 Probability of crack control with time.

The probabilities of crack control associated with each of weather condition shown in Table 5-1 are illustrated in bar charts in Figure 5-4 with respect to three different sawcut methods:

1. Early-entry sawing 3~5 hours after placement

2. Conventional sawing at the near-limit (the near limit occurs approximately 8 hours after placement of the concrete near the end of the day)

3. Conventional sawing 24 hours after placement (when many sawcutting operations are undertaken)

The results of each case shown in Figure 5-4 represent the condition that prevail associated with different methods of sawcutting under the climatic conditions delineated in Table 5-1. The results in each of these conditions are helpful in identifying limits associated with sawcutting operations. Typical cracking behavior can be derived from various combinations of the results at each climatic limit as to whether or not cracking can be controlled. In this respect, certain findings can be drawn from the charts shown in Figure 5-4.

Examination of each case in Figure 5-4 clearly indicates the superiority of early-entry sawcutting over conventional methods with respect to the control of random cracking in jointed pavement construction. A greater potential for crack control exists under the early-entry sawing due to its characteristically lower fracture toughness at an early age. The use of the early entry method shows the highest potential of crack control for all the climatic conditions while the conventional method shows much lower potential particularly in the low humidity condition. It is interesting to note that the most stringent condition for conventional sawing occurs with a low temperature and low humidity condition while early entry sawing has greater potential for crack control over 50% for all the climatic conditions.
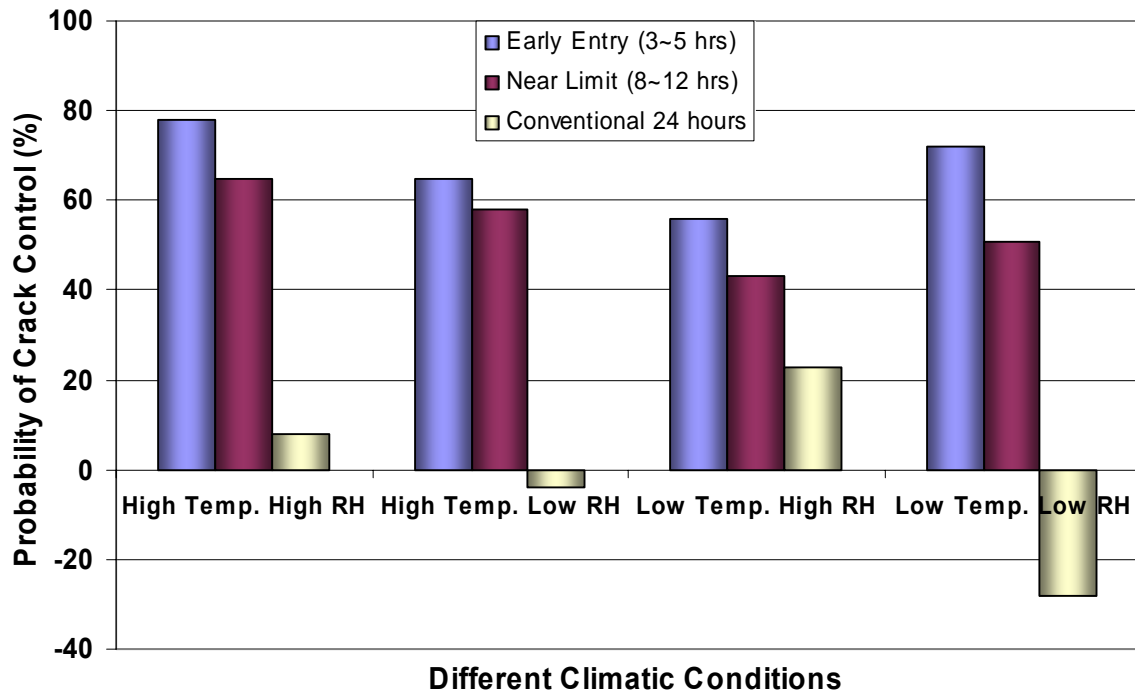
Figure 5-4 Probability of crack control for different methods of sawcutting.

Example II of C⁴M Procedure (Longitudinal Crack Control)

The jointing layout for a concrete pavement is shown in Figure 5-5. The slab has thickness of 13 inches, slab width of 18 feet, and 0.5 inch diameter reinforcing steel located 5.5 inches from the top of slab with 0.61 percent steel. It is assumed that sawcutting was operated to create a longitudinal contraction joint at 6 feet distance from the edge of concrete slab with two different sawcut depth, h/4 notch depth of 3.25 inches, and h/8 of 1.62. In this example, the effect of weather conditions and sawcut depth on cracking control will be demonstrated relative to two key factors of ambient temperature and initial crack ratio as illustrated in Table 5-2.

Table 5-2 Four combinations on longitudinal crack control

Case	Condition	Ambient Temperature	Initial Crack Ratio
1	High Temperature h/4, Initial crack ratio	90~105˚F	3.25 inches
2	High Temperature h/8, Initial crack ratio	90~105˚F	1.62 inches
3	Low Temperature h/4, Initial crack ratio	60~80˚F	3.25 inches
4	Low Temperature h/8, Initial crack ratio	60~80˚F	1.62 inches

Note: Ambient relative humidity is constant as 50~95%.

Longitudinal Sawcut with h/4 and h/8 notch depth

h = 13in
(Slab thickness)

6ft

18ft (Slab width)
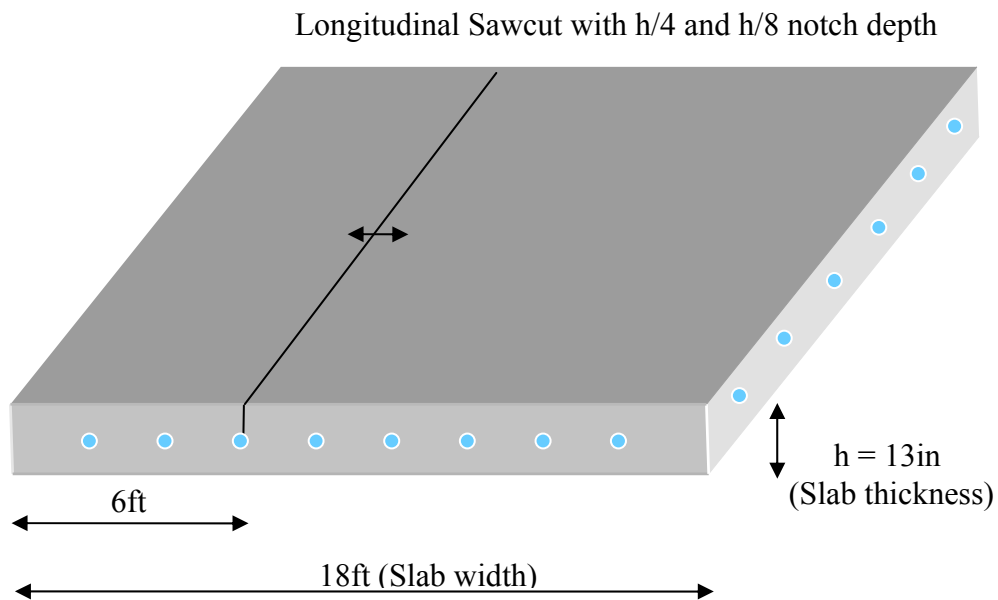
0.5 inch diameter reinforcing steel located 5.5 inches from surface
0.61 percent steel

Figure 5-5 Designed slab on longitudinal crack control.

First of all, the set temperatrure at the depth of steel was calculated under two different weather conditions as shown in table 5-3 using the TMAC^2 program. It is assumed that concrete placed in the morning, 7AM.

Table 5-3 Set temperature at steel depth for different ambient temperature

	High temperature (90~105˚F)	Low temperature (60~80˚F)
Set temp. at the depth of steel	118.9	82.96

This analysis presented below focuses on the control and incidence of longitudinal cracking as defined in terms of the difference between the probability of initiating a crack at the tip of sawcut notch and the greatest probability of a random crack developing at or prior to the time of initiation. Figure 5-6 shows that probability of controlled crack and random crack patterns as a function of time under high ambient temperature and h/4 sawcut depth. This figure shows that the probability of random cracking is dominant at an early age due to putting longitudinal sawcut in the wrong location. Although the probability of random cracking is greater than the probability of controlled cracking during most period for the first 36 hours, there is some period that the probability of controlled cracking is higher than the probability of random cracking for the first 10 hour after concrete paving. However, the probability of controlled cracking is less than 50% even though it has greater

value than the probability of random cracking within first 10 hours. It implies that there might be no chance to control cracking by sawcutting in this case.
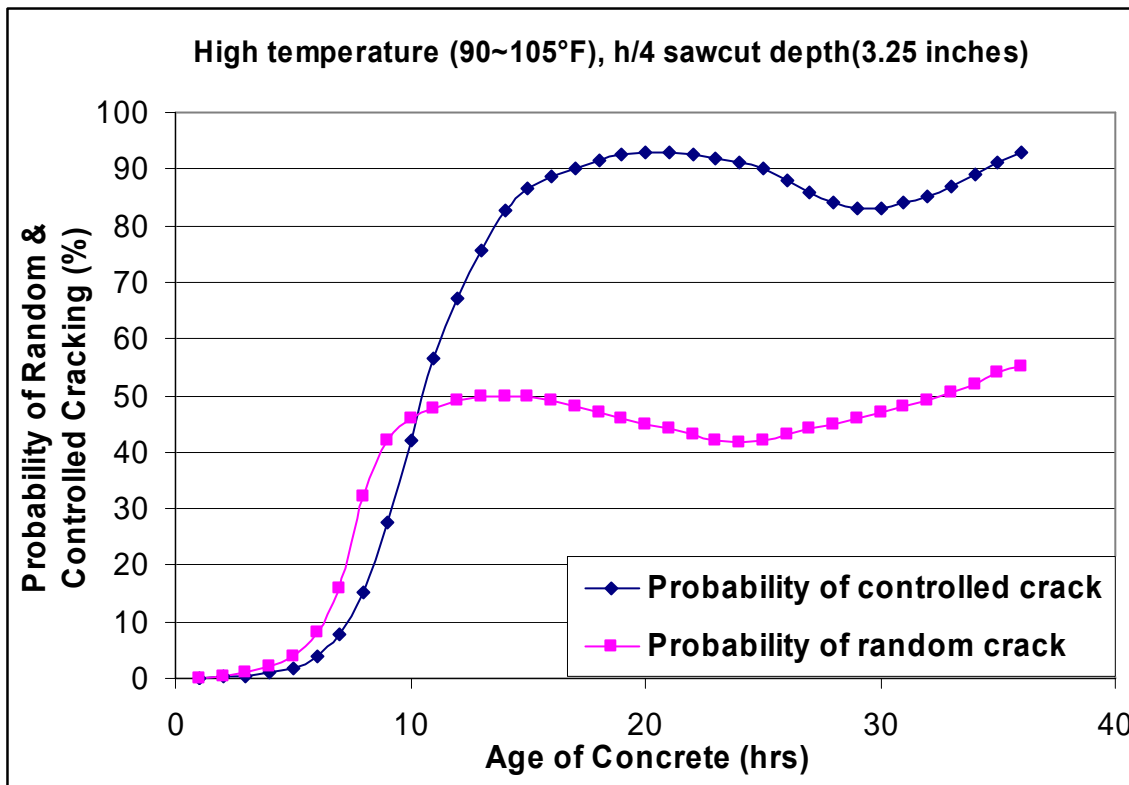

Figure 5-6 Probability of random and controlled cracking at high temperature and h/4 sawcut depth.

By subtracting the probability of a random crack from the probability of initiating a crack at the tip of sawcut notch, an indicator of the best time for crack control can be obtained as shown in Figure 5-7. In the same manner as case I (high ambient temperature and h/4 sawcut depth), the probability of crack control for other three cases listed in table 5-2 were also calculated.
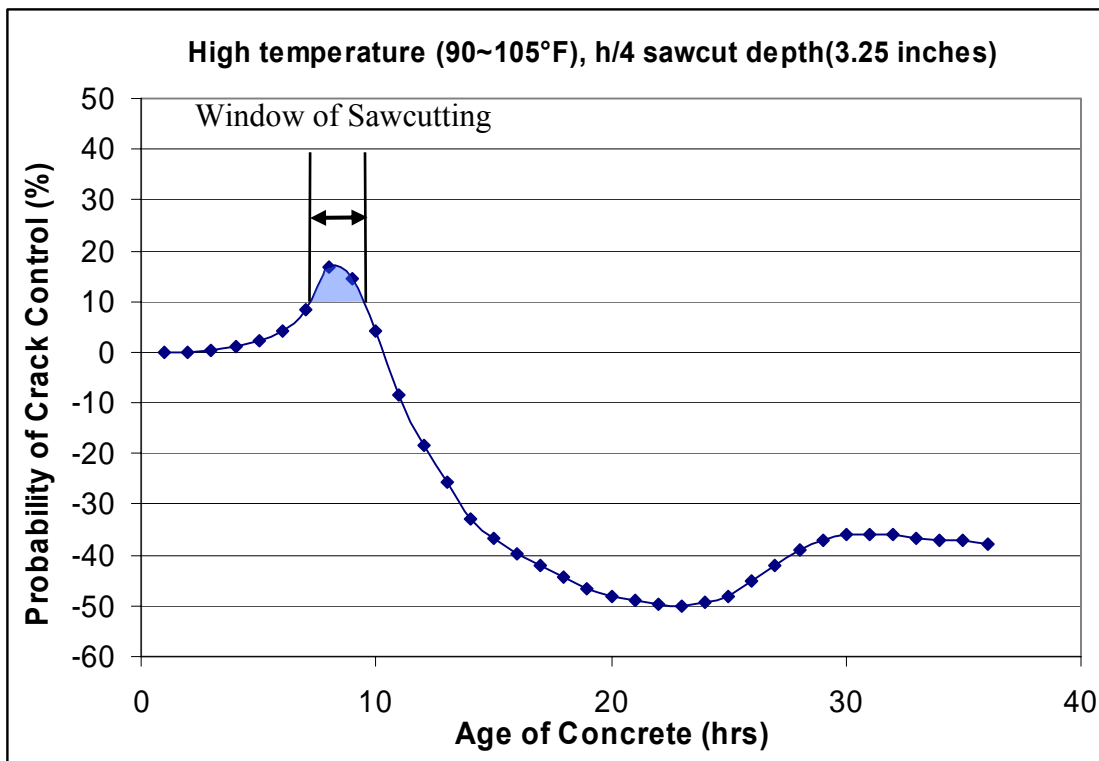
Figure 5-7 Probability of crack control with time.

The probabilities of crack control associated with each case shown in Table 5-2 are illustrated in bar charts in Figure 5-8 with respect to three different sawcut methods in the same manner as example of case I:

1. Early-entry sawing 3~5 hours after placement

2. Conventional sawing at the near-limit (the near limit occurs approximately 8 hours after placement of the concrete near the end of the day)

3. Conventional sawing 24 hours after placement (when many sawcutting operations are undertaken)

The results of each case shown in Figure 5-8 represent the condition that prevail associated with different methods of sawcutting for each case listed in Table 5-2. The results in each of these conditions are helpful in identifying limits associated with sawcutting operations. Examination of each case in Figure 5-8 clearly indicates that it is difficult to induce longitudinal controlled crack at the sawcut notch for all the types of sawcutting methods. However, early-entry sawcutting has positive probability of crack control compared to conventional methods with respect to in this case of jointing layout (putting longitudinal sawcut in the wrong location). It is interesting to note that crack control with h/8 sawcut depth has higher probability of crack control than those with h/4. A misconception held by many is that the deeper sawcut notch depth, the easilier it is to induce a crack at the tip of sawcut notch.
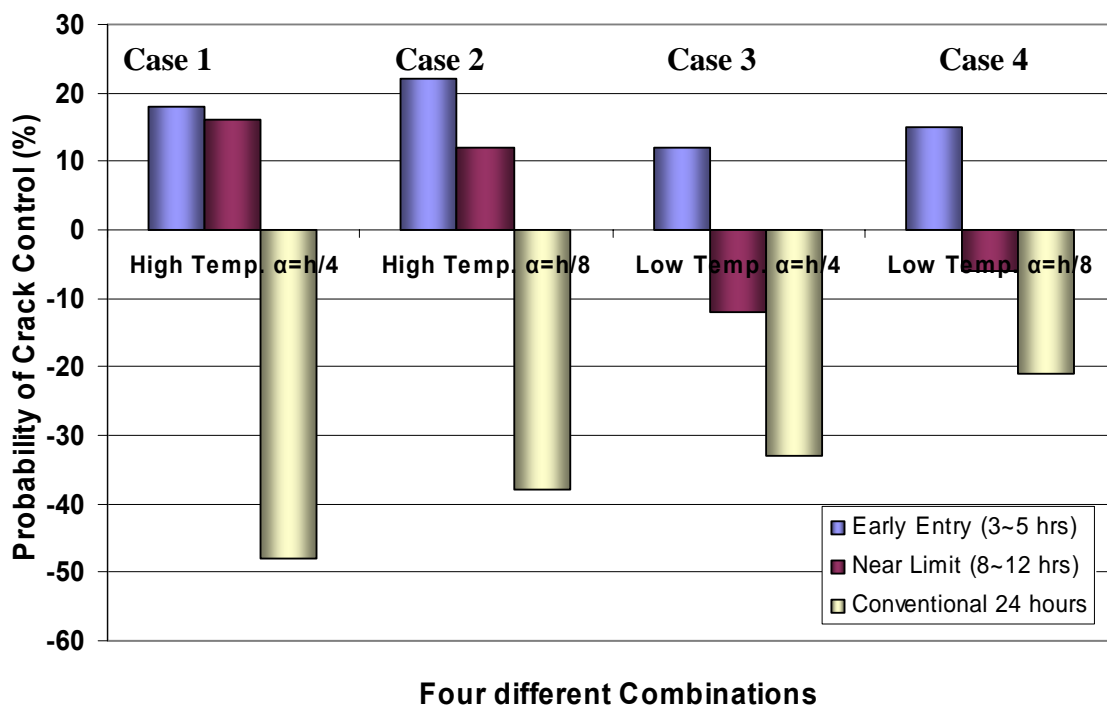
Figure 5-8 Probability of crack control for four different cases.

CHAPTER VI

CONCLUSIONS

It is observed that the controlled cracking formation occurred earlier at high placement temperature condition compared with at low placement temperature. In addition, concrete with high cement content such as cement factor 6 experienced cracking earlier than concrete with low cement content due to a high thermal (curling) stress induced by high positive set temperature gradient. However, the use of fly ash content greater than 25-30% is an effective way to delay the crack formation time up to 3 hours. From the results, the latest time of crack formation 67 hours was predicted for a concrete slab with mixture I (25% FA and CF 5) placed at 75°F (Test 1) whereas the earliest time of crack formation 53 hours was predicted for a concrete slab with mixture II (25% FA and CF6) placed at 105^0F (Test 5). Consequently, it is summarized that the sawcut timing is more sensitive under hot weather conditions compared with the contrary conditions.

As analyzed above, the tests conducted show that the cracking control of concrete slabs at sawcut notches at an early age can be achieved by estimating the cracking formation time using the predicted tensile strengths calculated by fracture mechanics and early aged tensile stresses caused by moisture and temperature changes throughout the depth of the concrete slab. Using the previous mentioned principles, the C^4M (Curing Concrete Crack Control and Management) program was developed to analyze the control of cracking in concrete slab. If the exact time when the cracking at the tip of a sawcut notch

occurs can be calculated and compared with the time random crack occurred on the concrete slab, the sawcuttting with appropriate time and sawcut depth can be assessed. Therefore, the C^{4}M program can be used to determine a suitable time, depth and location of sawcutting to avoid random cracking on concrete surface.

REFERENCES

1. *Design and Construction of Joints for concrete Highway*, Concrete Paving Technology, TB010.01P, American Concrete Pavement Association, 1991.

2. Okamoto, P.A., *Guidelines for Timing Contraction Joint Sawing and Earliest Loading for Concrete Pavements*, Vol. I-Final Report, Federal Highway Administration, McLean, VA, FHWA-RD-91-079, October 1991.

3. Okamoto, P.A., *Guidelines for Timing Contraction Joint Sawing and Earliest Loading for Concrete Pavements*, Vol. II-Appendix, Federal Highway Administration, McLean, VA, FHWA-RD-91-080, October 1991.

4. *Concrete Intersections-A Guide for Design and Construction,* Concrete Paving Technology, TB019.01P, American Concrete Pavement Association, 1998.

5. Darter, M.I., *Design of Zero-Maintenance Plain Jointed Pavements*, FHWA-RD-77-111, Federal Highway Administration, Washington DC, June 1977.

6. *Standard Specification for Deformed and Plain Billet-Steel Bars for Concrete Reinforcement*, Annual Book of ASTM Standards, Specification A615, West Conshohocken, PA, 1996.

7. *Corrosion-Resistant Coated Dowel Bars*, American Association of State Highway and Transportation Officials, Specification M254-77, Washington, D.C., 2000.

8. *Proper Use of Isolation and Expansion Joints in Concrete Pavemenets*, Concrete Paving Technology, IS400.01P, American Concrete Pavement Association, 1992.

9. *Epoxy Coated Steel Reinforcement*, American Association of State Highway and Transportation Officials, Specification M284-97, Washington, D.C., 2000.

10. *Standard Specification for Fabrication and Jobsite Handling of Epoxy-Coated Steel Reinforcing Bars*, Annual Book of ASTM Standards, Specification D3963, West Conshohocken, PA, 1994.

11. Jeong, J.H., *Characterization of Slab Behavior and Related Material Properties due to Temperature and Moisture effects*, Ph.D. Dissertation, Texas A&M University, College Station, TX.

12. Zollinger D.G., *Guide for Design of Jointed Concrete Pavements for Streets and Local Roads*, Proceedings, 7th International Conference on Concrete Pavements, Orlando, FL, Reported by Committee 325, March-2002, pp. 4-5.

13. Byfers, J., *Plane Concrete at Early Ages*, Research Report No.3-80, Swedish Cement and Concrete Research Institute, Stockholm, Sweden, 1980.

14. Neville, A.M., *Properties of Concrete*, 4th edition, John Wiley & Sons, Inc., New York, 1996.

15. Mindess, S. and J.F. Young, *Concrete*, Prentice-Hall, Inc., Englewood Cliffs, NJ.

16. Altoubat, S.A. and D.A. Lange, *Creep, Shrinkage, and Cracking of Restrained Concrete at Early Ages*, ACI Materials Journal, Vol. 98, No. 4, July-Aug. 2001.

17. Vepakomma, S., *Characterization of Cracking Restraint at Sawcut Joints Using the German Cracking Frame*, Thesis, Texas A&M University, College Station, TX.

18. Springenschmid, R., R. Breitenbucher, and M. Mangold, *Development of the Cracking Frame and the Temperature-Stress Testing Machine*, Proceedings of the International RILEM Symposium, Barcelona, 1994, pp. 90-115.

19. Bazant, Z.P., and S.T. Wu, *Creep and Shrinkage Law for Concrete at Variable Humidity*, J.Eng.Mech., ASCE, 100(6), pp. 1183-1209.

20. Reis, E.E., *Causes and Control of Cracking in Concrete Reinforced with High Strength Steel Bars-A Review of Research*, Engineering Experiment Station Bulletin 479, Amhearst, MA, 1992.

21. Jeong, J.H., N. Chapke, and D.G. Zollinger, *A Probabilistic Approach to Sawcut Timing and Depth Requirements for Newly Constructed Portland Cement Concrete Pavements*, Proceedings, 7th International Conference on Concrete Pavements, Vol.1, Orlando, Fl, Sept. 9-13, 2001, pp. 421-435.

22. Soares, J.B., *Concrete Characterization Through Fracture Mechanics and Selected Pavement Application*, Ph.D. Dissertation, Texas A&M University, College Station, 1997.

23. Tang, T., D. G. Zollinger, *Field Tests and Analysis of Concrete Pavement in Texarkana and La Porte,TX*, T.T.I Research Report 1244-7, Texas Transportation Institute, TX, 1996.

24. Mohamed, A.R. and W. Hansen, Effect of Nonlinear Temperature Gradient on Curling Stress in Concrete Pavement, *Transportation Research Record 1568*, Transportation Research Board, Washington DC,1996, pp. 128-132.

25. Bradbury, R.D., *Reinforced Concrete Pavement*, Wire Reinforcement Institute, Washington, DC, 1938.

26. Huang, Y.H., *Pavement Analysis and Design*, Prentice Hall, Inc., Englewood Cliffs, NJ, 1993.

27. Yoder, E.J., and M.M. Witczak, *Principles of Pavement Design*, 2nd Edition, A Wiley- Interscience Publication, Washington, D.C., 1975.

28. Tang, T., S.C. Yang, and D.G. Zollinger, *Determination of Fracture Energy and Process Zone Length Using Variable-Notch One-Size Specimens*, ACI Materials Journal, Vol. 96, No. 1, Jan.-Feb. 1999, pp. 3-10.

29. Yang, S.C., *A Temperature Prediction Model in New Concrete Pavement and A New Test Method for Concrete Fracture Parameters*, Ph.D. Dissertation, Texas A&M University, College Station, 1996.

30. Wang, L., *Precess and Prediction of Moisture and Temperature Distributions and History in Hardening Concrete*, Ph.D. Dissertation, Texas A&M University, College Station, 2000.

APPENDIX   A

MIX DESIGN AND RESULTS FOR SEVEN TEST RUNS

Table A-1 Mix component of *Mixture I* in a batch size (1 cubic yard)

Mixture Component	Proportions	Batch (lbm)
Cement	0.75	352.50
Fly Ash Class F	0.25	117.50
Coarse Aggregate	4.22	1985.28
Fine Aggregate (Sand)	2.87	1350.17
Net water	0.49	228.70
Air-entraining Admixture (ml)		150.40
Medium Range Water-reducing Admixture (ml)		1222.00
Water/Cementitious material Ratio	0.45	
Cement Factor	5	
Fly Ash Replacement Percent	25%	

Table A-2 Mix component of *Mixture II* in a batch size (1 cubic yard)

Mixture Component	Proportions	Batch (lbm)
Cement	0.75	423.00
Fly Ash Class F	0.25	141.00
Coarse Aggregate	3.52	1985.28
Fine Aggregate (Sand)	2.05	1154.98
Net water	0.48	269.86
Air-entraining Admixture (ml)		180.48
Medium Range Water-reducing Admixture (ml)		1466.40
Water/Cementitious material Ratio	0.45	
Cement Factor	6	
Fly Ash Replacement Percent	25%	

Table A-3 Mix component of *Mixture III* in a batch size (1 cubic yard)

Mixture Component	Proportions	Batch (lbm)
Cement	0.60	282.00
Fly Ash Class F	0.40	188.00
Coarse Aggregate	4.22	1985.28
Fine Aggregate (Sand)	2.83	1328.61
Net water	0.49	228.57
Air-entraining Admixture (ml)		150.40
Medium Range Water-reducing Admixture (ml)		1222.00
Water/Cementitious material Ratio	0.45	
Cement Factor	5	
Fly Ash Replacement Percent	40%	

Table A-4 Mix component of *Mixture IV* in a batch size (1 cubic yard)

Mixture Component	Proportions	Batch (lbm)
Cement	0.60	338.40
Fly Ash Class F	0.40	225.60
Coarse Aggregate	3.52	1985.28
Fine Aggregate (Sand)	2.00	1129.12
Net water	0.48	269.71
Air-entraining Admixture (ml)		180.48
Medium Range Water-reducing Admixture (ml)		1466.40
Water/Cementitious material Ratio	0.45	
Cement Factor	6	
Fly Ash Replacement Percent	40%	

Table A-5 Set maturity and set temperature

	Initial Set Time (hr)	Initial Set Maturity (℃-hr)	Final Set Time (hr)	Final Set Maturity (℃-hr)	Final Set Temp. (℃)	Final Set Temp. (℉)
Test 1 (75℉/25/5)	7.60	287.80	9.78	372.62	28.9	84.02
Test 2 (95℉/25/5)	6.34	262.70	8.03	334.80	34.8	94.64
Test 3 (95℉/25/6)	6.66	280.53	8.20	349.29	35.4	95.72
Test 4 (105℉/25/5)	5.08	245.35	6.51	324.88	39.5	103.10
Test 5 (105℉/25/6)	5.36	266.76	6.55	333.15	42.6	108.68
Test 6 (105℉/40/5)	5.4	269.73	6.82	345.59	42.9	109.22
Test 7 (105℉/40/6)	5.75	274.83	6.93	335.57	42.3	108.14

Table A-6 Development of heat of hydration (J/gm)

AHS (J/gm)	1 Day	2 Days	3 Days	4 Days	28 Days	90 Days
Test 1 (75˚F/25/5)	151.0	214.00	238.0	-	258.0	260.0
Test 2 (95˚F/25/5)	198.41	256.56	277.49	291.12	312.15	317.50
Test 3 (95˚F/25/6)	209.11	267.96	286.80	293.77	311.22	314.01
Test 4 (105˚F/25/5)	213.0	269.0	288.0	298.5	330.5	346.0
Test 5 (105˚F/25/6)	218.64	278.65	299.59	309.36	335.87	349.37
Test 6 (105˚F/40/5)	193.06	145.16	266.33	281.12	326.57	355.65
Test 7 (105˚F/40/6)	193.29	257.49	281.45	291.68	310.98	317.03

Table A-7 Compressive strength for each test

Strength (psi)	Test 1 (75˚F/25/5)	Test 2 (95˚F/25/5)	Test 3 (95˚F/25/6)	Test 4 (105˚F/25/5)	Test 5 (105˚F/25/6)	Test 6 (105˚F/40/5)	Test 7 (105˚F/40/6)
1 Day	1378.36	1419.91	2135.53	1619.86	2120.95	1703.12	2156.0
3 Days	2313.37	2518.09	3318.72	3081.11	3332.27	2553.52	3185.0
7 Days	3015.14	3553.48	4395.20	4199.95	4531.31	3469.67	4077.1
28 Days	4514.79	5039.92	5344.23	5057.26	5553.47	4686.82	5237.2
Required time to achieve 555psi MoR	55days	35days	30days	34days	21days	49days	41days

APPENDIX   B

DATA FROM ANALYSIS OF CRACKING FRAME TEST

Age (Hrs)	ΔT	Total Strain	Epcc	Cki	Stress at top surface	Stress at tip of notch	Tensile Strength
0	0.0000	0.000000	0.00		0.00	0.00	0.00
1	-0.1333	0.000015	407542.54	0.46	3.70	2.46	15.01
2	-0.2000	0.000020	416267.98	0.45	4.94	3.29	15.34
3	-0.1667	0.000038	434283.29	0.44	9.61	6.41	16.00
4	-0.1000	0.000043	472686.65	0.41	11.84	7.89	17.41
5	-0.1667	0.000043	559981.63	0.37	14.16	9.44	20.63
6	-0.2000	0.000042	785913.34	0.29	19.49	12.99	28.95
7	-0.0667	0.000043	1065009.98	0.22	26.90	17.93	39.24
8	-0.1000	0.000045	1257670.00	0.19	33.56	22.38	46.34
9	-0.1667	0.000046	1405861.24	0.18	38.33	25.56	51.79
10	-0.1333	0.000047	1526279.06	0.16	41.84	27.89	56.23
11	-0.1000	0.000046	1627553.14	0.16	44.09	29.40	59.96
12	-0.0667	0.000045	1714794.42	0.15	45.85	30.57	63.18
13	0.1333	0.000046	1791300.45	0.14	48.25	32.17	66.00
14	0.0667	0.000045	1859329.55	0.14	48.79	32.52	68.50
15	0.1000	0.000044	1920498.33	0.13	50.02	33.35	70.76
16	0.1000	0.000043	1976004.54	0.13	50.43	33.62	72.80
17	0.1333	0.000043	2026760.44	0.13	50.70	33.80	74.67
18	0.1000	0.000042	2073476.78	0.13	50.81	33.87	76.39
19	-0.2000	0.000039	2116717.95	0.12	48.63	32.42	77.98
20	-0.2667	0.000039	2156939.47	0.12	49.06	32.71	79.47
21	-0.3000	0.000040	2194514.17	0.12	51.02	34.01	80.85
22	0.1333	0.000044	2229750.95	0.12	57.79	38.53	82.15
23	0.1333	0.000044	2262908.55	0.12	58.49	39.00	83.37
24	0.6000	0.000048	2294205.74	0.11	64.55	43.03	84.52
25	0.9667	0.000050	2323829.12	0.11	68.81	45.87	85.61
26	1.1000	0.000050	2351939.08	0.11	69.42	46.28	86.65
27	1.1333	0.000049	2378674.42	0.11	68.86	45.91	87.64
28	1.1333	0.000049	2404156.09	0.11	68.86	45.91	88.57
29	1.2333	0.000050	2428490.02	0.11	71.07	47.38	89.47
30	1.2333	0.000051	2451769.55	0.11	74.17	49.44	90.33
31	1.2000	0.000054	2474077.30	0.11	78.17	52.11	91.15

Age	ΔT	Total Strain	Epcc	Cki	Stress at top surface	Stress at tip of notch	Tensile Strength
32	1.2000	0.000057	2495486.74	0.11	83.62	55.75	91.94
33	1.2000	0.000061	2516063.47	0.11	90.46	60.31	92.70
34	1.1667	0.000066	2535866.32	0.10	97.87	65.24	93.43
35	1.1667	0.000070	2554948.22	0.10	105.71	70.48	94.13
36	1.1000	0.000075	2573356.96	0.10	112.81	75.21	94.81
37	0.9333	0.000078	2591135.84	0.10	118.83	79.22	95.46
38	0.8667	0.000082	2608324.17	0.10	125.32	83.55	96.10
39	0.8000	0.000085	2624957.81	0.10	131.78	87.85	96.71
40	0.8000	0.000088	2641069.48	0.10	136.99	91.33	97.30
41	0.8000	0.000090	2656689.17	0.10	140.50	93.67	97.88
42	0.7667	0.000091	2671844.41	0.10	142.57	95.05	98.44
43	0.7667	0.000091	2686560.52	0.10	143.62	95.75	98.98
44	0.6667	0.000089	2700860.87	0.10	142.03	94.68	99.51
45	0.6667	0.000089	2714767.02	0.10	141.84	94.56	100.02
46	0.6000	0.000088	2728298.96	0.10	141.07	94.04	100.52
47	0.5333	0.000087	2741475.22	0.10	140.53	93.69	101.00
48	0.5000	0.000087	2754313.00	0.10	140.62	93.74	101.47
49	0.5667	0.000087	2766828.33	0.10	142.40	94.93	101.94
50	0.6000	0.000088	2779036.15	0.10	143.94	95.96	102.39
51	0.4333	0.000087	2790950.39	0.10	142.80	95.20	102.82
52	0.3667	0.000087	2802584.08	0.10	143.52	95.68	103.25
53	0.3333	0.000087	2813949.44	0.09	144.58	96.38	103.67
54	0.3333	0.000088	2825057.90	0.09	146.81	97.87	104.08
55	0.3333	0.000089	2835920.20	0.09	149.13	99.42	104.48
56	0.2667	0.000091	2846546.43	0.09	152.02	101.34	104.87
57	0.2667	0.000093	2856946.10	0.09	155.94	103.96	105.26
58	0.2333	0.000094	2867128.16	0.09	159.10	106.07	105.63
59	0.2667	0.000096	2877101.04	0.09	161.83	107.89	106.00
60	0.2667	0.000097	2886872.71	0.09	164.35	109.57	106.36
61	0.3000	0.000099	2896450.71	0.09	168.20	112.13	106.71
62	0.3000	0.000100	2905842.15	0.09	170.72	113.81	107.06
63	0.2000	0.000100	2915053.79	0.09	171.43	114.29	107.40

Age	ΔT	Total Strain	Epcc	Cki	Stress at top surface	Stress at tip of notch	Tensile Strength
64	0.0333	0.000100	2924092.02	0.09	171.55	114.37	107.73
65	-0.1000	0.000100	2932962.92	0.09	172.00	114.67	108.06
66	-0.1333	0.000100	2941672.23	0.09	173.34	115.56	108.38
67	-0.0333	0.000102	2950225.43	0.09	176.60	117.73	108.69
68	0.0000	0.000103	2958627.74	0.09	179.19	119.46	109.00
69	-0.0333	0.000103	2966884.11	0.09	180.62	120.41	109.31
70	-0.3333	0.000101	2974999.25	0.09	177.14	118.09	109.61
71	-0.5000	0.000100	2982977.67	0.09	175.89	117.26	109.90
72	-0.5000	0.000101	2990823.66	0.09	178.39	118.93	110.19
73	-0.5333	0.000102	2998541.32	0.09	179.72	119.81	110.47
74	-0.5333	0.000102	3006134.57	0.09	181.09	120.73	110.75
75	-0.4667	0.000101	3013607.14	0.09	178.81	119.20	111.03
76	-0.4667	0.000082	3020962.61	0.09	145.58	97.06	111.30
77	-0.5333	0.000074	3028204.42	0.09	132.61	88.41	111.57
78	-0.5667	0.000074	3035335.83	0.09	131.90	87.94	111.83
79	-0.6000	0.000073	3042360.00	0.09	131.11	87.41	112.09
80	-0.5667	0.000074	3049279.93	0.09	132.42	88.28	112.34
81	-0.6333	0.000074	3056098.52	0.09	132.22	88.15	112.59
82	-0.6333	0.000076	3062818.55	0.09	136.47	90.98	112.84
83	-0.6000	0.000079	3069442.67	0.09	141.79	94.52	113.08
84	-0.5667	0.000081	3075973.45	0.09	146.79	97.86	113.33
85	-0.5000	0.000084	3082413.35	0.09	151.82	101.21	113.56
86	-0.4000	0.000087	3088764.73	0.09	157.41	104.94	113.80
87	-0.3667	0.000089	3095029.88	0.09	161.23	107.49	114.03
88	-0.3333	0.000090	3101210.98	0.09	164.21	109.47	114.26
89	-0.2667	0.000093	3107310.15	0.09	169.19	112.80	114.48
90	-0.2333	0.000096	3113329.42	0.09	175.95	117.30	114.70
91	-0.2000	0.000099	3119270.76	0.09	181.94	121.29	114.92
92	-0.1667	0.000100	3125136.05	0.09	183.50	122.34	115.14
93	-0.1333	0.000099	3130927.13	0.09	181.60	121.06	115.35
94	-0.0667	0.000098	3136645.74	0.09	180.23	120.15	115.56
95	0.0333	0.000097	3142293.59	0.09	179.69	119.80	115.77

Age	ΔT	Total Strain	Epcc	Cki	Stress at top surface	Stress at tip of notch	Tensile Strength
96	0.0000	0.000097	3147872.33	0.09	179.65	119.77	115.97
97	0.0667	0.000099	3153383.54	0.09	183.90	122.60	116.18
98	0.0667	0.000100	3158828.76	0.09	185.88	123.92	116.38
99	0.1000	0.000101	3164209.47	0.09	187.24	124.83	116.58
100	0.0667	0.000101	3169527.10	0.09	188.16	125.44	116.77
101	0.1000	0.000101	3174783.04	0.08	188.74	125.83	116.97
102	0.1667	0.000102	3179978.64	0.08	190.78	127.19	117.16
103	0.1667	0.000103	3185115.20	0.08	192.74	128.50	117.35
104	0.1333	0.000104	3190193.98	0.08	194.46	129.64	117.53
105	-0.0333	0.000104	3195216.20	0.08	195.23	130.15	117.72
106	-0.0333	0.000106	3200183.05	0.08	200.18	133.45	117.90
107	0.0000	0.000110	3205095.67	0.08	206.59	137.73	118.08
108	-0.0333	0.000112	3209955.18	0.08	211.32	140.88	118.26
109	0.0333	0.000113	3214762.65	0.08	212.87	141.91	118.44
110	0.0333	0.000112	3219519.14	0.08	212.08	141.38	118.61
111	0.0000	0.000111	3224225.66	0.08	210.73	140.49	118.79
112	-0.0333	0.000110	3228883.20	0.08	209.16	139.44	118.96
113	0.0333	0.000110	3233492.72	0.08	209.09	139.39	119.13
114	0.0333	0.000109	3238055.15	0.08	208.10	138.73	119.30
115	0.0667	0.000109	3242571.40	0.08	208.56	139.04	119.46
116	0.0000	0.000111	3247042.35	0.08	211.21	140.80	119.63
117	0.0000	0.000112	3251468.85	0.08	214.53	143.02	119.79
118	-0.0333	0.000113	3255851.73	0.08	217.35	144.90	119.95
119	0.0000	0.000115	3260191.81	0.08	220.54	147.03	120.11
120	-0.0333	0.000114	3264489.88	0.08	219.85	146.57	120.27
121	-0.2333	0.000112	3268746.69	0.08	215.15	143.44	120.43
122	-0.2000	0.000111	3272963.00	0.08	213.78	142.52	120.58
123	0.0333	0.000113	3277139.53	0.08	217.10	144.73	120.74
124	0.0333	0.000112	3281276.99	0.08	216.65	144.43	120.89
125	0.0333	0.000112	3285376.08	0.08	216.21	144.14	121.04
126	0.0333	0.000112	3289437.45	0.08	216.08	144.05	121.19

Age	FrameStrain	Force(lb)	Force Strain	Incremental Creep strain	Accumulative Creep Strain
0	0.00E+00	0.00E+00	0.00E+00	0.00E+00	0.00E+00
1	1.20E-06	2.32E+01	3.25E-06	1.10E-05	1.10E-05
2	1.80E-06	3.48E+01	4.77E-06	1.36E-05	2.46E-05
3	3.00E-06	5.80E+01	7.62E-06	2.70E-05	5.16E-05
4	4.80E-06	9.28E+01	1.12E-05	2.66E-05	7.82E-05
5	7.20E-06	1.39E+02	1.42E-05	2.16E-05	9.98E-05
6	7.80E-06	1.51E+02	1.09E-05	2.34E-05	1.23E-04
7	8.40E-06	1.62E+02	8.70E-06	2.58E-05	1.49E-04
8	9.60E-06	1.86E+02	8.42E-06	2.74E-05	1.76E-04
9	1.08E-05	2.09E+02	8.47E-06	2.71E-05	2.03E-04
10	1.38E-05	2.67E+02	9.97E-06	2.28E-05	2.26E-04
11	1.68E-05	3.25E+02	1.14E-05	1.79E-05	2.44E-04
12	2.04E-05	3.94E+02	1.31E-05	1.19E-05	2.56E-04
13	2.22E-05	4.29E+02	1.37E-05	9.93E-06	2.66E-04
14	2.58E-05	4.99E+02	1.53E-05	3.51E-06	2.70E-04
15	2.94E-05	5.68E+02	1.69E-05	-2.00E-06	2.68E-04
16	3.06E-05	5.92E+02	1.71E-05	-4.29E-06	2.63E-04
17	3.48E-05	6.73E+02	1.89E-05	-1.12E-05	2.52E-04
18	3.72E-05	7.19E+02	1.98E-05	-1.53E-05	2.37E-04
19	4.08E-05	7.89E+02	2.13E-05	-2.30E-05	2.14E-04
20	4.50E-05	8.70E+02	2.30E-05	-2.93E-05	1.84E-04
21	4.62E-05	8.93E+02	2.32E-05	-2.99E-05	1.55E-04
22	4.74E-05	9.16E+02	2.34E-05	-2.68E-05	1.28E-04
23	4.98E-05	9.63E+02	2.43E-05	-3.01E-05	9.76E-05
24	5.40E-05	1.04E+03	2.59E-05	-3.21E-05	6.55E-05
25	5.58E-05	1.08E+03	2.65E-05	-3.19E-05	3.36E-05
26	5.52E-05	1.07E+03	2.59E-05	-3.09E-05	2.69E-06
27	5.64E-05	1.09E+03	2.61E-05	-3.33E-05	-3.06E-05
28	5.70E-05	1.10E+03	2.61E-05	-3.44E-05	-6.51E-05
29	5.64E-05	1.09E+03	2.56E-05	-3.23E-05	-9.73E-05
30	5.52E-05	1.07E+03	2.48E-05	-2.86E-05	-1.26E-04

Age	FrameStrain	Force(lb)	Force Strain	Incremental Creep strain	Accumulative Creep Strain
31	5.46E-05	1.06E+03	2.43E-05	-2.52E-05	-1.51E-04
32	5.40E-05	1.04E+03	2.39E-05	-2.09E-05	-1.72E-04
33	5.28E-05	1.02E+03	2.31E-05	-1.48E-05	-1.87E-04
34	5.46E-05	1.06E+03	2.37E-05	-1.27E-05	-2.00E-04
35	5.34E-05	1.03E+03	2.30E-05	-6.10E-06	-2.06E-04
36	5.16E-05	9.98E+02	2.21E-05	8.17E-07	-2.05E-04
37	5.04E-05	9.74E+02	2.14E-05	6.12E-06	-1.99E-04
38	4.98E-05	9.63E+02	2.10E-05	1.08E-05	-1.88E-04
39	4.92E-05	9.51E+02	2.07E-05	1.55E-05	-1.72E-04
40	4.98E-05	9.63E+02	2.08E-05	1.76E-05	-1.55E-04
41	5.10E-05	9.86E+02	2.12E-05	1.77E-05	-1.37E-04
42	5.04E-05	9.74E+02	2.08E-05	1.95E-05	-1.18E-04
43	5.10E-05	9.86E+02	2.09E-05	1.90E-05	-9.86E-05
44	5.34E-05	1.03E+03	2.18E-05	1.42E-05	-8.44E-05
45	5.04E-05	9.74E+02	2.05E-05	1.80E-05	-6.65E-05
46	4.98E-05	9.63E+02	2.01E-05	1.80E-05	-4.85E-05
47	4.92E-05	9.51E+02	1.98E-05	1.82E-05	-3.04E-05
48	5.04E-05	9.74E+02	2.02E-05	1.62E-05	-1.41E-05
49	5.10E-05	9.86E+02	2.03E-05	1.62E-05	2.03E-06
50	5.16E-05	9.98E+02	2.05E-05	1.60E-05	1.80E-05
51	5.22E-05	1.01E+03	2.06E-05	1.42E-05	3.22E-05
52	5.28E-05	1.02E+03	2.08E-05	1.35E-05	4.57E-05
53	5.34E-05	1.03E+03	2.09E-05	1.30E-05	5.87E-05
54	5.64E-05	1.09E+03	2.20E-05	9.94E-06	6.86E-05
55	5.94E-05	1.15E+03	2.31E-05	6.91E-06	7.55E-05
56	6.06E-05	1.17E+03	2.35E-05	6.72E-06	8.22E-05
57	6.12E-05	1.18E+03	2.36E-05	7.97E-06	9.02E-05
58	6.18E-05	1.19E+03	2.38E-05	8.77E-06	9.90E-05
59	6.24E-05	1.21E+03	2.39E-05	9.31E-06	1.08E-04
60	6.36E-05	1.23E+03	2.43E-05	8.89E-06	1.17E-04
61	6.42E-05	1.24E+03	2.44E-05	1.01E-05	1.27E-04
62	6.24E-05	1.21E+03	2.37E-05	1.38E-05	1.41E-04

Age	FrameStrain	Force(lb)	Force Strain	Incremental Creep strain	Accumulative Creep Strain
63	6.12E-05	1.18E+03	2.31E-05	1.56E-05	1.57E-04
64	6.00E-05	1.16E+03	2.26E-05	1.71E-05	1.74E-04
65	6.06E-05	1.17E+03	2.28E-05	1.63E-05	1.90E-04
66	6.18E-05	1.19E+03	2.32E-05	1.52E-05	2.05E-04
67	6.12E-05	1.18E+03	2.29E-05	1.77E-05	2.23E-04
68	6.18E-05	1.19E+03	2.30E-05	1.81E-05	2.41E-04
69	6.12E-05	1.18E+03	2.27E-05	1.96E-05	2.61E-04
70	6.24E-05	1.21E+03	2.31E-05	1.57E-05	2.76E-04
71	6.30E-05	1.22E+03	2.33E-05	1.40E-05	2.90E-04
72	6.18E-05	1.19E+03	2.28E-05	1.68E-05	3.07E-04
73	6.30E-05	1.22E+03	2.32E-05	1.57E-05	3.23E-04
74	6.42E-05	1.24E+03	2.35E-05	1.47E-05	3.38E-04
75	6.24E-05	1.21E+03	2.28E-05	1.56E-05	3.53E-04
76	6.30E-05	1.22E+03	2.30E-05	1.40E-05	3.67E-04
77	6.36E-05	1.23E+03	2.32E-05	1.20E-05	3.79E-04
78	6.42E-05	1.24E+03	2.33E-05	1.10E-05	3.90E-04
79	6.48E-05	1.25E+03	2.35E-05	1.00E-05	4.00E-04
80	6.54E-05	1.26E+03	2.36E-05	9.00E-06	4.09E-04
81	6.42E-05	1.24E+03	2.32E-05	7.00E-06	4.16E-04
82	6.48E-05	1.25E+03	2.33E-05	6.00E-06	4.22E-04
83	6.36E-05	1.23E+03	2.28E-05	4.00E-06	4.26E-04
84	6.30E-05	1.22E+03	2.26E-05	2.00E-06	4.28E-04
85	6.24E-05	1.21E+03	2.23E-05	1.00E-06	4.29E-04
86	6.30E-05	1.22E+03	2.25E-05	1.15E-06	4.30E-04
87	6.36E-05	1.23E+03	2.27E-05	2.30E-06	4.33E-04
88	6.48E-05	1.25E+03	2.30E-05	2.18E-06	4.35E-04
89	6.42E-05	1.24E+03	2.28E-05	1.00E-06	4.36E-04
90	6.30E-05	1.22E+03	2.23E-05	1.00E-06	4.37E-04
91	6.36E-05	1.23E+03	2.25E-05	1.00E-06	4.38E-04
92	6.42E-05	1.24E+03	2.26E-05	2.00E-06	4.40E-04
93	6.48E-05	1.25E+03	2.28E-05	1.00E-06	4.41E-04
94	6.36E-05	1.23E+03	2.24E-05	1.00E-06	4.42E-04

Age	FrameStrain	Force(lb)	Force Strain	Incremental Creep strain	Accumulative Creep Strain
95	6.30E-05	1.22E+03	2.21E-05	1.00E-06	4.43E-04
96	6.24E-05	1.21E+03	2.19E-05	1.00E-06	4.44E-04
97	6.36E-05	1.23E+03	2.22E-05	2.00E-06	4.46E-04
98	6.24E-05	1.21E+03	2.18E-05	2.00E-06	4.48E-04
99	6.18E-05	1.19E+03	2.15E-05	1.00E-06	4.49E-04
100	6.12E-05	1.18E+03	2.13E-05	1.00E-06	4.50E-04
101	6.30E-05	1.22E+03	2.19E-05	1.00E-06	4.51E-04
102	6.24E-05	1.21E+03	2.16E-05	1.00E-06	4.52E-04
103	6.42E-05	1.24E+03	2.22E-05	1.00E-06	4.53E-04
104	6.48E-05	1.25E+03	2.24E-05	1.00E-06	4.54E-04
105	6.54E-05	1.26E+03	2.26E-05	1.00E-06	4.55E-04
106	6.18E-05	1.19E+03	2.13E-05	2.32E-05	4.78E-04
107	6.12E-05	1.18E+03	2.11E-05	2.73E-05	5.05E-04
108	6.06E-05	1.17E+03	2.08E-05	3.05E-05	5.36E-04
109	6.24E-05	1.21E+03	2.14E-05	2.88E-05	5.65E-04
110	6.30E-05	1.22E+03	2.16E-05	2.74E-05	5.92E-04
111	6.48E-05	1.25E+03	2.22E-05	2.42E-05	6.16E-04
112	6.54E-05	1.26E+03	2.23E-05	2.24E-05	6.39E-04
113	6.60E-05	1.28E+03	2.25E-05	2.14E-05	6.60E-04
114	6.72E-05	1.30E+03	2.29E-05	1.92E-05	6.79E-04
115	6.54E-05	1.26E+03	2.22E-05	2.17E-05	7.01E-04
116	6.42E-05	1.24E+03	2.18E-05	2.46E-05	7.26E-04
117	6.48E-05	1.25E+03	2.20E-05	2.54E-05	7.51E-04
118	6.54E-05	1.26E+03	2.21E-05	2.59E-05	7.77E-04
119	6.42E-05	1.24E+03	2.17E-05	2.91E-05	8.06E-04
120	6.24E-05	1.21E+03	2.11E-05	3.10E-05	8.37E-04
121	6.30E-05	1.22E+03	2.12E-05	2.76E-05	8.65E-04
122	6.42E-05	1.24E+03	2.16E-05	2.52E-05	8.90E-04
123	6.48E-05	1.25E+03	2.18E-05	2.60E-05	9.16E-04
124	6.54E-05	1.26E+03	2.20E-05	2.49E-05	9.41E-04
125	6.60E-05	1.28E+03	2.21E-05	2.37E-05	9.64E-04
126	6.72E-05	1.30E+03	2.25E-05	2.19E-05	9.86E-04

VITA

Name   Se Hoon Jang

Education

Master of Science in Civil Engineering
Texas A&M University, College Station, TX, 2005

Bachelor of Science in Civil Engineering
Kyungpook National University, Daegu, Korea, 2002

Work Experience

Research Assistant   (02/01/2004 ~ Present)
Texas Transportation Institute, Texas A&M System, College Station, Texas
- Perform Concrete Lab. Tests such as Strength Test, Heat of Hydration Test, Drying Shrinkage Test, Penetration Test, Cracking Frame Test, etc
- Analyze Concrete Test Data and Conduct Concrete Pavement Properties Modeling
- Simulate Random and Controlled Cracking Formation on CRCP utilizing VBA
- Prepare Proposals and Technical Reports

Permanent Address

Samsung Remian Apt. 104-dong #1702, Daegok-dong, Dalseo-gu, Daegu, South Korea

---

Publication

Sehoon Jang, Anal Mukhopadhyay, Dan G. Zollinger
"Hydration Modulation Measures to Mitigate the Negative Effect of Paving Concrete in Hot Weather", *Proceedings, 8th International Conference on Concrete Pavements*, August 2005